Alexander Arnitz, BSc

Model based predictive control of a heat pump system

MASTERARBEIT

zur Erlangung des akademischen Grades

Diplom-Ingenieur

Masterstudium Maschinenbau

eingereicht an der

Technischen Universität Graz

Beurteiler

Ao.Univ.-Prof. Dipl.-Ing. Dr.techn. René Rieberer

Betreuer

Mag.rer.nat. Ing. Martin Pichler M.Sc.

Institut für Wärmetechnik

Graz, November 2014

Statutory declaration

I declare that I have authored this thesis independently, that I have not used other than the declared sources/resources, and that I have explicitly indicated all material which has been quoted either literally or by content from the sources used. The text document uploaded to TUGRAZonline is identical to the present master's thesis.

Graz, am ………………………………….	…………………………………………………………..

(Alexander Arnitz)

Abstract

Title: Model based predictive control of a heat pump system

Author: Alexander Arnitz

1st keyword: Model based predictive control

2nd keyword: Heat pump

3rd keyword: Thermal storage

4th keyword: PV output prediction

This thesis presents and investigates a model based predictive control (MPC) approach to control the heating of a thermal storage with a heat pump. Aside from achieving the required temperatures in the storage the heat pump ought to maximize the utilization of electricity produced from an on-site photovoltaic (PV) installation.

Predictions for the PV output and the electricity price are combined with characteristic diagrams of the heat pump and a model of the thermal storage to determine an optimum heat pump operation. The optimum is found through solving a convex optimization problem. Different hydraulic circuits for the connection of the heat pump to the thermal storage are investigated. The nonlinear charging process of the thermal storage required an iterative MPC routine. The simulation results for the various hydraulic circuits are analyzed for a defined set of parameters.

Comparing simulation results from the MPC case against results obtained with a hysteresis control showed that the capacity utilization of the on-site PV – for driving the heat pump – is significantly higher for the MPC case. In addition, the MPC case shows a higher degree of compliance for all relevant temperature bandwidths. Finally, the robustness of the developed approach was proven through a number of annual simulations, however, further investigations and parameter optimization are required to allow for an assessment of the MPC performance in terms of energy demand and comfort, on an annual base.

Kurzfassung

Titel: Modellbasierte prädiktive Regelung einer Wärmepumpenanlage

Autor: Alexander Arnitz

1. Stichwort: Modellbasierte prädiktive Regelung

2. Stichwort: Wärmepumpe

3. Stichwort: Thermischer Speicher

4. Stichwort: Photovoltaik Ertragsprognose

In dieser Arbeit wird ein Ansatz zur modellbasierten prädiktiven Regelung der Beheizung eines thermischen Speichers mit einer Wärmepumpe untersucht. Ziel der Regelung ist einerseits die Einhaltung der erforderlichen Temperaturen im thermischen Speicher und andererseits ein überwiegender Betrieb der Wärmepumpe mit produziertem Strom aus einer Photovoltaikanlage.

Der optimale Betrieb der Wärmepumpe wird durch die Lösung eines konvexen Optimierungsproblems ermittelt. Dazu werden Photovoltaik Ertragsprognosen und Strompreisprognosen mit Kennfeldern der Wärmepumpe sowie einem Model des thermischen Speichers kombiniert. Für den Anschluss der Wärmepumpe an den thermischen Speicher wurden unterschiedliche hydraulische Schaltungen untersucht. Der nichtlineare Beladungsvorgang des thermischen Speichers führte zu einem iterativen Ansatz der modellbasierten prädiktiven Regelung. Dieser Ansatz wurde für die unterschiedlichen hydraulischen Schaltungen in Simulationen analysiert.

Ein Vergleich der Simulationsergebnisse der modellbasierten prädiktiven Regelung mit den Ergebnissen einer Hysterese Regelung zeigte einen erhöhten Eigenverbrauch des Photovoltaik Ertrags und eine bessere Einhaltung der erforderlichen Temperaturen mit der modellbasierten prädiktiven Regelung. Die Stabilität des entwickelten Ansatzes wurde in Jahressimulationen getestet. Um den Energieverbrauch zu bewerten sind jedoch weitere Untersuchungen notwendig.

Preface

This master thesis was written in the year 2014 at the Institute of Thermal Engineering at Graz University of Technology to support the development of a model based predictive control approach for a heat pump system for the project "*The Bat: The thermal battery in Smart grids in combination with heat pumps*".

First of all I would like to thank Ao. Univ.-Prof. Dipl.-Ing. Dr. techn. René Rieberer, for agreeing to evaluate this work and for his support during the writing of this thesis.

My special thanks go to my supervisor Mag.rer.nat. Ing. Martin Pichler M.Sc.. He organised everything down to the last detail and gave me the decisive impetus to continue making progress. Without him this work would not have been possible.

Furthermore, I would like to thank Dipl.-Ing. Dr. techn Andreas Heinz and Dipl.-Ing. Franz Hengel BSc, who were very helpful and supportive regarding all questions, especially concerning the heat pump system. I also want to thank everybody at the Institute of Thermal Engineering who contributed to this work. Additional thanks go to MA Silke Jandl for her support in writing this thesis in English.

I am grateful to my whole family, who supported me during all my years of study, my mother Kornelia, my father Ludwig, my brother Bernhard and my aunt Hildegard. Moreover, I would like to thank all my friends who have always backed me up.

Last but not least my thanks go to my girlfriend Elisabeth for her support and understanding during the writing of this thesis.

Graz, 10.11.14

Alexander Arnitz

Contents

1   Introduction

This work was conducted at the Institute of Thermal Engineering at the Graz University of Technology as a part of the project "The Bat - The thermal battery in smart grids in combination with heat pumps". It was carried out in cooperation with the company Heliotherm, a manufacturer of domestic hot water (DHW) systems and heat pumps, and the department of energy efficient buildings at the University of Innsbruck as designer of the reference system.

The motivation for this project is a result of the continuous efforts to reduce CO_2 emissions through lower fossil energy consumption, in addition to the long term phasing out of the nuclear energy program in Germany (see http://www.bundestag.de, 09.09.2014). Both of them lead to a push of renewable energies such as solar and wind power. The energy provided by solar and wind is, in contrast to conventional energy production, dependent on exterior factors, like weather and location. This is a challenge, when it comes to the integration into the grid and is referred to as *smart grid*.

Smart grids control the interaction between producers and consumers of electricity to find an economic and energetic balance (see http://www.smartgrids.at, 09.09.2014). This can be further improved by the use of energy storages which are able to compensate frequency fluctuations caused by the increasing displacement between demand and production of electricity. An overview of current storage methods can be found in "Uninterrupted renewable power through chemical storage cycles" (Gencer et al., 2014). A classification can be made according to the target group of energy storages. Pumped storage plants and air compression plants are, due to high investment costs, reserved for industrial purposes in contrast to batteries and thermal storages which can also be used privately. At the moment, pumped-storage plants are mainly used for this purpose. However, the possibilities for the construction of these plants are limited; hence alternative concepts increasingly gain significance.

Nowadays many single family houses are equipped with heat pump systems. Reasons for this development are low operating costs, security of supply and environmentally friendly heat generation (see www.waermepumpe-austria.at, 17.09.2014). Furthermore, heat pumps based on traditional control strategies are already used as flexible power consumers in restricted periods. These strategies, however, are unable to consider external input variables such as economic factors. Therefore, there is still a need to further exploit the potential of heat pumps using renewable energies.

This work deals with a predictive control approach for a heating system in combination with a photovoltaic (PV) array of a typical single family home. Thermal storages are the mass of

the building and the DHW storage. Within this work, the heating system is a monovalent heat pump with ground as the heat source. The aims are to minimize the costs for heating and to guarantee comfortable temperatures for the residents. For this, predictions for electricity prices and weather forecasts to predict PV output are used. Other achievements of conventional control strategies, like reasonable on and off cycles of the heat pump, should be maintained with this new control approach.

To achieve this, a model to control the reference system has to be found. This work investigates the combination of the heat pump with the thermal storage and the modeling of external input variables. The modeling of the thermal storage was particularly challenging because of the nonlinear convective heating process. The performance of the heat pump is mainly influenced by the temperatures of the heat source and sink. To keep the problem simple, the temperature of the heat source is assumed to be constant with the effect that a model for the geothermal probe is not necessary. The weather forecast is an ideal forecast. In real systems this is not possible. Therefore, some considerations about weather forecasts are discussed. Finally, the simulation results for different parameter settings of the model based predictive control (MPC) are analyzed and compared to the classical control concept.

This work is divided into the following chapters:

Chapter two gives an introduction into the fundamentals used in this work. At first the principle of compression heat pumps and PV cells is explained. After a brief overview on fluid dynamics and heat transfer, the concept of MPC is presented. This includes models used in control theory as well as the model predictive control toolbox in MATLAB which is used for solving the optimization problem. Finally, a short review about MPC in heating applications is provided.

Chapter three deals with the reference system which is represented by a simulation model implemented in TRNSYS. The chapter starts with an overview on the whole system followed by some information about the thermal storage and the building. Then the heat pump is explained with regard to the variable speed compressor, economizer and desuperheater. Subsequently the implementation of the PV array in TRNSYS is discussed. Finally, the external input variables (weather and electricity data) are dealt with.

Chapter four explores the modeling of the reference system used in the control algorithm followed by the parameterization of the MPC. After dealing with the modeling of the heat pump, by means of characteristic diagrams, the idea for the linear model of the thermal storage is explained. This explanation starts with a nonlinear approach followed by the introduction of the linear model used in the optimization problem. After this, the calculations to adapt the nonlinear behavior to the linear model are explained. The parameterization of the MPC is shown subsequent to the modeling of the disturbances.

Chapter five looks at the simulation results for a defined set of parameters. The simulations over a short period of two days and a long period of a year are compared between the MPC and a classical control concept based on a hysteresis.

Chapter six summarizes the most important findings and provides insights into further expansions.

2 Fundamentals

This chapter deals with the principle of compression heat pumps and PV cells. In the subchapter "Fluid mechanics and heat transfer" the basics used for the modeling of the thermal storage are introduced. This is followed by an introduction into the concept of MPC. Finally, some heating applications based on MPC are discussed.

2.1 Compression heat pumps

The information given in this chapter is mainly based on the lecture notes "Heat pump technology" (Rieberer et al., 2009). Compression heat pumps invert the natural heat flow by raising heat to a higher temperature level with the use of external energy. Figure 2-1 shows the working principle of a heat pump. Heat at a low temperature level is extracted from air, water or ground to evaporate the working fluid. Then the working fluid is compressed to reach a higher temperature level. This heat can be used to heat buildings or thermal storages. After the expansion of the working fluid through an expansion valve the cycle is complete.
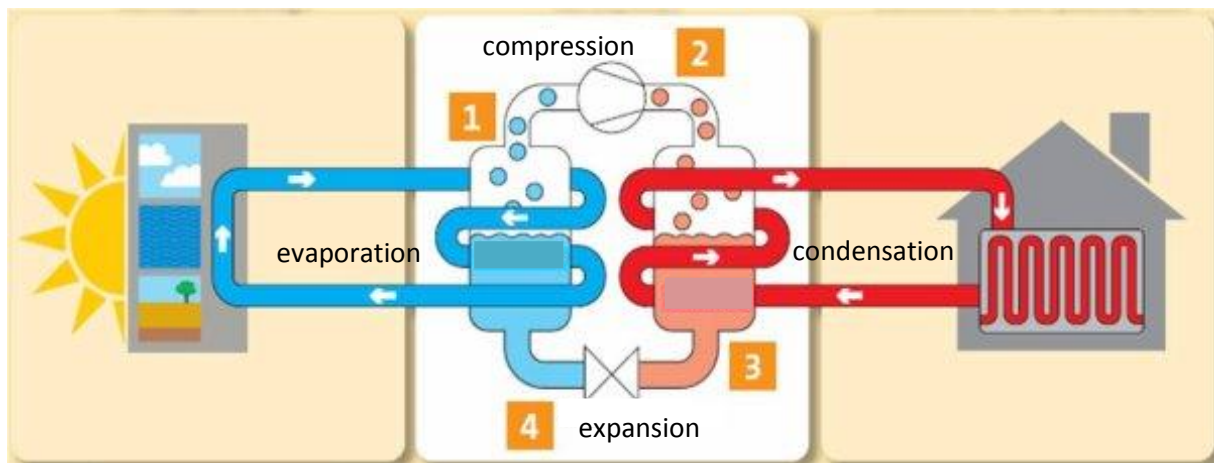
Figure 2-1: General form of a heat pump cycle (http://www.beama.org.uk/en, 13.09.2014)

The efficiency of a heat pump is expressed by the coefficient of performance (COP) and represents the current ratio of thermal output to electrical power input. Eq. 2-1 shows the COP of the Carnot cycle. This is the maximum possible efficiency reached by a process with reversible state changes.

$$COP_{Carnot} = \frac{T_{cr}}{T_{cr} - T_{er}}$$

Eq. 2-1

Although the Carnot cycle cannot be realized, the COP of heat pumps is mainly dependent on the temperatures at the source and sink (see Rieberer et al., 2009). Air as heat source has the disadvantage that the highest efficiency is reached in times of low heating demand. This aspect is important because lower investment costs for a heat pump with air as heat source

will be compensated by higher operating costs. The use of geothermal energy as heat source avoids partly this mismatch. The Fraunhofer Institute for Solar Energy Systems (ISE) investigated the COP of different heat pump systems (see Miara et al., 2011). The evaluated COP values for given temperatures at the source and sink are shown in Figure 2-2.
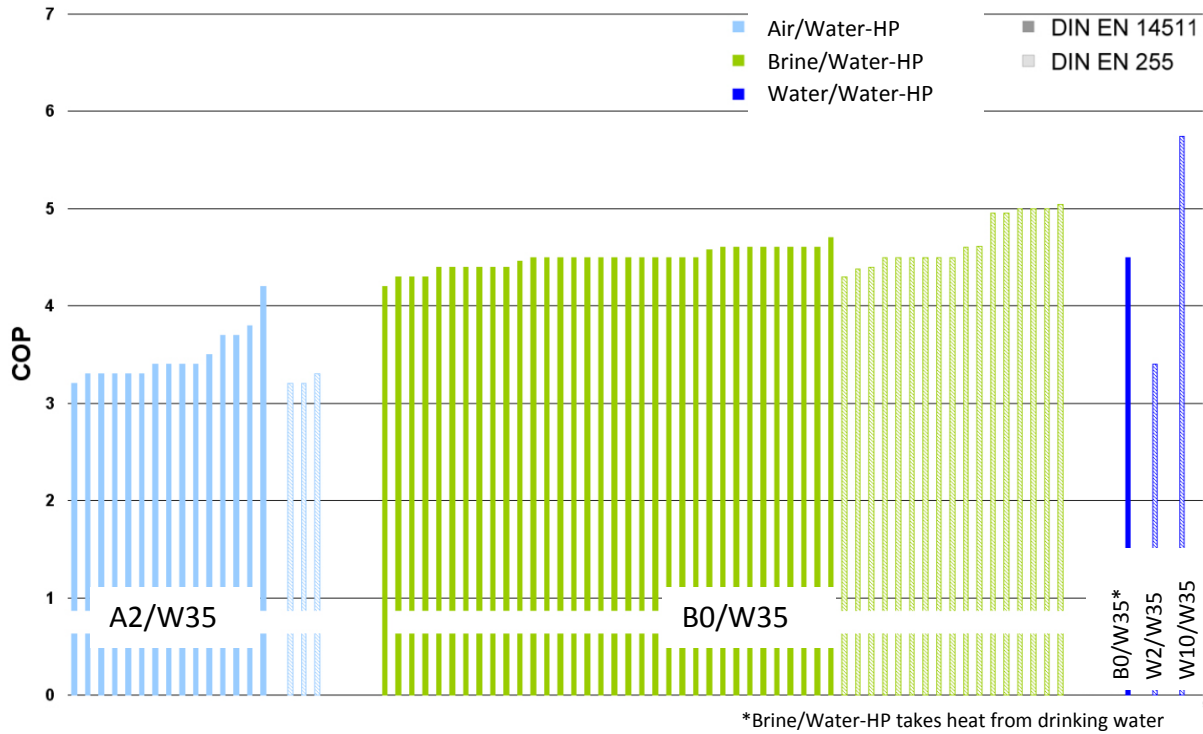

Figure 2-2: COP values of heat pumps divided by the heat source and certification standard (Miara et al., 2011)

Another quantity to measure the efficiency of heat pumps is the seasonal performance factor (SPF). The SPF is a mean average value of the COP usually over one year and is defined with Eq. 2-2 as the ratio of delivered heat Q_H to consumed energy W_{el} (see Rieberer, 2012).

$$SPF = \frac{Q_H}{W_{el}}$$

Eq. 2-2

The SPF for heat pumps with ground as the heat source and low temperature, heat distribution systems lies around 4 or higher (see Rieberer et al., 2009).

The efficiency is also affected by the working fluid because each refrigerant has certain pressure ratios for condensation and evaporation temperatures. Other thermodynamic properties are the volumetric heating capacity which influences size and costs of the heat pump, the temperature at the compressor outlet as a measure for the thermal stress of the compressor and the condensing pressure which has to be considered in the design. Furthermore, a good miscibility with the compressor oil, the possibility to use it as safety refrigerant as well as the impact on the environment is important. The environmental impact is characterized by the ozone depletion potential (ODP) and the global warming potential (GWP).

2.2 Photovoltaic arrays

Semiconductor materials, such as silicon, are able to absorb photons and release electrons. This is called *photoelectric effect*, which is used in PV cells. Semiconductor material contains unbound electrons known collectively as the conduction band. The bounded electrons form the valence band. The electrons are able to switch between the two bands. Figure 2-3 shows the cross section of a PV cell consisting of an n-doped side (e.g. phosphorus has one more electron then silicon) which faces the sun and a p-doped side (e.g. boron has one less electron then silicon) at the back. The p-n junction forms a strong, permanent electric field at the junction of these two sides. In the presence of incident light, electrons are separated from the atoms in the n-doped side and the p-n junction. This causes a flow of electrons along the electric field. If the front side and the back side are connected to a load, a current is produced (see Fry, 1998).
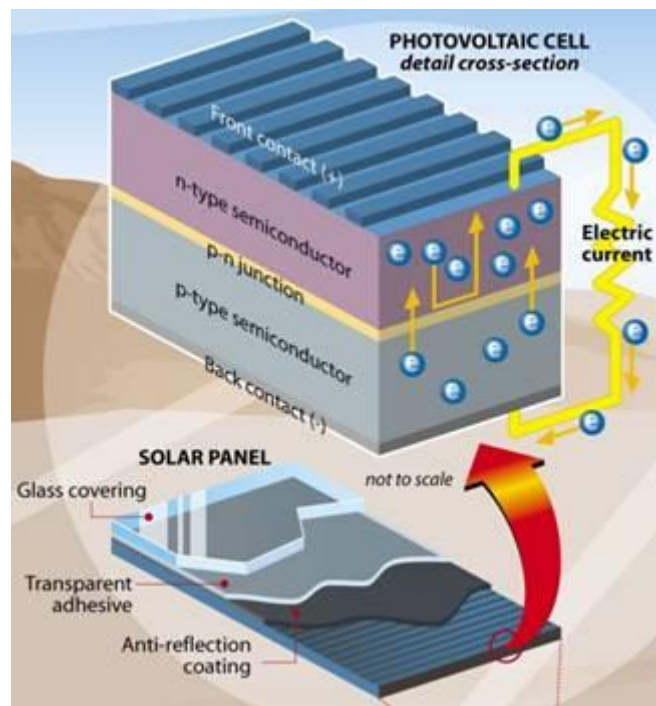
Figure 2-3: PV principle (http://www.sunbirdenergy.com/, 25.09.2014)

The output of a PV system depends mainly on the solar irradiation, the cell temperature which is further affected by the wind velocity, the angle of incidence and the load resistance. There are two operating modes possible, a connection to the grid or the operation in an island mode. Figure 2-4 schematically shows the steps to feed electricity, produced by a PV array, into the grid.
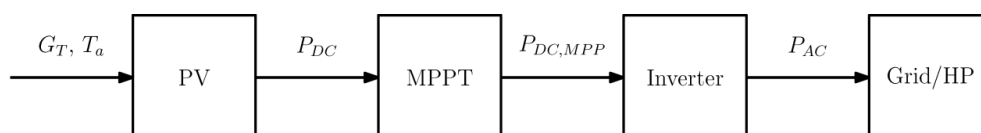
Figure 2-4: Steps to feed electricity, produced by a PV array, into the grid

First of all, the total solar irradiation G_T meets the PV array under ambient conditions T_a, then the PV effect enables that direct voltage is available at the output. The maximum power point tracker (MPPT) is installed to ensure that current and voltage deliver maximum power. Before the electricity is fed into the grid, an inverter is used to switch from direct current to alternating current, which influences the efficiency.

If a PV array is directly coupled to a load, the system will operate at the intersection of the current-voltage-curve of the PV array and the current-voltage-curve of the load. The current-voltage-curve of a load represents all possible operating points for this load. This equally applies for the current-voltage-curve of PV arrays (see Eckstein, 1990). Figure 2-5 on the left shows the current-voltage curve of the PV array. In the middle the current-voltage curve for a load with constant resistance is shown. On the right the resulting operating point is shown, which lies on the intersection of these curves. Furthermore the maximum power point (MPP) of the PV array is illustrated. As already mentioned, a PV array with MPPT operates at this point.
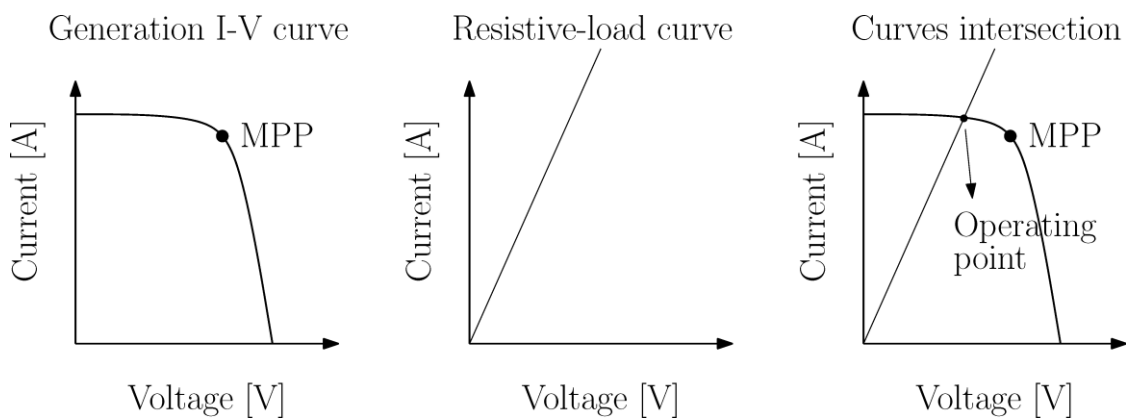
Figure 2-5: Operating point of a PV array directly coupled to a load (Coelho et al., 2012)

2.3 Fluid mechanics and heat transfer

This subchapter focuses on the basics for the modeling of the thermal storage. The specific heat capacity of water as an incompressible fluid can be expressed in Eq. 2-3 (see Brenn et al., 2010).

$$c_v = c_p = c$$

Eq. 2-3

The one dimensional conservation equation used for the modeling of the thermal storage is derived as shown in Figure 2-6. The heat flow across the boundaries can be divided into two streams. Forced convection is caused by the constant fluid flow u_{vel} and conduction is caused by a temperature gradient.

Figure 2-6: Control volume with heat flows

The energy balance for this control volume is shown in Eq. 2-4.

$$\frac{\partial Q}{\partial \tau} = \dot{Q}_{conv,x} + \dot{Q}_{cond,x} - \dot{Q}_{conv,x+dx} - \dot{Q}_{cond,x+dx}$$

Eq. 2-4

Using a Taylor series expansion for $\dot{Q}_{conv,x+dx}$ and $\dot{Q}_{cond,x+dx}$ leads to Eq. 2-5. This approach is similar to that applied in "Thermal engineering 1" (see Hochenauer, 2012).

$$\frac{\partial Q}{\partial \tau} = \frac{\partial \dot{Q}_{conv}}{\partial x} + \frac{\partial \dot{Q}_{cond}}{\partial x}$$

Eq. 2-5

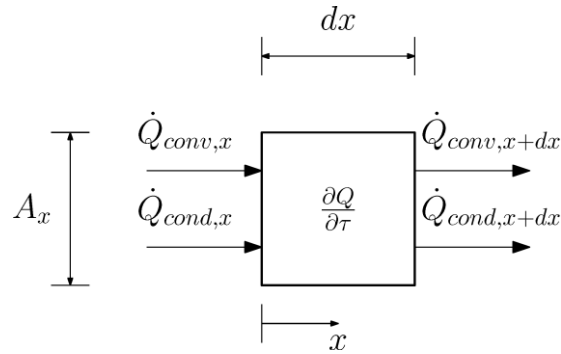The amount of heat in the control volume can be written as Eq. 2-6.

$$Q = m \, c \, T = \rho \, A_x \, c \, T \int dx$$

Eq. 2-6

The convective heat flow is represented by Eq. 2-7.

$$\dot{Q}_{conv} = \dot{m} \, c \, T = \rho \, A_x \, u_{vel} \, c \, T$$

Eq. 2-7

The heat flow caused by conduction is based on the heat conduction equation according to Fourier (see Brenn et al., 2010).

$$\dot{Q}_{cond} = -\lambda \, A_x \, \frac{\partial T}{\partial x}$$

Eq. 2-8

Substituting Eq. 2-6 - Eq. 2-8 for Q, $\dot{Q}_{conv}$, $\dot{Q}_{cond}$ in Eq. 2-5 leads with $\rho = constant$ to Eq. 2-9.

$$\frac{\partial T}{\partial \tau} = u_{vel} \, \frac{\partial T}{\partial x} - a \, \frac{\partial^2 T}{\partial x^2}$$

Eq. 2-9

Whereby a is called thermal diffusivity and is defined by Eq. 2-10 (see Brenn et al., 2010).

$$a = \frac{\lambda}{\rho \, c}$$

Eq. 2-10

The thermal storage is furthermore in heat exchange with the environment. This is the heat loss and can be written with the heat transition coefficient and the area dA_{yz} as shown in Eq. 2-11.

$$\dot{Q}_{loss} = U\,(T - T_a)\int dA_{yz}$$

Eq. 2-11

Adding the heat losses to the energy balance, written in Eq. 2-9, leads to Eq. 2-12. This equation is used for the nonlinear model of the thermal storage.

$$\frac{\partial T}{\partial \tau} = -u_{vel}\,\frac{\partial T}{\partial x} + a\,\frac{\partial^2 T}{\partial x^2} - \frac{U\int dA_{yz}}{\rho\,c\int dV}\,(T - T_a)$$

Eq. 2-12

2.4   MPC in a nutshell

This chapter introduces the basic idea behind MPC, starting with a list of benefits and areas of application. Then some possibilities to characterize optimization algorithms used in control theory are discussed. After an explanation of the idea of the receding horizon and an overview on models used in control theory, the model predictive control toolbox is explained. Finally, an alternative to the model predictive toolbox is presented.

The concept of MPC is used since the 1970's mainly in process industries. A reason for this is the ability to handle a large number of manipulated and controlled variables including constraints as well as plants with large time constants or time delays. Other advantages are that firstly, a cost function can be formulated and secondly, that predicted disturbances can be considered (see Morari et al., 1998). The cost function is also called objective or quality factor. Examples for the use of MPC in applications other than the process industry are the control of locks in canal systems, heating and air conditioning systems or the control of seasonal heat storage systems (see Grötschel et al., 2008).

MPC is based on an optimization algorithm. Optimization algorithms in control theory can be separated as follows:

A real time optimization performed at each sampling instant is called *online optimization*. A sampling instant specifies the times the controller is called upon. The time between two sampling instants is called sampling interval. In contrast to an *offline optimization* where the optimization is performed to obtain a control rule which can be implemented into the controller (see Wimmer, 2004).

A classification can be made with regard to the dimension of the optimization variables. If they are represented by scalars it is called *parameter optimization* and if the optimization

variables are represented by trajectories within a time horizon, as it is in MPC, then it is called *dynamic optimization* (see Hofer, 2014).

Algorithms can be distinguished with respect to the manipulated variable in *direct* or *indirect optimization*. In an indirect optimization the optimization variables do not contain the manipulated variable needed for the actuator. This means that the solution of the optimization problem is further processed to obtain the manipulated variable. Direct optimization, on the other hand, directly optimizes the manipulated variable needed for the actuator (see Wimmer, 2004).

The last classification can be made according to the form of the cost function and the constraints. In this context, the popular approach for a linear, time invariant system with quadratic cost function, also called linear quadratic regulator (LQR) is specified. This is shown in Eq. 2-13. Whereby J represents an arbitrary cost function in quadratic form and the system equations, which have to be fulfilled, are represented by a linear, time invariant state space model (see chapter 2.4.2). This constellation leads to a optimization problem which can be solved exactly (see Hofer, 2014). In this case the optimization is performed offline with the advantage that the computational effort for the determination of the manipulated variable is reduced.

$$\min J$$
$$\text{with subject to the } system\ equations$$

<div align="right">Eq. 2-13</div>

The drawback of an optimization problem in the form of Eq. 2-13 is that inequality constraints in the form of Eq. 2-14 and Eq. 2-15 are not considered. If the manipulated variable u is not constrained, high or negative values may occur, which cannot be handled by the actuator. If constraints in the form of Eq. 2-14 and Eq. 2-15 are incorporated, an exact solution of the optimization problem is no longer possible. The optimization problem has to be evaluated online at each sampling instant. This leads to higher requirements on computational power (see Wimmer, 2004).

$$y_{min} \leq y \leq y_{max}$$

<div align="right">Eq. 2-14</div>

$$u_{min} \leq u \leq u_{max}$$

<div align="right">Eq. 2-15</div>

The cost function offers the opportunity to impose a certain behavior to a system. Hence the cost function differs according to the requirements of the system. Eq. 2-16 and Eq. 2-17 show two cost functions for a system with one manipulated variable and one controlled variable. The first cost function (Eq. 2-16) has the aim to minimize the difference between a reference value y_{ref} and the controlled variable y. In the second cost function (Eq. 2-17) a second term is added and consequently, two different aims are pursued. The second aim is to reduce e.g. the energy consumption of the manipulated variable u. The aims may be

contradictory. Therefore, a weighting factor w^u is introduced to set a priority. For instance, if the weighting factor is very high, the energy consumption has priority, and if the weighting factor is zero, the energy consumption is not considered.

$$J = \sum_{i=0}^{p-1} \left(y_{i+1} - y_{ref,i+1} \right)^2 \qquad \text{Eq. 2-16}$$

$$J = \sum_{i=0}^{p-1} \left[\left(y_{i+1} - y_{ref,i+1} \right)^2 + (w_i^u \ u_i)^2 \right] \qquad \text{Eq. 2-17}$$

2.4.1   The receding horizon

The principle of MPC is based on the idea of the receding horizon which is explained for a system with one controlled variable y and one manipulated variable u in Figure 2-7. The main objective is to reach the reference (or setpoint) y_{ref} with the controlled variable y under the consideration of constraints on the controlled variable (y_{max}, y_{min}) and the manipulated variable (u_{max}, u_{min}). The MPC is called upon and obtains measured values for y at the sampling instant k.

The lower part of the Figure 2-7 shows a trajectory of u. This trajectory consists of a set of present and future control moves over the control horizon m. The control horizon can be smaller than the prediction horizon, which stabilizes the system. If $m < p$ the missing values remain constant (see Bemporad et al., 2014).

The prediction of y over the prediction horizon p is shown in the upper part. This prediction is obtained with the system equations (e.g. state space model of the plant) based on the measured state and the input trajectory u. The optimization algorithm chooses different trajectories of u and evaluates the impact on y until an optimal solution is found which minimizes the cost function. Even though a trajectory of control moves is calculated only the first value is set. This procedure is repeated at each sampling instant by shifting the control and prediction horizon. The feedback is generated as each set of control moves is based on a new measured output (see Morari et al., 1998).

For a controlled system based on a perfect model without disturbances the trajectory of u shown in Figure 2-7 at the bottom would be sufficient to reach the predicted curve of the controlled variable y shown in Figure 2-7 at the top. Whereas in reality this is rarely the case for this a feedback is used to compensate this.
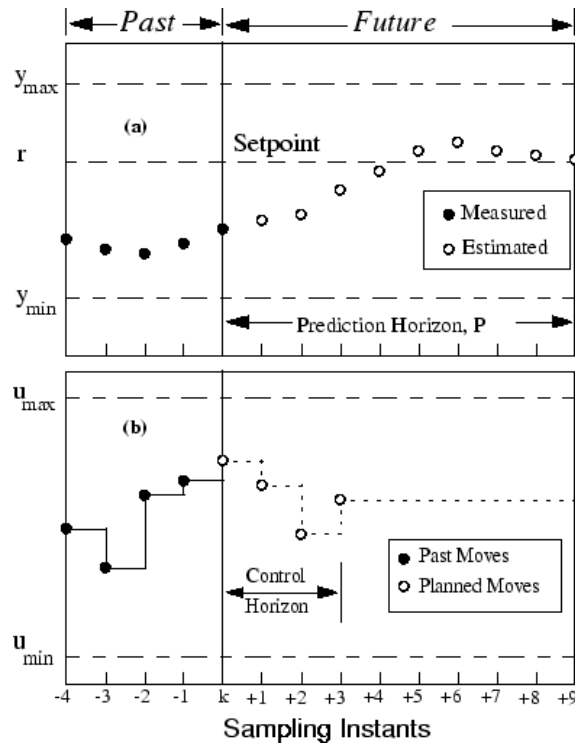
Figure 2-7: The predicted curve of the controlled variable (a) within the receding horizon based on a set of manipulated variables (b) within the receding horizon (Bemporad et al., 2014)

2.4.2 Models used in control theory

The name MPC suggests that a mathematical model is necessary to represent the physical behavior of the system. For this different models can be used. Impulse or step response models describe the behavior of the output in dependence of an impulse or step on the input. These models are derived by measurements on the real plant. If a linear physical model can be found state space models or transfer functions can be used (see Wimmer, 2004).

Eq. 2-18 - Eq. 2-20 show a continuous, linear, time invariant state space model with the parameters dynamic matrix A, the input matrix B, the output matrix C and the variables for state x, input u and output y (see Hofer, 2009).

$$\dot{x} = A \cdot x + B \cdot u \qquad \text{Eq. 2-18}$$

$$y = C \cdot x \qquad \text{Eq. 2-19}$$

$$x(0) = x_0 \qquad \text{Eq. 2-20}$$

State space models correspond to systems of ordinary, linear differential equations of first order. If state space models are used in digital control loops they are discretized in time. Discretized models correspond to a system of linear equations in the state variables between two successive time steps (see Horn et al., 2004).

The challenge in the modeling process is to find a linear model, as for problems based on linear models high quality optimization algorithms are available. Despite this, many technical systems are nonlinear and operate in a wide range. In those cases, a linear or linearized model is not sufficient. For these situations there are methods for nonlinear systems available. These methods are more complex because the optimization problem changes from a convex quadratic problem to a non-convex nonlinear problem and there is no guarantee that a global minimum can be found (see Camacho et al., 1999).

2.4.3 The MPC toolbox

The MPC toolbox of MATLAB is used to implement the MPC problem. The content of this chapter is mainly based on the "Model Predictive Toolbox Users Guide" (Bemporad et al., 2014).
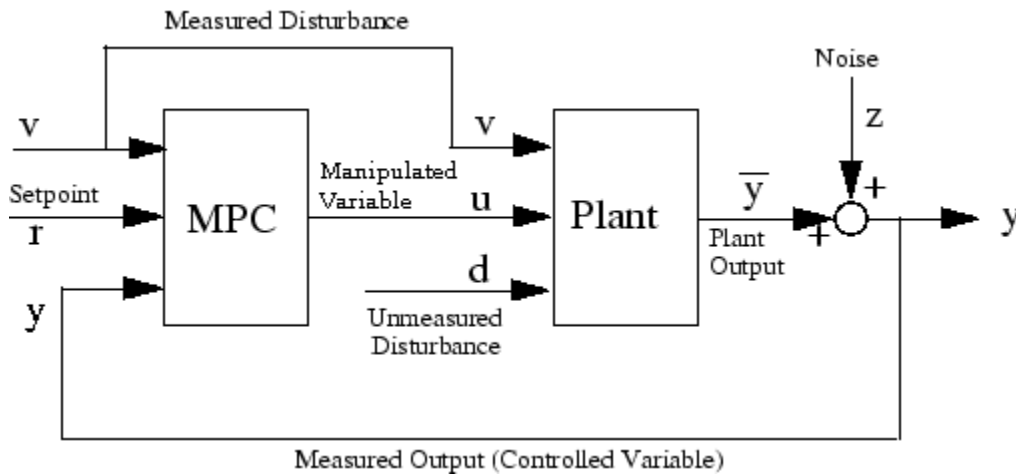

Figure 2-8: Schematic representation of a MPC application (Bemporad et al., 2014)

A general schematic representation of a single-input single output MPC toolbox application is shown in Figure 2-8. The plant represents the process to be controlled. The output value of the plant $\bar{y}$ is the signal to be held at the reference value $r = y_{ref}$. Therefore $\bar{y}$ is measured under the influence of measurement noise z that impairs measurement precision and accuracy. The measured output y is the feedback signal for the MPC controller. When the controller receives the measured output variable all state variables have to be updated. Therefore a state estimation is necessary at the beginning of each sampling instant. If all plant states are measured, the state estimation has only to consider measurement noise effects. Other input variables of the MPC controller are the reference value y_{ref} and the measured disturbances v. These values are trajectories within the prediction horizon and can vary in time. Based on these input variables the MPC controller adjusts the manipulated variable u by minimizing a cost function. The manipulated variable in addition to the unmeasured d and the measured disturbances are the input of the plant. The difference between measured disturbances and unmeasured disturbances is that the controller receives measured disturbances in advance. This allows a feed forward compensation of the

impact on the output signal. Unmeasured disturbances are present in almost every process and are handled by feedback compensation.

Bellman's principle of optimality states that infinite horizons ensure stability, as for an infinite horizon at each sampling instant the same optimization problem is solved. This is due to the fact that no additional information comes between two successive optimization problems because they consider the same infinite horizon. In finite horizons optimizations are based on different problems because each optimization is performed above a receding horizon and the behavior behind is not considered (see Maciejowski, 2000). The MPC toolbox provides the possibility to set terminal constraints or terminal weights to achieve closed loop stability for the LQR. For problems with constraints this is not possible. Consequently, the constraints, weights and equal concerns for relaxation (ECR) factors have to be chosen to ensure stability.

Constraints on manipulated and output variables defined for a MPC toolbox application may be hard or soft. If a hard constraint is violated the controller assumes the system as unstable. Such a violation occurs under certain conditions (e.g. an unexpected large disturbance). The MPC toolbox handles this by specifying a degree of softness for each constraint. The constraints are relaxed by introducing the slack variable ϵ with the corresponding ECR factors V. V should be chosen large for a soft constraint. If V is equal to zero the constraint is defined as a hard constraint.

For the further investigations the denomination $y(k + i + 1|k)$ is interpreted as the predicted output at time $k + i + 1$ based on the actuator $u(k + i|k)$ obtained at the current sampling instant k. The optimization problem solved by the MPC toolbox uses the cost function shown in Eq. 2-21 and handles constraints in the form of equation Eq. 2-26.

$$\min_{\Delta u(k|k),\dots,\Delta u(m-1+k|k),\epsilon} \left\{ \sum_{i=0}^{p-1} \left[\left(w_{i+1}^y \left(y(k + i + 1|k) - y_{ref}(k + i + 1) \right) \right)^2 \right. \right.$$
$$\left. \left. + \left(w_i^{\Delta u} \Delta u(k + i|k) \right)^2 + \left(w_i^u u(k + i|k) \right)^2 \right] + \rho_\epsilon \epsilon^2 \right\}$$

Eq. 2-21

The optimization algorithm chooses $\Delta u(k|k), \dots, \Delta u(m - 1 + k|k), \epsilon$ to minimize Eq. 2-21 above the whole prediction horizon. The first term represents the deviation of the output variable from the reference. The second term of the cost function considers the alteration rate of the manipulated variable. The third term minimizes the manipulated variable. The last term penalizes the violation of the constraints. The first three terms are weighted with the non-negative weights $w_i^{\Delta u}, w_i^u, w_i^y$. As already mentioned a high value of w raises the importance of the corresponding term to the overall performance.

Eq. 2-22 - Eq. 2-24 define lower and upper bounds on the corresponding variables. Eq. 4-26 ensures that the manipulated variable remains constant for $h = m, \dots, p - 1$. This is relevant if the control horizon m is smaller than the prediction horizon p. Eq. 2-26 defines a positive value for the slack variable.

$$u_{min}(i) - \epsilon V_{min}^u(i) \leq u(k + i|k) \leq u_{max}(i) + \epsilon V_{max}^u(i) \qquad \text{Eq. 2-22}$$

$$\Delta u_{min}(i) - \epsilon V_{min}^{\Delta u}(i) \leq \Delta u(k + i|k) \leq \Delta u_{max}(i) + \epsilon V_{max}^{\Delta u}(i) \qquad \text{Eq. 2-23}$$

$$y_{min}(i) - \epsilon V_{min}^y(i) \leq y(k + i + 1|k) \leq y_{max}(i) + \epsilon V_{max}^y(i) \qquad \text{Eq. 2-24}$$

$$\Delta u(k + h|k) = 0 \qquad \text{Eq. 2-25}$$

$$\epsilon \geq 0 \qquad \text{Eq. 2-26}$$

2.4.4 Alternatives to the MPC toolbox

The MPC toolbox provides a valuable framework to solve optimization problems in MATLAB. For this, the parameters explained in the previous section are arranged in matrices which can be handled by a solver for quadratic programs. But this also leads to restrictions on the form of the optimization problem. One alternative to avoid these restrictions would be to set up the matrices manually for a suitable solver which is available in MATLAB. This, however, is a time consuming task.

Another alternative, which is free of charge to use and openly distributed, can be found in YALMIP. Further information about the license can be found in the "YALMIP Wiki" (Löfberg, 2014). It is a toolbox which can be used in MATLAB for advanced modeling and the solution of convex and non convex optimization problems. YALMIP can be used for a wide range of applications. For instance, it can be used for simple parameter optimizations as well as for MPC (see Löfberg, 2014).

One interesting application can be found in hybrid MPC. Models for hybrid MPC are based on linear time invariant models in addition to logic operators. For instance, if the behavior of a system can be described by two state space models depending on the state or input variable. The optimization problem can be expressed as Eq. 2-27 - Eq. 2-31 (see Löfberg, 2014).

$$\min J \qquad \text{Eq. 2-27}$$

$$\dot{x} = A_1 \cdot x + B_1 \cdot u \quad if \ u > 0 \qquad \text{Eq. 2-28}$$

$$\dot{x} = A_2 \cdot x + B_2 \cdot u \quad if \ u = 0 \qquad \text{Eq. 2-29}$$

$$y_{min} \leq y \leq y_{max} \qquad \text{Eq. 2-30}$$

$$u_{min} \leq u \leq u_{max}$$

<div align="right">Eq. 2-31</div>

This method is highlighted, as it offers another possibility to model the thermal storage described in chapter 4.2. It has one essential drawback, however, with increasing order of the system or prediction horizon the number of possible solution increases significantly and thus the computational effort.

2.5 Predictive control for heating applications – A short review

The most common traditional control strategy for central heating applications is based on a heating curve to represent the relationship between the ambient temperature and the flow temperature. The connection between the measured ambient temperature and the flow temperature as controlled variable is established by a heating curve. This curve may vary in time to enable a night reduction (see Thron, 2001).

Thron (2001) starts with a good overview on different control concepts for predictive heating applications. She investigates an adaptive MPC approach for a building to improve the use of solar heat gains. The heating system is not considered in her work. The approach is compared to the traditional control strategy by simulations in different building constructions. The results show a reduction of heating energy consumption in lightweight construction of approximately 3% and in massive construction of approximately 7%.

Wimmer (2004) investigates three different MPC approaches for a building with integrated heat pump system. The heat pump with air as heat source is equipped with a compressor of constant speed. The model for the building is based on a physical state space model of third order. The state variables are return flow temperature, the temperature of the floor and the room temperature. The heat pump is modeled according to a nonlinear model of first order with the flow temperature as state variable. The identification of the parameters for the models is performed offline with the System Identification Toolbox in MATLAB. This is a non adaptive approach because the parameters are not updated during the operation. Two MPC approaches are based on indirect optimizations which optimize the required heat flow. These are the LQR without constraints and the linear quadratic MPC with constraints. In these concepts the heat flow provided by the heat pump is determined by a characteristic diagram. The third concept is based on a nonlinear approach and directly optimizes the manipulated variable of the heat pump by using the model of the heat pump. The LQR algorithm was implemented and tested in a real system. The COP is considered as a function of the ambient temperature and the temperature at the heat sink is not considered. This enables an optimization of the electrical energy. For the electricity prices Wimmer (2004) only makes a distinction between low tariff and high tariff times. In the simulation the MPC approaches are compared to a traditional control strategy. The results show an

improvement with the innovative concepts, especially in terms of economic costs. The economic costs can be reduced by 13% and the electrical energy consumption is reduced by 3%. The nonlinear approach, despite higher technical effort, does not show significant improvement compared to the linear quadratic MPC.

The work of Bianchi (2006) is based on the results found by Wimmer (2004). He improved the approach with an online identification algorithm to determine the physical parameters of the building during the operation. The heating system is represented by a heat pump with ground as heat source. Furthermore, the control concept is expanded for a combined regulation of a building in combination with a thermal storage for DHW preparation. The thermal storage is regulated with a classical hysteresis that a physical model is not necessary. The control concept is compared and emulated in a test bench. The results show economic cost reductions of 10-20% through shifting the operating time of the heat pump in low tariff periods. Furthermore, longer operating periods of the heat pump are achieved(see Bianchi, 2006).

The work of Pichler et al. (2014) investigates a MPC approach for a solar thermal combistorage. The storage is heated with solar yields in addition to auxiliary heating. The reference system is represented in a simulation model implemented in TRNSYS. The model used for control is represented by a linear time invariant state space model. The optimization algorithm can be classified as direct optimization. The heat flow due to solar yields is interpreted as disturbances. Such disturbances are derived by a simulation, based on predicted weather data. Load profiles take DHW demand and SH into consideration. The results demonstrate the strength of the MPC approach for months where relatively high irradiance meets an according SH demand.

3 Reference system implemented in TRNSYS

This chapter introduces the reference system of the project "The Bat" to derive comfort limits for the design of the control unit and to guarantee a correct operation. At first the software tool TRNSYS is presented, followed by an overview of the whole system to show how the components are connected. Then the components of the system are explained with special focus on the thermal storage, the heat pump and the PV array. Finally, the weather and electricity data is analyzed.

TRNSYS is a complete and extensible simulation environment for the transient simulation of systems. It is mainly used for the design and simulation of buildings and their equipment. This includes control strategies, occupant behavior, weather data as well as a wide range of components in connection with heating systems. The individual extensibility is one reason why TRNSYS is such a powerful tool (TRNSYS, 2012). A TRNSYS model for a compression heat pump has been developed at the Institute of Thermal Engineering at the Graz University of Technology (see Heinz et al., 2014).

The whole system is shown in Figure 3-1. It consists of a heat pump, a thermal storage, a PV panel and a building model. External input variables are a DHW load profile and weather data. The heat pump is illustrated in a simplified form to show the external connections. The internal cycle of the heat pump is investigated in chapter 3.3.2. The heat pump is used to heat up the storage or to heat up the building, these two operating modes are controlled by the valves $V1$ and $V2$. The building can only be heated with the condenser c, the heat flow of the desuperheater d is in both modes injected into the top node. If space heating (SH) is not necessary the heat flow of the condenser is injected into the middle node of the thermal storage. The evaporator e is connected to the heat source.

The classical control approach is realized with an ON/OFF control for the heat pump in the two operating modes whereby the heating of DHW has priority against SH. The reference value of the flow temperature for the storage is $45\,°C$. To hold this temperature at the connection to the DHW station a volume has to be defined which is able to fulfill the daily demand of DHW (see chapter 3.1). The classical control is based on a hysteresis to hold this volume of the storage above the temperature limit (see chapter 3.1). The reference value of the return temperature for the floor heating is calculated according to a heating curve (see Brychta, 2014).

The MPC application designed in this work is used to control the heating process of the thermal storage. The heating requirements of the building are not considered in this MPC application.
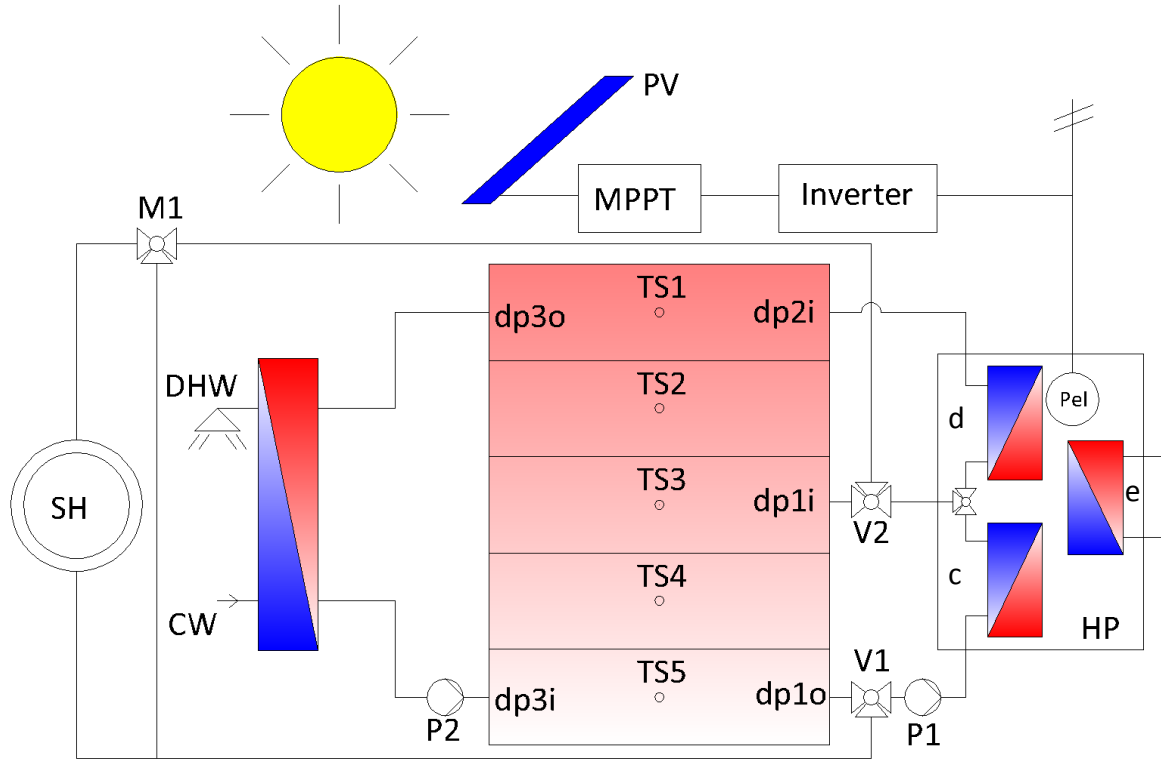
Figure 3-1: Reference system

Table 3-1 is an overview of the simulation results collected over one year, based on the classical control concept. The values fit a typical single family home with a living area of $160 \, m^2$. Important quantities are the SPF in combination with the heating demand Q_H. The heating demand is the sum of the DHW demand Q_{DHW}, the SH demand Q_{SH} and the heat losses of the thermal storage $Q_{S,loss}$. Further heat losses occur in the heat distribution system. These values are not listed in Table 3-1. The heating demand has to be covered by the thermal output of the condenser Q_c and the desuperheater Q_d. The work required to drive the heat pump W_{Comp} can consequently be calculated with Eq. 3-1.

$$W_{Comp} = \frac{Q_H}{SPF} = \frac{Q_c + Q_d}{SPF}$$

Eq. 3-1

As already mentioned, the SPF for heat pumps with ground as the heat source and low temperature, heat distribution systems lies around 4 or higher (see Rieberer et al., 2009). In this project an innovative heat pump is used, so a SPF of 5.07 is achieved.

Although the PV array is connected to the grid via the inverter, its main purpose is to drive the heat pump. The MPPT ensures that the PV array operates at the maximum power point (MPP). The PV array has a total surface of $13.14 \, m^2$ which faces south with an angle of 45°. The PV output W_{PV} and the tilted total irradiation $G_{T,S,45}$ in Table 3-1 are referred to this area. The PV output does not contain losses caused by the inverter. The comparison of the

PV output with the electricity requirement of the heat pump can be interpreted as a motivation of the MPC.

Table 3-1: Characteristic quantities of the system based on an annual simulation

Quantity	$[kWh]$	$[kWh/m^2]$
W_{Comp}	2193	14
Q_c	10253	64
Q_d	871	5.4
Q_{DHW}	2142	13.4
Q_{SH}	7694	48
$Q_{S,loss}$	1230	7.7
W_{PV}	3579	272
$G_{T,S,45°}$	20856	1587

3.1 Thermal storage

This chapter investigates the thermal storage. At first some aspects for hot water preparation are introduced. After the discussion of a charging process, the positions of the sensors, and the temperature limits are explained.

Central systems for hot water preparation are available as instantaneous water heating systems or hot water storage systems. In instantaneous water heating systems the storage water is separated from the drinking water. This has the advantage that higher hygienic standards can be achieved because the growth of legionella is avoided. The thermal storage used in this work represents the type ZH-S5101 distributed by Heliotherm (see Brychta, 2014). This is a thermal storage with a fresh water counter flow heat exchanger and a total volume of $500\ l$ (see Heliotherm, 2014). Figure 3-2 shows a schematic representation of the thermal storage without the heat pump. The instantaneous water heating system is connected to the cold water source and the hot water distribution system. If a DHW draw off occurs the circulation pump feeds water through the heat exchanger for instantaneous heating of the cold water. The temperature distribution inside the storage is stratified. If the return temperature into the storage is lower than the temperature at the bottom of the storage or higher than the temperature above the inlet, a mixing process caused by natural convection occurs.
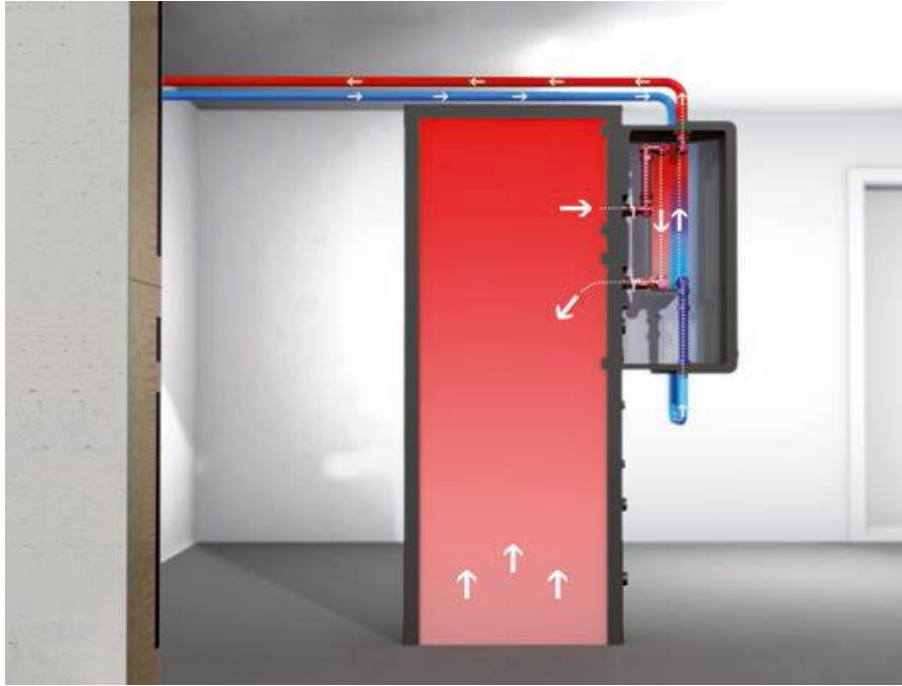
Figure 3-2: Heliotherm fresh water system (http://www.heliotherm.com, 17.09.2014)

The thermal storage is connected to the heat pump through the condenser and the desuperheater (see Figure 3-1). The mass flow through the heat exchangers is regulated to reach a certain temperature difference between the inlet and the outlet (see chapter 3.3.2). The left picture of Figure 3-3 shows a simulation example of the charging from $30\,°C$ to $55\,°C$ in a thermal storage with an external heat exchanger. The recorded temperatures refer to the numbering of the nodes shown in Figure 3-1. The cold water is taken from the bottom. It is additional heated for $5\,K$ and injected at the top of the thermal storage. The effect of stratified charging is pronounced at the first two stages. For the other stages this is not so clear because of mixing effects and the thermal inertia of the thermal storage. This behavior was also observed by Bianchi (2006) through measurements in a real storage.

DHW must be available at every time. For this a volume has to be defined which is able to fulfill the daily demand of DHW. This volume is set to the half of the whole thermal storage volume (see Brychta, 2014). The sensor position to control the temperature of this volume can be calculated with Eq. 3-2. $h_{S,DHW}$ represents the height of the sensor position in the thermal storage and h_S represents the total height of the thermal storage. The right picture of Figure 3-3 shows an example of the discharging of the thermal storage for an arbitrary load.

$$h_{S,DHW} = \frac{1}{2}\,h_S$$
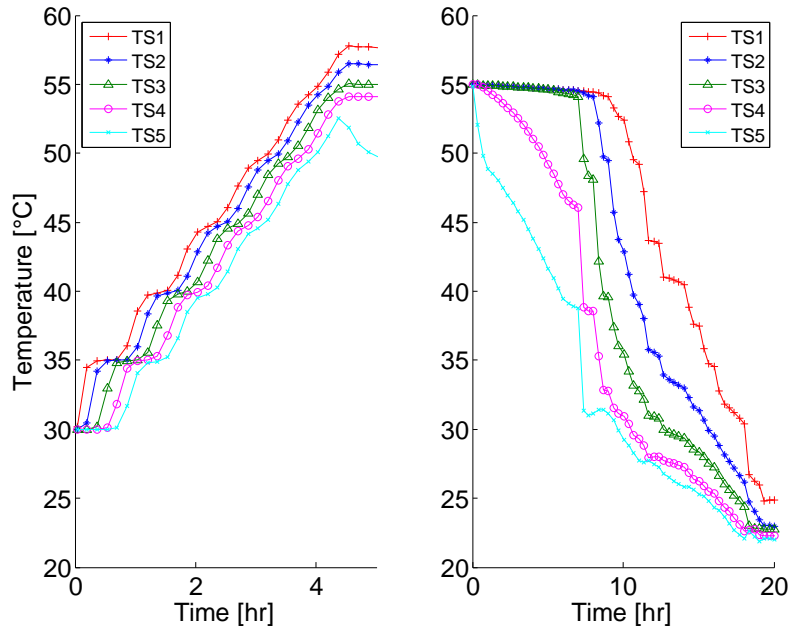
<div align="right">**Eq. 3-2**</div>

Figure 3-3: Simulated charging and discharging of the thermal storage with an external heat exchanger connected to the bottom and the top (without the desuperheater), the temperatures refer to the nodes shown in Figure 3-1

As a general rule the temperature of the DHW should be chosen as low as possible in order to achieve a high efficiency of the heat pump. For a heat exchanger with instantaneous water heating system a temperature of approximately $45\,°C$ is sufficient. The classical control uses a hysteresis to switch on if the temperature at the sensor position falls below $45\,°C$ and switches off if the temperature exceeds $50\,°C$ (see Brychta, 2014).

Temperature limits of the thermal storage are necessary to avoid vaporization and to prevent damages. These limits cannot be achieved with heat pumps. It would be crucial, however, if an auxiliary heater or a solar system is installed. For the control of the limits for the heat pump a sensor should be placed at the top or bottom of the thermal storage (see chapter 3.3.2).

Table 3-2 shows evaluated quantities of the thermal storage based on an annual simulation. These are the heat losses to the ambient $\dot{Q}_{S,loss}$ and the temperatures at the nodes t_{sj} of the thermal storage (see Figure 3-1).

Table 3-2: Characteristic quantities of the thermal storage based on an annual simulation

Quantity	*mean ± std. dev.*	*min*	*max*
$\dot{Q}_{S,loss}$ $[kW]$	0.14 ± 0.02	0	0.2
t_{S1} $[°C]$	43 ± 2	20	50
t_{S2} $[°C]$	40 ± 3	20	50
t_{S3} $[°C]$	39 ± 3	20	50
t_{S4} $[°C]$	29 ± 5	20	49
t_{S5} $[°C]$	29 ± 5	20	49

3.2 Building

This chapter introduces a few aspects concerning the building, as this work mainly focuses on the thermal storage. As already mentioned the building represents a single family home. Buildings with integrated heat pumps are often characterized by high energy efficiency and are equipped with under floor heating systems. Such systems have a good storage capability in comparison to radiators and the return temperature for SH is lower, resulting in a positive aspect for the COP of the heat pump.

Besides the thermal storage, the building represents the second storage and is also directly coupled to the heat pump. The building has two floors. To keep the temperature constant inside the building the heating requirements have to cover the losses through windows, roof, basement and the outside walls reduced by heat gains. The losses depend on the thermal insulation and the ambient temperature. Heat gains arise through solar irradiation, technical equipment, artificial light or high occupancy. For the ambient conditions the weather data of Innsbruck is used.

Table 3-3 shows evaluated quantities of the building based on an annual simulation. These are the room air temperatures in the ground floor $t_{air,GF}$ and the first floor $t_{air,1stFl.}$, the operative room temperatures of the ground floor $t_{op,GF}$ and the first floor $t_{op,1stFl.}$ and the SH demand of the ground floor $\dot{Q}_{SH,GF}$ and the first floor $\dot{Q}_{SH,1stFl.}$. The maximum values of the SH demand in Table 3-3 are outliers and appear for short periods only. The operative room temperatures which are listed in Table 3-3 are an output value of the simulation model of the building implemented in TRNSYS. The operative room temperature is relevant for the thermal comfort. Eq. 3-3 approximates this temperature with the room air temperature t_{air}, the surface temperature t_{surf} of the total wall area and the heat transfer coefficient for the heat convection α_{conv} and the fictitious heat transfer coefficient of the heat radiation α_{rad} (see Rieberer, 2012).

$$t_{op} \cong \frac{\alpha_{conv}\ t_{air}\ + \alpha_{rad}\ t_{surf}}{\alpha_{conv}\ + \alpha_{rad}} \qquad \text{Eq. 3-3}$$

Table 3-3: Characteristic quantities of the building based on an annual simulation

Quantity	*mean* $\pm$ *std. dev.*	*min*	*max*
$t_{air,GF}$ $[°C]$	23 ± 1.3	18	28
$t_{air,1stFl.}$ $[°C]$	22 ± 1.3	18	27
$t_{op,GF}$ $[°C]$	23 ± 1.2	18	28
$t_{op,1stFl.}$ $[°C]$	23 ± 1.2	18	27
$\dot{Q}_{SH,GF}$ $[kW]$	0.43 ± 1.0	0	11
$\dot{Q}_{SH,1stFl.}$ $[kW]$	0.45 ± 1.0	0	11

3.3 Heat pump

This chapter deals with the heat pump. The given information is mainly based on the lecture notes "Heat pump technology" (Rieberer et al., 2009). At first the refrigerant is introduced, then the heat pump is investigated with a focus on the innovative modifications, the variable compressor speed, the economizer and the desuperheater. Finally, the operating limits of the compressor are discussed.

3.3.1 Refrigerant R410A

The heat pump used in this work uses R410A as refrigerant which is an almost azeotropic mixture of 50 % R32 and 50 % R125. R410A replaces mainly R22 because the European Union has decided an early phase out of hydro chlorofluorocarbons (HCFC's). The ODP value of R410A is zero because it does not contain chlorine atoms and the GWP related to CO_2 over 100 years is 1720 according to IPCC II[1]. A further comparison of R410A and R22 shows that R410A has 50 % more refrigeration capacity at higher pressure levels. Therefore R410A cannot be handled with $30\ bar$ technology. The thermodynamic properties at high condensation temperatures lead to worse COP values but this effect can be compensated by higher compressor efficiencies and higher heat transfer coefficients (see Bitzer, 2008).

3.3.2 Investigation of the heat pump cycle

Figure 3-4 is a schematic representation of the heat pump cycle. The most innovative components are the scroll compressor, the economizer and the desuperheater. A scroll compressor is a displacement compressor and is suited perfectly for variable speeds because of the pure rotational movement. Scroll compressors are usually available in fully hermetic designs. Other advantages are the insensitivity against liquid particles in the vapor at the suction side and the possibility to use an economizer cycle. With an economizer a similar behavior to a two stage compression can be achieved. This means that the decrease of the performance as well as the increase of the temperature at the compressor outlet for low evaporation temperatures is less pronounced (see Self et al., 2013). The positive effect on the performance is due to a better adaption to the Carnot cycle. The economizer consists of another expansion valve and an internal heat exchanger with vapor injection into the compressor at a medium pressure level. However, the effect of the economizer is not explicit considered in the modeling process of the heat pump (see chapter 4.1).The desuperheater is a second heat exchanger at the sink. It is used to reach higher temperature levels for DHW preparation. The temperature at the inlet of the desuperheater d_1 is equal to the temperature at the outlet of the condenser w_2 and the water mass flow is divided according to the desired temperature at the desuperheater outlet d_2. The liquid receiver is mainly used to compensate different filling quantities caused by different operating points. The

---

[1] IPCC II (1996) is the basis for the Kyoto protocol

thermostatic expansion valves regulate the refrigerant mass flow through the evaporators for a certain superheating level.

Figure 3-4: Heat pump cycle

Figure 3-5 is a representation of the heat pump cycle in the t-h diagram for a compressor speed of $75\ Hz$ and inlet temperatures of $10\ °C$ of the heat source and $35\ °C$ of the heat sink. The pressure of condensation and evaporation result from the temperatures of the source b_1 and sink w_1. The temperature difference between the two sides of a heat exchanger is dependent on the area of the heat exchanger, the heat transfer coefficient and the capacities at the source and sink. For a heat exchanger with an infinitely large area and an infinitely high thermal capacity of the fluid flows the temperature difference in the condenser and evaporator would be zero. For a finite thermal capacity the slope of the fluid temperature at the source and sink rises and for a finite heat exchanger area the difference at the pinch point rises. The pinch point is characterized by the smallest temperature difference between the cold and hot side of the heat exchanger.

For the heat exchangers two basic control concepts are possible, constant mass flow or constant temperature difference through the heat exchanger. This can be regulated by a pump, if the pump delivers a constant mass flow of heating water the temperature at the outlet of the heat exchanger varies depending on the operating conditions. If the temperature difference of the heat exchanger is kept constant then the mass flow must be varied. In this work the mass flow through the heat exchangers is determined for a constant

temperature difference of $5\ K$ at the sink side (see Eq. 3-4) and $3\ K$ at the source side (see Eq. 3-5). The temperature at the desuperheater outlet t_{d2} is set to $55\ °C$. This temperature is higher than the required minimum temperature for DHW mentioned in chapter 3.1. A reason for this is that the classical control switches off at $50\ °C$, therefore the temperature at the desuperheater outlet must be higher otherwise this temperature cannot be reached. A further reduction of the temperature at the desuperheater outlet seems to be possible if the temperature remains higher than $50\ °C$.

$$t_{w2} - t_{w1} = 5\ K \tag{Eq. 3-4}$$

$$t_{b1} - t_{b2} = 3\ K \tag{Eq. 3-5}$$
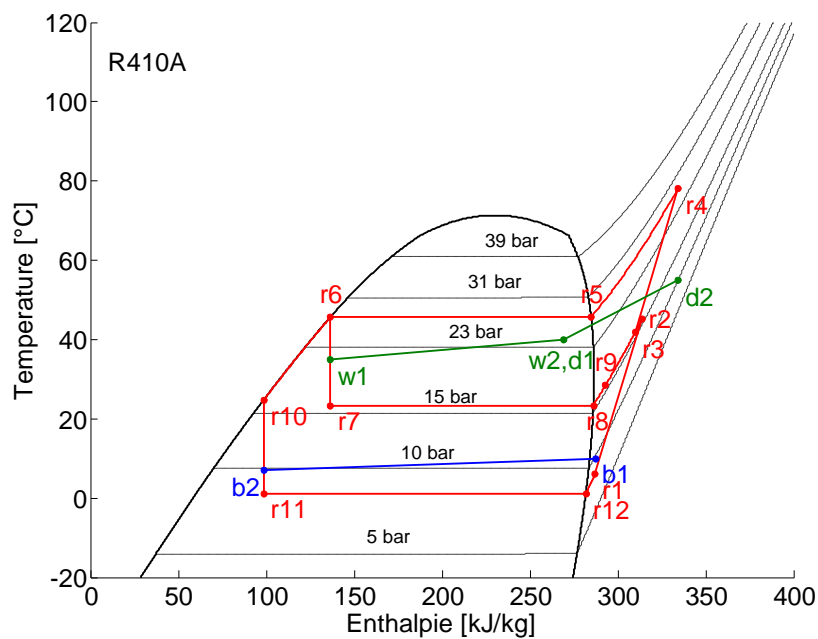
Figure 3-5: t-h diagram of the heat pump cycle

The state changes of the refrigerant cycle are the following:

$r_1 \rightarrow r_2$	Polytropic compression
$r_2 + r_9 \rightarrow r_3$	Adiabatic mixing of r_2 and r_9
$r_3 \rightarrow r_4$	Polytropic compression
$r_4 \rightarrow r_5$	Isobar heat transfer in the desuperheater
$r_5 \rightarrow r_6$	Isobar heat transfer in the condenser
$r_6 \rightarrow r_7$	Isenthalp reexpansion in valve 1
$r_7 \rightarrow r_8 \rightarrow r_9$	Isobar heat transfer with superheating in the economizer (cold side)
$r_6 \rightarrow r_{10}$	Isobar heat transfer in the economizer (hot side)
$r_{10} \rightarrow r_{11}$	Isenthalp reexpansion in the valve 2
$r_{11} \rightarrow r_{12} \rightarrow r_1$	Isobar heat transfer with superheating in the evaporator

3.3.3 Limits of the compressor

The compressor speed is selected to achieve a certain heating output and can be set continuously between the minimum and maximum speed limit as seen in Eq. 3-6.

$$f = 0 \text{ or } 25 \, Hz \leq f \leq 117 \, Hz \qquad \textbf{Eq. 3-6}$$

Figure 3-6 shows the operating envelope of the compressor for R410A in dependence of the condensing and evaporating temperature. These limits have been defined by Emerson Climate Technologies through testing and experience. Operating outside of the envelope might lead to compressor failure (see Copeland, 2013). For a compressor with variable speed, different envelopes have to be considered.
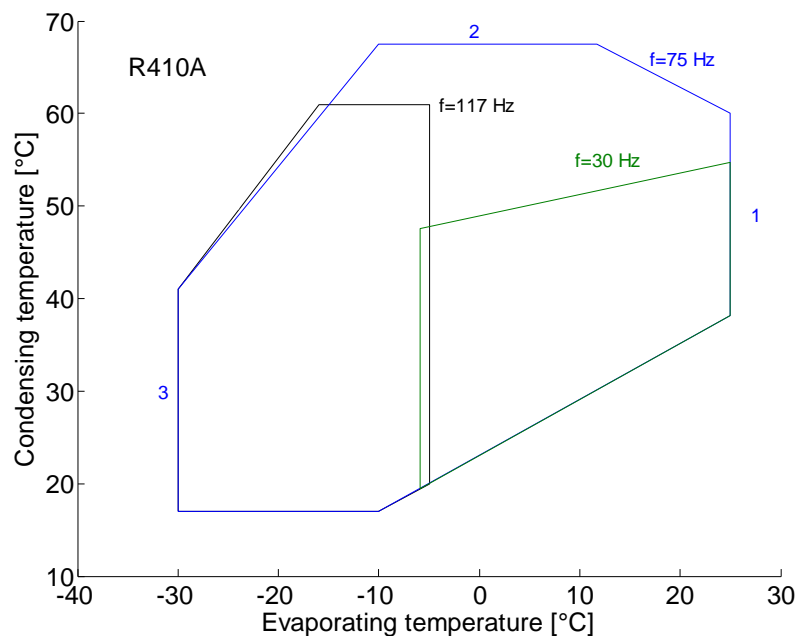
Figure 3-6: Safe operating envelope of the compressor (the numbers are attributed to the limits of the 75 Hz envelope)

According to the training manual "Air Conditioning and Refrigeration" Webasto, 2000 the limits shown in Figure 3-6 for $f = 75 \, Hz$ can be interpreted as follows:

1	Upper limit for the evaporation temperature; above this temperature the motor becomes overloaded because of the high suction gas density. This is because the compressor sucks a constant volume. Therefore, high density leads to higher mass flow which in turn leads to higher drive power.
2	Upper limit for the condensation temperature, above this temperature the high pressure and the temperature at the compressor outlet become too high (oil coking, thermal stress). The temperature limit at the compressor outlet lies between $120 - 140 \, °C$.
3	Lower limit for the evaporation temperature; lower temperatures cause high temperatures at the compressor outlet and small mass flows. Small mass flows are not able to carry the waste heat of the motor.

The heat pump cycle is monitored with measuring devices to stop the motor and avoid damages. Activation leads to disturbances in the heat pump cycle. These disturbances must be avoided by the MPC. To control the temperature of the refrigerant in the condenser the temperature at the top or at the bottom of the thermal storage could be chosen whereby the temperature at the top is strongly coupled with the high pressure and consequently fits better for off control (see Bianchi, 2006). In this work the temperature at the bottom is used as the characteristic diagrams of the heat pump are based on the water temperature at the inlet of the condenser. The details for the evaluation of the evaporation and condensation temperature can be found in chapter 4.1.

Table 3-4 shows evaluated quantities of the heat pump based on an annual simulation. These are the COP, the electric driving power of the compressor P_{el}, the thermal output of the condenser $\dot{Q}_c$, the thermal output of the desuperheater $\dot{Q}_d$ and the thermal input of the evaporator $\dot{Q}_e$. As already mentioned, the COP represents the current ratio of thermal output to electrical power input. The current ratio of thermal output is the sum of the thermal output of the condenser and the thermal output of the desuperheater. For the electrical power input the electric driving power of the compressor is used and the electrical consumption of auxiliary devices is neglected. The COP is calculated with Eq. 3-7. The low minimum value of the COP in Table 3-4 results during the start up of the heat pump.

$$COP = \frac{\dot{Q}_c + \dot{Q}_d}{P_{el}}$$

<div align="right">Eq. 3-7</div>

Table 3-4: Characteristic performance data of the heat pump based on an annual simulation

Quantity	mean ± std. dev.	min	max
$COP\ [-]$	5.4 ± 1	0.9	7.4
$P_{el}\ [kW]$	1.4 ± 0.7	0.4	3.3
$\dot{Q}_c\ [kW]$	6.7 ± 2.4	0.4	12
$\dot{Q}_d\ [kW]$	0.6 ± 0.3	0	1.3
$\dot{Q}_e\ [kW]$	6.3 ± 2	2	10.8

3.4 Photovoltaic array

This chapter introduces the PV array with a general description because the PV array was implemented in TRNSYS as part of this work. Solar modules are available as crystalline (mono, poly), thin film or amorphous types. The behavior of the types differs and has to be taken into consideration by the simulation model. The investigations in this work focus on crystalline modules. Two different types are available in TRNSYS to simulate PV arrays. Both are able to calculate the output of a polycrystalline PV array at different ambient conditions.

Type 194 is the more complex one which can be used to simulate all different cell technologies. It is based on a five parameter model with the drawback that 5 parameters have to be determined in advance by solving a nonlinear system of five equations (see TRNSYS, 2012). In "Improvement and validation of a model for PV array performance" (Beckmann et al., 2006) a method to derive these parameters with EES is described.

Type 94 is used in this work. It is a special case of type 194 whereby one of the five parameters is equal to zero. Type 94 is a four parameter model and has the advantage over type 194 that the evaluation of the four parameters is performed by TRNSYS (see TRNSYS, 2012).

Figure 3-7 shows the electrical circuit of the 4 parameter model following Eckstein (1990). The light current I_L represents the current in dependence of the irradiation. The diode represents the semiconductor junction. The internal dissipative electrical losses are represented by the resistance R_S. The light current is linearly dependent on the total incident irradiation G_T and calculated with known reference conditions ($I_{L,Ref}$, $G_{T,Ref}$) as seen in Eq. 3-8. The diode reverse saturation current I_O is dependent on the cell temperature T_{Cell} and calculated with known reference conditions ($T_{Cell,Ref}$, $I_{O,Ref}$) as seen in Eq. 3-9 (see Eckstein, 1990).

$$I_L = I_{L,Ref} \frac{G_T}{G_{T,Ref}}$$

<div align="right">**Eq. 3-8**</div>

$$I_O = I_{O,Ref} \left(\frac{T_{Cell}}{T_{Cell,Ref}}\right)^3$$

<div align="right">**Eq. 3-9**</div>
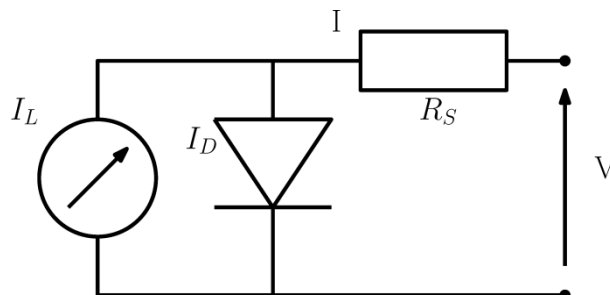
Figure 3-7: Electrical circuit of the 4 parameter model

Applying Kirchhoff's law on the electrical circuit (shown in Figure 3-7) and substituting the diode current I_D by the Shockley equation (Eq. 3-10) leads to a correlation between current and voltage. This can be written in the form of Eq. 3-11. The equation represents the current voltage curve of a single cell and is illustrated in Figure 3-8.

$$I_D = I_O * \left(\exp\left(\frac{q(V + IR_S)}{\gamma k T_{Cell}}\right) - 1\right)$$

<div align="right">**Eq. 3-10**</div>

$$I = I_L - I_O \left(\exp\left(\frac{q}{\gamma k T_{Cell}} (V + IR_S) \right) - 1 \right)$$ **Eq. 3-11**

Eq. 3-11 contains four unknown parameters γ, R_S, I_L and I_O. The dependence of I_L and I_O is shown in Eq. 3-8 and Eq. 3-9 and γ and R_s are constants. To obtain equations for the determination of these parameters different methods can be found in the literature (see Eckstein (1990), Fry (1998), Townsend (1989)). They are all based on measured data provided by the manufacturer. These values are the current and voltage at short circuit, open circuit and at the MPP. These points are illustrated in Figure 3-8 and are used with Eq. 3-11 to obtain three equations. The fourth equation is based on the temperature coefficient of the open circuit voltage (Eq. 3-12). A datasheet with the measured reference values can be found in Appendix A-1.

$$\mu_{V,OC} = \frac{\partial V_{OC,Ref}}{\partial T_{Cell,Ref}}$$ **Eq. 3-12**
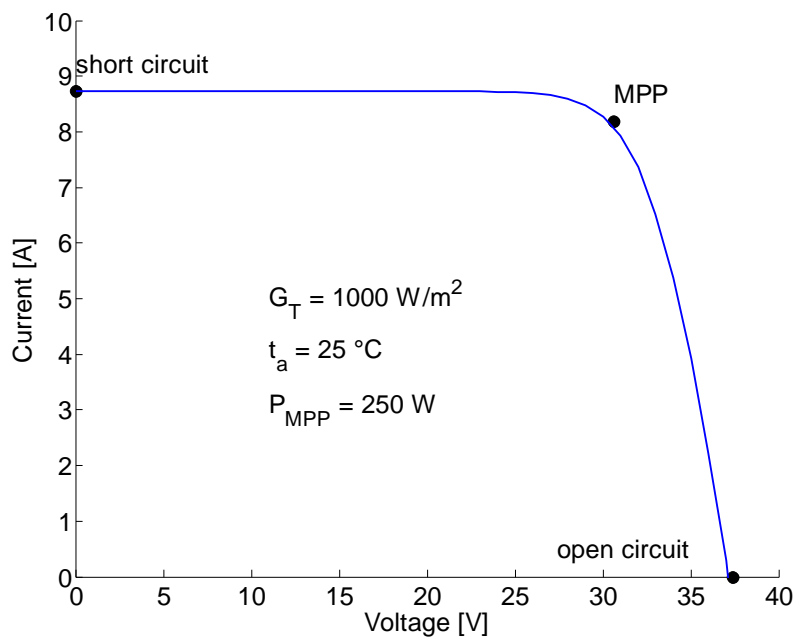
Figure 3-8: IV-curve of a PV module with reference points obtained by a TRNSYS simulation at standard test conditions

It should be mentioned that these equations represent the behavior of one solar module with a maximum power at standard test conditions of $P_N = 250\,W$. The standard test conditions are defined as $G_{T,Ref} = 1000\,W/m^2$ and $t_a = 25\,°C$. These modules are put in series three times and in parallel three times to reach a reasonable power output. The maximum power output of the system at standard test conditions is then $250 \cdot 3 \cdot 3 = 2250\,W$ with an area of $A = 13.14\,m^2$. Modules in series increase the voltage and modules in parallel increase the current.

Table 3-5 shows the evaluated values for the cell temperature t_{Cell} and the PV output P_{PV} based on a annual simulation.

Table 3-5: Characteristic quantities of the PV array based on annual simulation

Quantity	$mean \pm std.dev.$	*min*	*max*
t_{Cell} $[°C]$	12.6 ± 11.5	-13.7	50.9
P_{PV} $[kW]$	0.4 ± 0.6	0	2.6

3.5 External input variables

This chapter presents the external input variables in general. The modeling of the external input variables is shown in chapter 4.3 and the combination of the PV output with the electricity prices is shown in chapter 4.4.2.

3.5.1 Weather data

The weather data is represented by standard weather data and comprises the climate in Innsbruck. It is mainly used in connection with the building and the PV array. As weather data is not freely available and costs should be held at a minimum, possibilities to model an internal weather forecast are shown below.

For an internal temperature forecast of the ambient temperature the temperature curve of the last day $T_{a,(k-24h)}$, with a correction to the actual temperature$(T_{a,0} - T_{a,-24h})$, can be used as seen in Eq. 3-13 (see Wimmer, 2004). This is called *persistent weather prediction*.

$$T_{a,k} = T_{a,(k-24h)} + T_{a,0} - T_{a,-24h} \qquad k = 0 \dots 24\,h \qquad \text{Eq. 3-13}$$

In "Solar irradiation forecast based on numerical weather models" a statistical method called *model output statistics* is investigated. This method improves large scale weather forecast data and makes it fit for the use of local weather forecasts. For this a prediction equation is necessary which has the form of Eq. 3-14 (see Girodo, 2006).

$$Y = a_0 + a_1 X_1 + \dots + a_k X_k \qquad \text{Eq. 3-14}$$

Maybe Eq. 3-14 can be used in addition to persistent weather data to predict the irradiation: Y represents the irradiation and $X_1, \dots, X_k$ are measured values (e.g. ambient temperature, humidity). The parameters $a_0, \dots, a_k$ are constants derived from historical weather data. It has to be mentioned that the combination of persistent weather data and model output statistics is a suggestion and has not been investigated by Girodo (2006).

Table 3-6 shows evaluated quantities of the weather data based on an annual simulation. These are the ambient temperature t_a and the total irradiation on a tilted surface which faces south with an angle of 45° $G_{T,S,45°}$.

Table 3-6: Characteristic quantities of the weather based on an annual simulation

$Quantity$	$mean \pm std.\,dev.$	min	max
$t_A\ [°C]$	9.2 ± 8.7	-13.7	33.8
$G_{T,S,45°}\ [kW/m^2]$	0.2 ± 0.3	0	1.2

3.5.2 Electricity data

The operation of the heat pump based only on PV output cannot be guaranteed. To ensure an economic operation in times of external power requirement, electricity prices have to be considered.

The liberalization of the Austrian electricity market in the year 2001 has set the general framework for the establishment of an electricity exchange named Energy Exchange Austria (EXAA). Historical data can be downloaded online (see http://exaa.de, 01.09.2014). In this work the electricity data of the year 2011 was used.

Table 3-7: Characteristic quantities of the electricity prices based on an annual simulation

$Quantity$	$mean \pm std.\,dev.$	min	max
$Price\ [EUR/MWh]$	51.8 ± 12.7	0	124

3.5.3 DHW load profile

The load profile for the DHW demand is the draw off of the storage. The demand of DHW is mainly dependent on the number of occupants and their habits. Furthermore, the demand of DHW increases simultaneously with higher hygienic standards (see Rieberer, 2012). Table 3-8 shows characteristic values of the load profile.

Table 3-8: Characteristic quantities of the DHW load profile based on an annual simulation

$Quantity$	$mean \pm std.\,dev.$	min	max
$\dot{Q}_{DHW}\ [kW]$	0.2 ± 0.8	0	14.8

4   Models used in the MPC framework

This chapter presents the modeling, starting with the heat pump followed by the thermal storage and the external input variables. To keep the problem clear, some simplifications have been made. The temperature of the heat source is assumed constant $10\,°C$. The heating of the building as well as the division of the heat flows between building and thermal storage will not be investigated in this work, this is why the building will not be considered.

Figure 4-1 shows the MPC application as used in this work. The reference system is implemented in TRNSYS with a sampling interval of $\tau_s = 2\,min$. The MPC-routine is called at each 5th TRNSYS sampling instant to generate a new signal for the compressor frequency. One call successively processes the preparation of external input variables into weights and disturbances over the prediction horizon. Then the optimization problem is solved online under consideration of the measured values y, the last control move and the trajectories for the reference $r = y_{ref}$, disturbances v, weights and constraints. The unmeasured disturbances d which affect the plant have to be compensated by the feedback of the MPC. The optimization determines the required heat flow into the thermal storage based on a linear model which does not consider the convective heat flow of the heating process. Hence a nonlinear model of the thermal storage is used in combination with equations of the heat pump to simulate the convective heat flows. Then the convective heat flow is converted into a disturbance which can be used in the online optimization. The optimization is performed again considering these additional disturbances. This is repeated until a termination criterion is fulfilled. The result of this iterative process is converted into a compressor frequency f and sent to the plant.
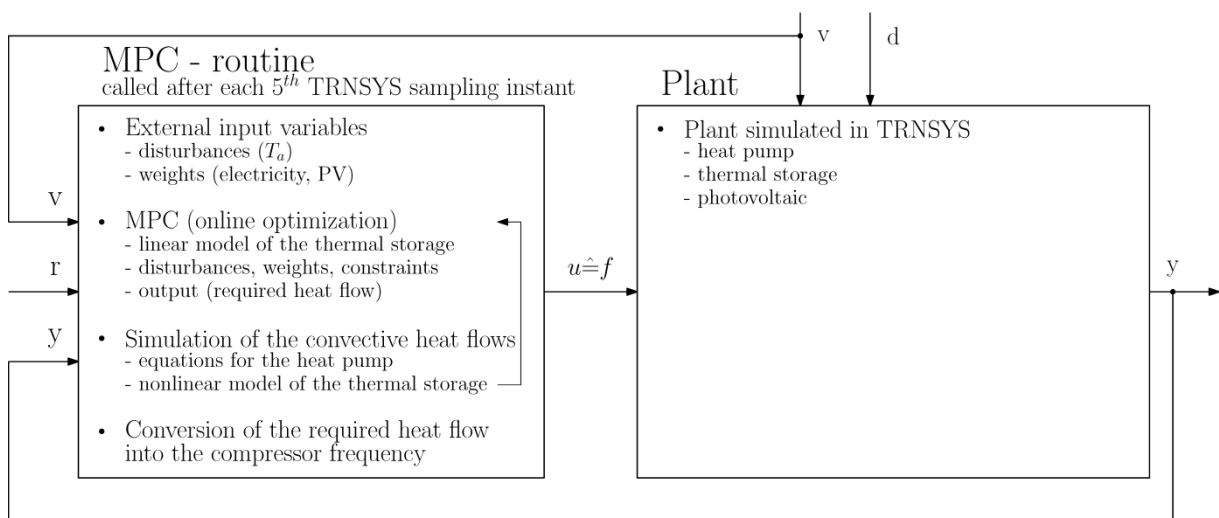
Figure 4-1: MPC-application used in this work

4.1 Heat pump

In this work an indirect optimization is used to avoid a nonlinear optimization problem. This means the optimization determines the required heat flow of the thermal storage instead of the frequency needed for the compressor. The interpretation of the required heat flow into the frequency is made after the optimization. The advantage of this method is that the restrictions to preserve a linear quadratic MPC do not apply for the modeling of the heat pump. A nonlinear model of the dynamical behavior of a heat pump has been found in "Accelerated test method for heat pump systems" (Reiner et al., 1998).

Heat pump specific parameters for a typical heat pump with this size are necessary for the TRNSYS simulation model. These are mainly the isentropic and volumetric efficiency of the compressor, UA values for the condenser, desuperheater and evaporator, the heat exchanger efficiency of the economizer and the heat losses of the compressor to the ambient. These values are based on empirical values which were available at the Institute of Thermal Engineering. With this parameters TRNSYS simulations are performed to obtain a map of required quantities dependent on the condenser water inlet temperature T_{ci} and the frequency of the compressor f. This is why the effect of the economizer is implicitly considered in the model used for the MPC. The required quantities are the heat flow of the condenser and desuperheater, the water mass flow through the condenser and desuperheater, the temperature at the desuperheater outlet, the COP and the temperatures of condensation and evaporation. The map covers the range from $25\,Hz \leq f \leq 115\,Hz$ and $15\,°C \leq T_{ci} \leq 45\,°C$. This range includes operating points outside the envelopes mentioned in chapter 3.3.3. The observance of the operating envelopes is explained in chapter 4.4.3.

The next subchapters will show the derivation of the equations for the heat pump quantities, based on a polynomial approach, for two different modes of the heat pump. In *mode one* the heat pump is only equipped with a condenser and in *mode two* a desuperheater is added. *Mode one* is characterized by two connections to the thermal storage (see chapter 4.2.1) and *mode two* is characterized by three connections to the thermal storage (see chapter 4.2.2). The coefficients for the polynomials are derived from MATLAB with the function "regress". For the verification of the quality of these regression areas the mean value and the standard deviation of the absolute residuals is used. The residuals represent the absolute deviation of the polynomial approximation from the simulated TRNSYS values. Therefore, the residuals have the same unit as the investigated value. The residuals are a return value of the MATLAB function.

4.1.1 Heat flow of the condenser and desuperheater

The left side of Figure 4-2 shows the heat flow through the condenser for *mode one*. The upper curves on the right of Figure 4-2 show the sum of the heat flows through the

condenser and desuperheater (*mode two*). The heat flow is mainly dependent on the compressor frequency. At the bottom of the right diagram the individual heat flow of the condenser and desuperheater for an inlet temperature in the condenser of 35 °C is shown.
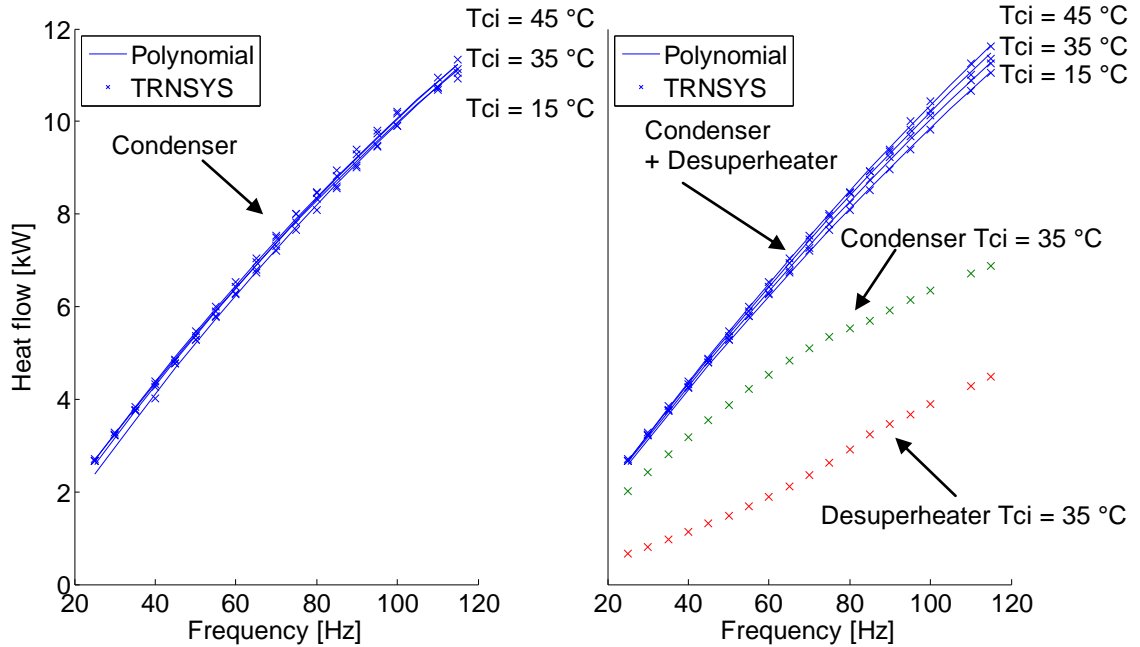
Figure 4-2: Heat flow of condenser (mode one, left) and heat flow of the condenser and desuperheater (mode two, right)

The heat flow is modeled with a quadratic polynomial approach. This is done as higher accuracy is reached as with a linear polynomial. A polynomial of third order does not show a significant improvement. The approximation accuracy for the quadratic polynomial approach is shown in Table 4-1. Eq. 4-1 and Eq. 4-2 are used for *mode one* and *mode two* with different coefficients. Eq. 4-2 is the positive solution for the frequency of the quadratic Eq. 4-1. These equations can be used for both modes as the model used for the MPC determines only the required heat flow $\dot{Q}_{HP}$ into the thermal storage. Based on $\dot{Q}_{HP}$ the compressor speed is calculated with Eq. 4-2. The equation for the heat flow can also be used to determine the heat flow as a function of the frequency and the temperature at the inlet of the condenser (see Eq. 4-1). For *mode one* the heat flow of the desuperheater $\dot{Q}_d$ in Eq. 4-3 is zero. For *mode two* the heat flow of the condenser $\dot{Q}_c$ and desuperheater $\dot{Q}_d$ are added (see Eq. 4-3).

$$\dot{Q}_{HP} = b_1 + b_2 \cdot f + b_3 \cdot T_{ci} + b_4 \cdot f^2 + b_5 \cdot T_{ci}^2 + b_6 \cdot T_{ci} \cdot f \qquad \text{Eq. 4-1}$$

$$f = \frac{\left(-b_2 - b_6 \cdot Tci + \sqrt{(b_2 + b_6 \cdot T_{ci})^2 - 4 \cdot b_4 \cdot \left(b_1 - \dot{Q}_{HP} + b_3 \cdot T_{ci} + b_5 \cdot T_{ci}^2\right)}\right)}{2 \cdot b_4} \qquad \text{Eq. 4-2}$$

$$\dot{Q}_{HP} = \dot{Q}_c + \dot{Q}_d \qquad \text{Eq. 4-3}$$

Table 4-1: Approximation accuracy of the heat flow regression

Quantity	Mode 1	Mode 2
Mean of the absolute residuals $\dot{Q}_{HP}$ [kW]	0.0882	0.0375
Standard deviation of the absolute residuals $\dot{Q}_{HP}$ [kW]	0.0658	0.0361

4.1.2 Mass flow of the condenser and desuperheater

The water mass flow through the heat exchangers is necessary to determine the convective heat flow in the thermal storage. For *mode one* the whole mass flow of the condenser is injected into the thermal storage at the top or middle node according to the hydraulic circuit (see chapter 4.2.1). For *mode two* a part of the condenser mass flow is diverted into the middle node and the other part of the mass flow is further heated in the desuperheater and injected into the top node (see Figure 4-12). Therefore an equation for each mass flow has to be found. The mass flows are regulated to achieve a certain temperature at the outlet. Eq. 4-4 calculates the temperature at the condenser outlet T_{co} which is equal the temperature at the desuperheater inlet T_{di} (see Eq. 4-5) and Eq. 4-6 defines the temperature at the desuperheater outlet T_{do} (see chapter 3.3.2).

$$T_{co} = T_{ci} + 5 \qquad\qquad \text{Eq. 4-4}$$

$$T_{di} = T_{co} \qquad\qquad \text{Eq. 4-5}$$

$$T_{do} = 55\,°C \qquad\qquad \text{Eq. 4-6}$$

The left picture of Figure 4-3 shows the mass flow through the condenser for *mode one*. The mass flow is strongly correlated to the heat flow and increases in accordance with higher compressor frequencies. The right picture of Figure 4-3 shows the individual mass flow of the condenser and desuperheater (*mode two*). The mass flows through the desuperheater for certain condenser inlet temperatures and a frequency of $f = 30\,Hz$ are $\dot{m}_{d,T_{ci}=15} = 14.4\,kg/h$ and $\dot{m}_{d,T_{ci}=35} = 46.5\,kg/h$. The mass flows through the condenser for the same conditions are $\dot{m}_{c,T_{ci}=15} = 415.6\,kg/h$ and $\dot{m}_{c,T_{ci}=35} = 483\,kg/h$. The mass flow of the desuperheater increases with rising inlet temperature in the condenser T_{ci}. This is due to the constant temperature at the desuperheater outlet ($55\,°C$). The inlet temperature of the desuperheater T_{di} increases with rising inlet temperature of the condenser. The mass flow through the condenser changes in opposite directions as the heat output differs slightly for different T_{ci} (see Figure 4-2).

For the mass flow of the condenser a sufficient accuracy is reached with a polynomial of third order (see Eq. 4-7). For the mass flow of the desuperheater a polynomial of third order leads to negative values at low inlet temperatures of the condenser. This would cause problems in the simulation of the nonlinear model. Therefore a polynomial of fourth order is

used (see Eq. 4-8). The approximation accuracy for the regression polynomials is shown in Table 4-2.
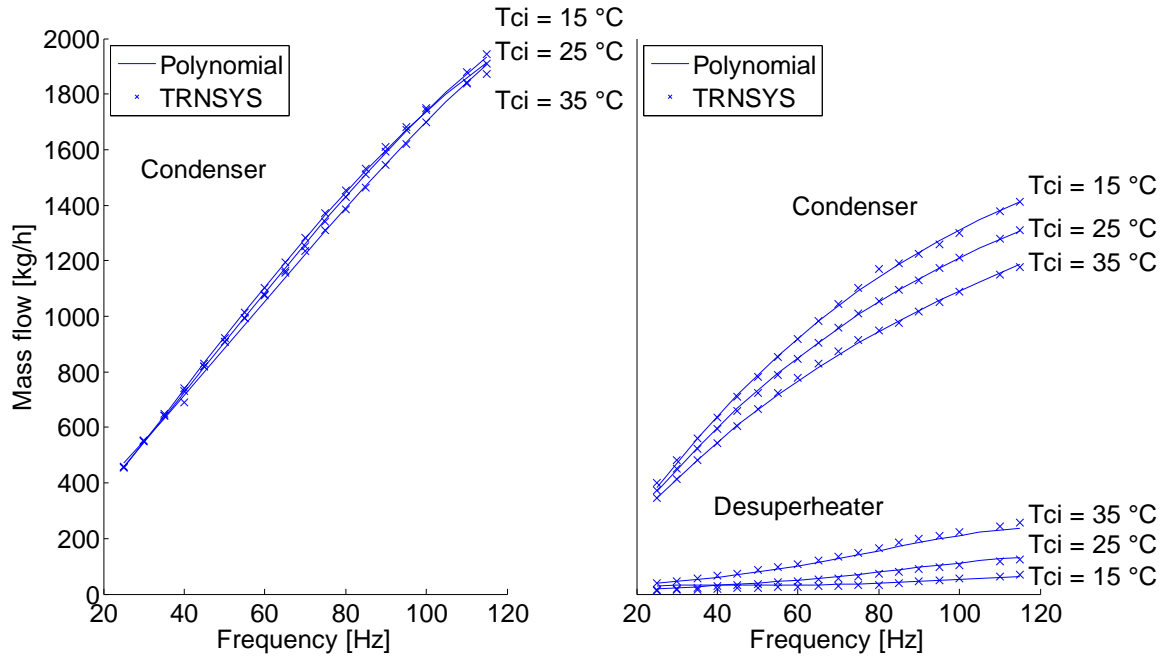
Figure 4-3: Mass flows through the condenser (mode one, left), mass flow through the condenser and desuperheater (mode two, right)

$$g(f, T_{ci}) = b_1 + b_2 \cdot f + b_3 \cdot T_{ci} + b_4 \cdot f^2 + b_5 \cdot T_{ci}^2 + b_6 \cdot T_{ci} \cdot f + b_7 \cdot f^3 + b_8 \cdot T_{ci}^3 \\ + b_9 \cdot f \cdot T_{ci}^2 + b_{10} \cdot f^2 \cdot T_{ci}$$

Eq. 4-7

$$g(f, T_{ci}) = b_1 + b_2 \cdot f + b_3 \cdot T_{ci} + b_4 \cdot f^2 + b_5 \cdot T_{ci}^2 + b_6 \cdot T_{ci} \cdot f + b_7 \cdot f^3 + b_8 \cdot T_{ci}^3 \\ + b_9 \cdot f \cdot T_{ci}^2 + b_{10} \cdot f^2 \cdot T_{ci} + b_{11} \cdot f^4 + b_{12} \cdot T_{ci}^4 + b_{13} \cdot f^2 \cdot T_{ci}^2 + b_{14} \\ \cdot f^3 \cdot T_{ci} + b_{15} \cdot f \cdot T_{ci}^3$$

Eq. 4-8

Table 4-2: Approximation accuracy of the mass flow regression

Quantity	Mode 1	Mode 2
Mean of the absolute residuals $\dot{m}_{Desup}$ $[kg/h]$	-	7.59
Standard deviation of the absolute residuals $\dot{m}_{Desup}$ $[kg/h]$	-	6.45
Mean of the absolute residuals $\dot{m}_{Cond}$ $[kg/h]$	8.41	6.26
Standard deviation of the absolute residuals $\dot{m}_{Cond}$ $[kg/h]$	9.59	6.74

4.1.3 Temperature at the outlet of the desuperheater

The temperature at the outlet of the desuperheater is set to $55\ °C$. For low condenser inlet temperatures and low frequencies the temperature at the compressor outlet is below this temperature. In this case the temperature at the desuperheater outlet has to be reduced to avoid that the mass flow through the desuperheater becomes zero. This has already been

considered in the TRNSYS simulation and means that for the outlet temperature of the desuperheater an equation is also necessary. If the temperature at the outlet of the desuperheater is lower than the temperature in the thermal storage a mixing process leads to a reduction of the temperature in the thermal storage.
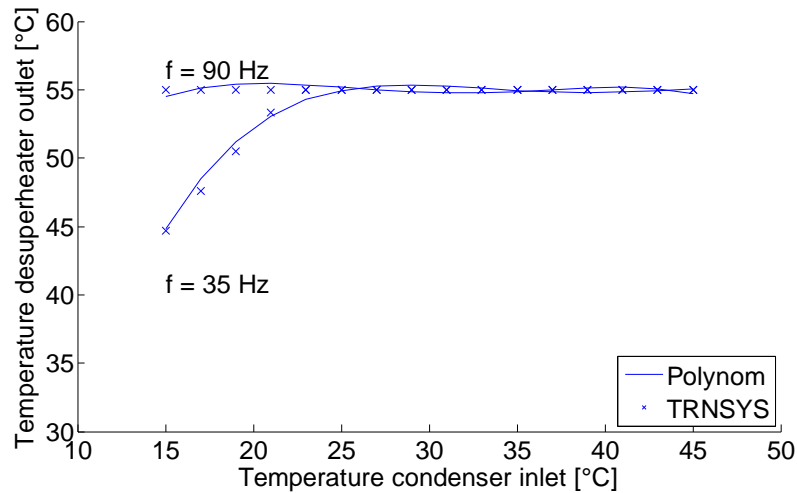
Figure 4-4: Temperature at the desuperheater outlet

To reach the curves shown in Figure 4-4 a polynomial of fourth order is used (see Eq. 4-8). The approximation accuracy of the regression polynomial is shown in Table 4-3.

Table 4-3: Approximation accuracy of the desuperheater outlet temperature regression

Quantity	Value
Mean of the absolute residuals $[K]$	0.27
Standard deviation of the absolute residuals $[K]$	0.28

4.1.4 Condensation and evaporation temperature of the heat pump

Figure 4-5 shows the condensation and evaporation temperatures in dependence of the frequency for different condenser inlet temperatures. The distance between the condensation and evaporation temperature can be interpreted as the pressure ratio π. The pressure ratio is relevant for the compressor power and can be determined with Eq. 4-9.

$$\pi = \frac{p_{cr}}{p_{er}} = \frac{p_{high}}{p_{low}}$$

Eq. 4-9

The evaporation and condensation temperature is determined to guarantee an undisturbed operation of the compressor inside the operating range. The condensation temperatures are dependent on the frequency and on the water temperature at the condenser inlet. The effect of different water temperatures at the condenser inlet on the evaporation temperature is not significant. The evaporation and condensation temperature are modeled

by a polynomial of third order (see Eq. 4-7). The approximation accuracy of the regression polynomials is shown in Table 4-4.
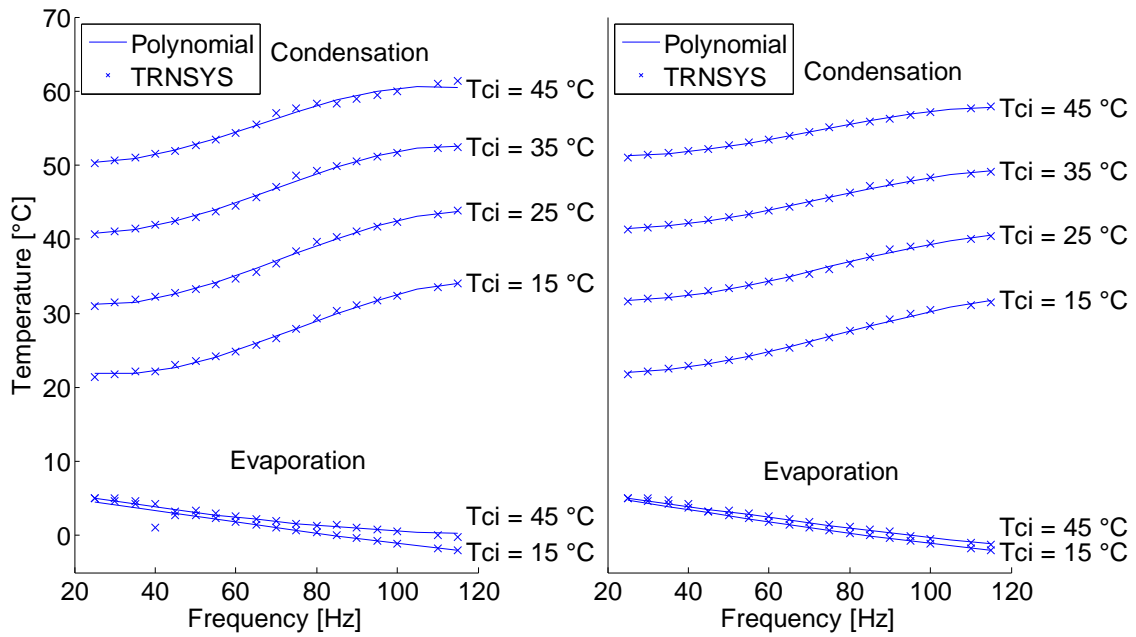
Figure 4-5: Condensation and evaporation temperatures without desuperheater (mode one, left) with desuperheater (mode two, right)

Table 4-4: Approximation accuracy of condensation and evaporation temperature regression

Quantity	Mode 1	Mode 2
Mean of the absolute residuals T_{cr} $[K]$	0.25	0.13
Standard deviation of the absolute residuals T_{cr} $[K]$	0.18	0.09
Mean of the absolute residuals T_{er} $[K]$	0.18	0.14
Standard deviation of the absolute residuals T_{er} $[K]$	0.35	0.31

4.1.5   COP of the heat pump

The COP has to be modeled to optimize the power consumption of the compressor. As mentioned in chapter 3.3 the COP is mainly dependent on the temperatures at the heat source and heat sink. The COP can be written in a general form:

$$COP = \frac{useful\ power}{required\ power}$$

<div align="right">Eq. 4-10</div>

The heat flow through the condenser and desuperheater is the useful power. In this work only the input power to drive the compressor is used for the required power the electricity consumption of auxiliary devices is neglected. The COP increases in accordance with lower condensation temperatures for a constant evaporation temperature until the optimum pressure ratio π is reached. A lower pressure ratio is also reached through lower

frequencies. This is caused by the lower heat output which leads to a lower condensation temperature (and condensation pressure) and a higher evaporation temperature (and evaporation pressure) for a constant inlet temperature of both heat source and heat sink.
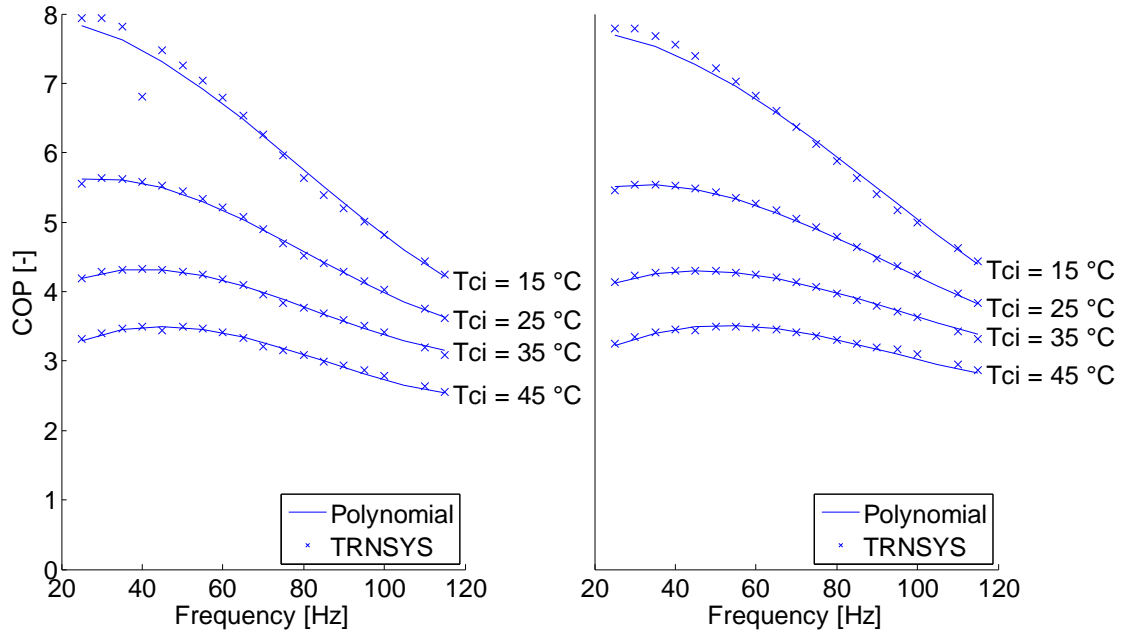
Figure 4-6: COP of the heat pump without desuperheater (mode one, left) with desuperheater (mode two, right)

Figure 4-6 shows the COP for *mode one* (left) and the COP for *mode two* (right). Comparing *mode one* against *mode two* shows slightly higher COP values at lower frequencies for *mode one* and slightly higher COP values at higher frequencies for *mode two*. However, the difference is not significant. The outliner in the curve of the COP for *mode one* is a result of the TRNSYS simulation. The deviation cannot be explained as the maximum number of iterations was not exceeded. The COP is modeled, for both modes, with a polynomial of third order (see Eq. 4-7). The approximation accuracy of the regression polynomials is shown in Table 4-5.

Table 4-5: Approximation accuracy of COP regression

Quantity	Mode 1	Mode 2
Mean of the absolute residuals [$-$]	0.04	0.03
Standard deviation of the absolute residuals [$-$]	0.07	0.06

4.1.6   Start and stop time of the heat pump

The analysis of the heat losses at the start and the heat gains at the stop of the heat pump is shown in Figure 4-7. The start time constant is set to $\tau_{start} = 2\,min$ and the stop time constant is set to $\tau_{stop} = 20\,min$. These values are recommended by the manufacturer of the compressor for all frequencies. For the start time constant similar values ($1 - 2\,min$) are

mentioned in Reiner et al. (1998). Wimmer (2004) also used a similar start time constant ($1\ min$) but a lower stop time constant ($6\ s$). The difference to the stop time constant recommended by the manufacturer cannot be explained.
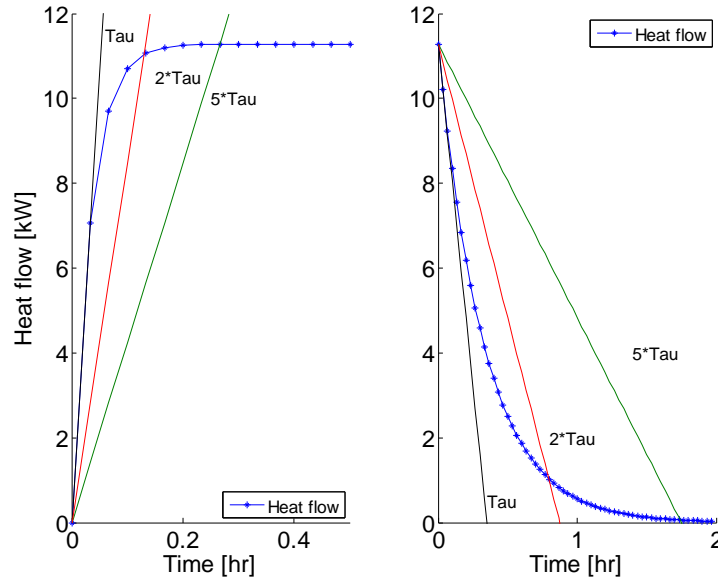
Figure 4-7: Start (left) and stop (right) behavior of the heat pump

The calculation of the starting losses in the TRNSYS model is performed with Eq. 4-11. The factor for the losses $f_{loss,start}$ is reduced at each time step from one to zero (see Eq. 4-12). If the heat pump switches on after a short shut down the start value for the factor of the losses has to be reduced. This is considered with Eq. 4-13 (see Heinz et al., 2014).

$$\dot{Q}_{loss,start,t} = \dot{Q}_{HP}\, f_{loss,start,t}$$

<div style="text-align:right">**Eq. 4-11**</div>

$$f_{loss,start,t} = f_{loss,start,t-\Delta t}\, e^{-\frac{\Delta t}{\tau_{start}}}$$

<div style="text-align:right">**Eq. 4-12**</div>

$$f_{loss,start,t} = 1 - \left(1 - f_{loss,start,t-\Delta t}\right) e^{-\frac{\Delta t}{\tau_{stop}}}$$

<div style="text-align:right">**Eq. 4-13**</div>

The MPC does not consider these losses/gains. These effects must be compensated by the feedback to the MPC. According to Martin Pichler is a consideration of these effects possible if the thermal state of the heat pump is simulated similar to the simulation of the convective heat flows in the thermal storage. In this work the start time constant is used to estimate the constraint on the manipulated variable rate (see chapter 4.4.3).

4.2 Thermal storage

This chapter deals with the modeling process of the thermal storage. Figure 3-1 shows that the thermal storage is connected to the heat pump with the condenser and desuperheater. The water mass flow of the condenser is taken from the bottom of the storage. At the outlet

of the condenser the mass flow is separated. The bigger part of the mass flow is diverted into the middle node. The smaller part is further heated in the desuperheater and inserted into the top node. The thermal storage is also connected to the DHW with an external heat exchanger. These connections cause forced convective heat flows inside the thermal storage. A mixing process caused by natural convection occurs if the inlet temperature into one node is higher than the temperature above this node or vice versa. Conductive heat flows occur if the temperature inside the thermal storage is stratified. The thermal storage is furthermore in heat exchange with the ambient.

Two models of the thermal storage are used in the MPC-routine (see Figure 4-1). The linear model is used to determine the optimal control action with the MPC, in this case the total required heat flow into the thermal storage. The nonlinear model is used to simulate the convective heat flows. In the following investigations DHW draw offs are omitted as they are not considered in the model used for the MPC. The prediction of the DHW draw off is discussed in chapter 4.3.1

Nonlinear models are derived for three different hydraulic circuits of a thermal storage with five nodes. The first hydraulic circuit (HC1) investigates the thermal storage connected to the condenser of the heat pump with the top and bottom node (see Figure 4-8). In the second circuit (HC2) the condenser is connected to the middle and bottom node (see Figure 4-10). For the third hydraulic circuit (HC3) the condenser is connected to the middle and bottom node and the desuperheater is connected to the top node (see Figure 4-12). The third hydraulic circuit represents the reference system (see Figure 3-1). For the first and second hydraulic circuit the equations derived for *mode one* are used and for the third hydraulic circuit the equations derived for *mode two* are used (see chapter 4.1).

Then a linear model suitable for the optimization algorithm is presented. This model can be used in combination with all three hydraulic circuits. However, this model is adapted for two different controlled variables. Firstly, the linear model which is able to control the temperature of the top node is presented. Then this model is adapted to control the temperature of the middle node.

Finally, the iterative approach to model the nonlinear processes within a linear MPC is presented. No information was found in the literature on this iterative approach[2].

4.2.1   Nonlinear model of the thermal storage (HC1 & HC2)

a) Nonlinear model for the hydraulic circuit HC1:

Figure 4-8 shows a schematic representation of the heat flows of the thermal storage connected to the condenser with the top and bottom node. The forced convective heat

---

[2] The iterative approach was found by Martin Pichler.

flows are caused by the heating through the condenser. Between the nodes an exchange of heat caused by thermal conduction occurs and each node has heat losses to the ambient.
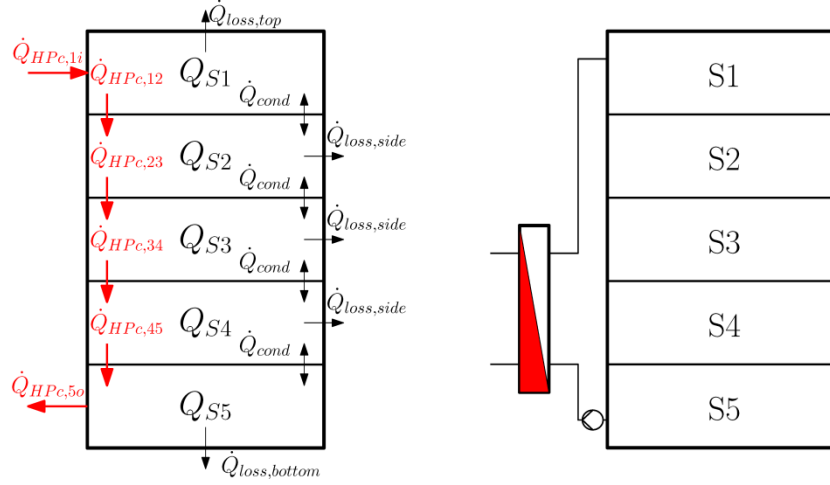
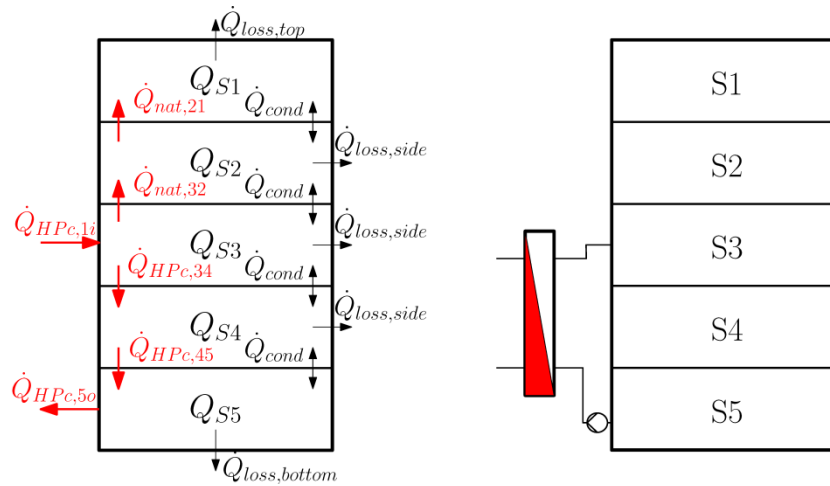**Figure 4-8: Heat flows of the thermal storage connected to the condenser at the top and bottom node (HC1)**

The energy balance for a node can be written as follows:

$$\frac{\partial Q_{Sj}}{\partial \tau} = \dot{Q}_{conv,j+1} + \dot{Q}_{conv,j-1} + \dot{Q}_{cond,j+1} + \dot{Q}_{cond,j-1} - \dot{Q}_{loss,j}$$

Eq. 4-14

The term on the left side of Eq. 4-14 represents the heat change at node j and the terms at the right side represent the heat flows across the border of node j. With Eq. 2-12 derived in chapter 2.3 and an explicit discretization the energy balance for a node can be written as Eq. 4-15. The UA_j value in Eq. 4-15 refers to the cylindrical surface of node j. Discretization schemes can be found in Sanz (2012). The whole system of equations can be found in Appendix A-2.

$$T_{Sj}^{N+1} = T_{Sj}^{N} - \frac{u_{vel,j}\,\Delta\tau}{\Delta x}\left(T_{Sj}^{N} - T_{Sj-1}^{N}\right) - \frac{a\,\Delta\tau}{\Delta x^2}\left(T_{Sj+1}^{N} - 2T_{Sj}^{N} + T_{Sj-1}^{N}\right)$$
$$- \frac{UA_j\Delta\tau}{m_j\,c}\left(T_{Sj} - T_a\right)$$

Eq. 4-15

For the conduction term a Neumann boundary condition with ghost cells (see Sanz, 2012) is applied (see Eq. 4-16 - Eq. 4-17). The UA values and the areas A_1 and A_5 in Eq. 4-17 refer to the circular area at the top and the bottom.

$$T_{S0} = T_{S1} - \frac{\Delta x\,UA_{top}}{\lambda\,A_1}\left(T_{S1} - T_a\right)$$

Eq. 4-16

$$T_{S6} = T_{S5} - \frac{\Delta x\,UA_{bottom}}{\lambda\,A_5}\left(T_{S5} - T_a\right)$$

Eq. 4-17

For the forced convection term the velocity is calculated with Eq. 4-18 based on the mass flow determined in chapter 4.1.2. The inlet temperature into node one is the temperature at

the condenser outlet T_{co} (see Figure 4-8). This temperature is calculated according to the temperature difference of the condenser (see Eq. 4-4).

$$u_{vel,j} = \frac{\dot{m}_{cond}}{\rho \, A_j}$$

Figure 4-9 compares the curves of the node temperatures of the thermal storage for the hydraulic circuit HC1 obtained by a TRNSYS simulation with the results obtained by a MATLAB simulation based on the nonlinear model of the thermal storage. The charging process is performed with two constant compressor frequencies ($f = 40\,Hz$ and $f = 90\,Hz$). The MATLAB model determines the mass flow for the forced convection in the thermal storage with the equation for *mode one* derived in chapter 4.1.2. The charging process starts from a uniform temperature distribution of $30\,°C$. Loads are not considered in this simulation. The upper curve shows the temperature of the top node and the lower curve shows the temperature of the bottom node. The curves of the TRNSYS model and MATLAB model match quite accurately. The TRNSYS model shows the stages during the charging process as already mentioned in chapter 3.1. The MATLAB model uses a time step of $\Delta\tau = 2\,min$. The MATLAB model may match the curves of the TRNSYS model with an adapted time step.
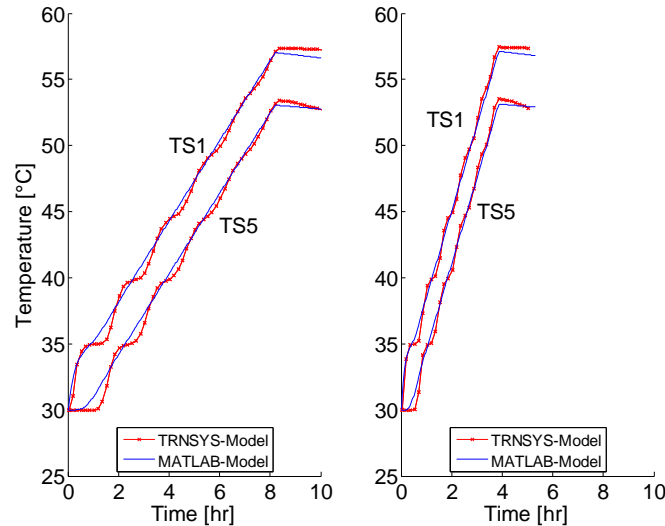
Figure 4-9: Comparison of simulated charging processes of the thermal storage with the condenser for hydraulic circuit HC1 with a compressor frequency of 40 Hz (left) and 90 Hz (right)

b) Nonlinear model for the hydraulic circuit HC2:

Figure 4-10 shows a schematic representation of the heat flows of the thermal storage connected to the condenser with the middle and bottom node. Forced convective heat flows due to the heating with the condenser affect nodes three, four and five. Node one and two are heated due to natural convection. Furthermore, between the nodes an exchange of heat caused by thermal conduction occurs and each node has heat losses to the ambient.

Figure 4-10: Heat flows of the thermal storage connected to condenser at the middle and bottom node (HC2)

The system of equations for this hydraulic circuit is similar to the equations for hydraulic circuit HC1 and can also be found in Appendix A-3. The term with the forced convection has to be removed from the first and second node and the temperature of the condenser outlet is the temperature of the mass flow injected into node three. Furthermore, the equations of the heat pump for *mode one* can also be applied on this hydraulic circuit.

A challenge in this hydraulic circuit is the consideration of the heat flows due to natural convection. Natural convection is a complex phenomenon. It is generated if the temperature at the bottom is higher than the temperature above. This results in a heat flow driven by density differences. A simplified model to handle the effect of natural convection by mixing is specified in Pichler et al. (2014). The natural convection is modeled by setting the according bordering nodes with Eq. 4-19 to their average value (see Pichler et al., 2014). This has to be done after each time step in the simulation. Eq. 4-19 is applied to each pair of nodes where the temperature of the node below is higher than the temperature of the node above. This has to be repeated until for each pair of nodes the temperature of the node below is lower or equal the temperature of the node above.

$$T_{Sj+1} = T_{Sj} = \frac{T_{Sj+1} + T_{Sj}}{2}$$

<div align="right">**Eq. 4-19**</div>

Figure 4-11 compares the curves of the node temperatures of the thermal storage for the hydraulic circuit HC2 obtained by a TRNSYS simulation with the results obtained by a MATLAB simulation based on the nonlinear model. The two constant frequencies, the initial temperature distribution and the consideration of the loads are equal to the simulation shown in Figure 4-9 for hydraulic circuit HC1. Figure 4-11 shows the temperature curves for all nodes of the thermal storage. The temperatures of node one, two and three are equal through the mixing process caused by natural convection. The temperature difference

between node three, four and five is due to the stratified charging process. The curves of the TRNSYS model and MATLAB model match quite accurately.
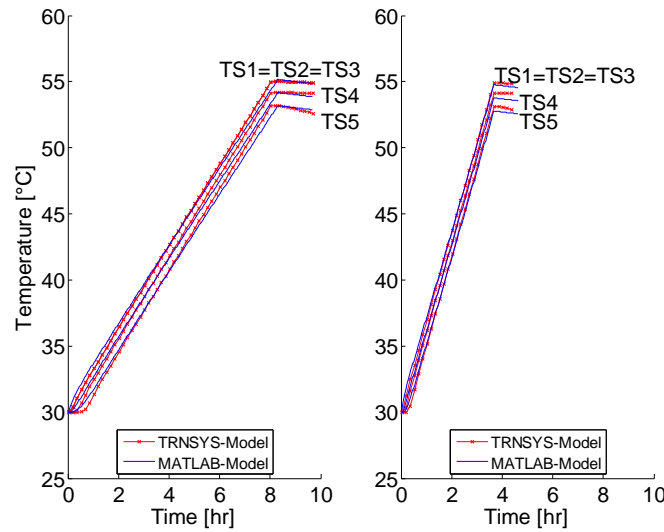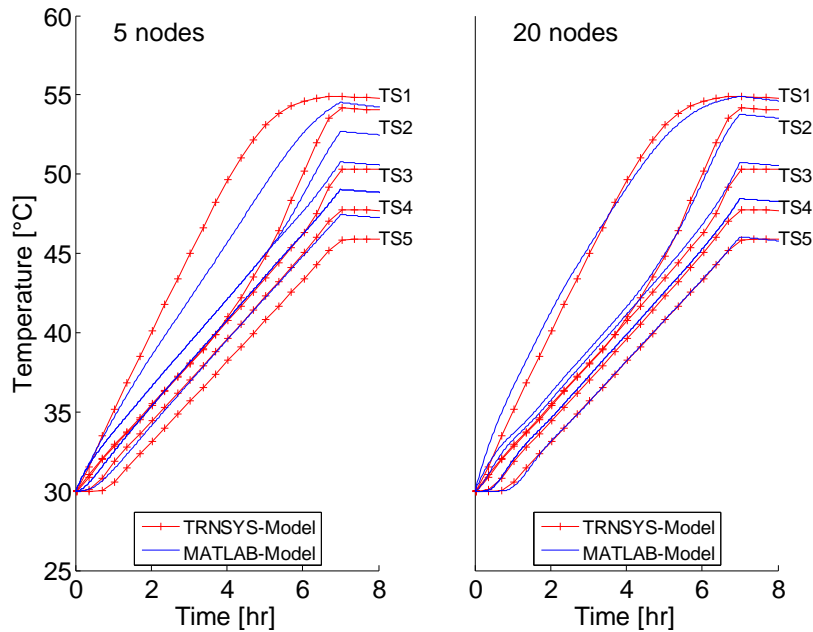

Figure 4-11: Comparison of simulated charging processes of the thermal storage with the condenser for hydraulic circuit HC2 with a compressor frequency of 40 Hz (left) and 90 Hz (right)
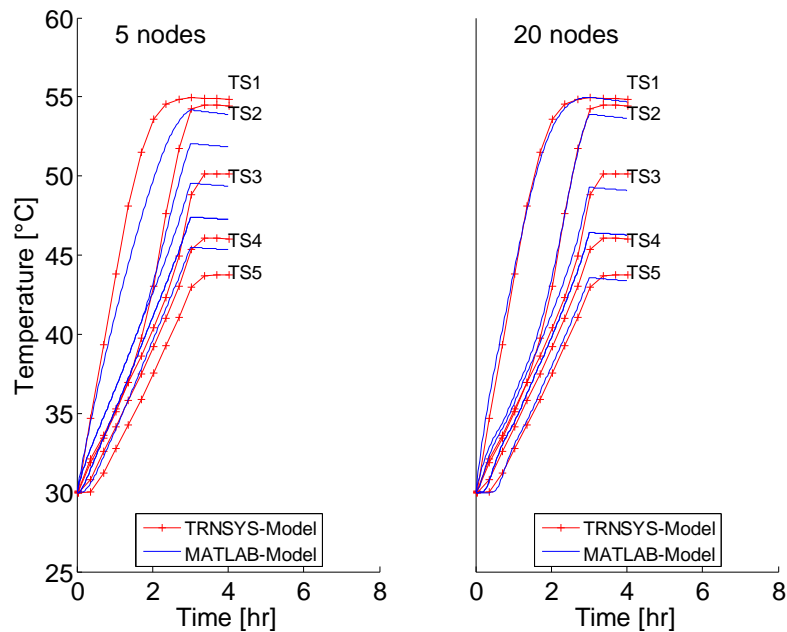
4.2.2 Nonlinear model of the thermal storage including desuperheater (HC3)

The hydraulic circuit HC2 will here be augmented by the desuperheater to hydraulic circuit HC3 (see Figure 4-12). The desuperheater is connected to the top node and the condenser is connected to the middle and bottom node.
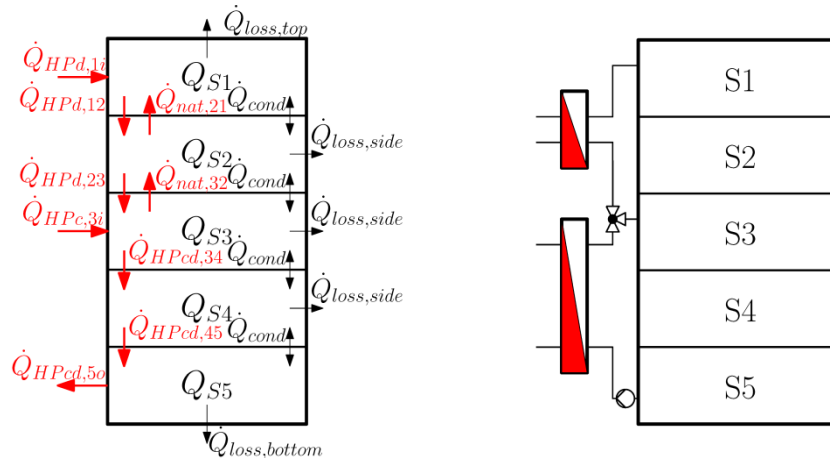
Figure 4-12: Heat flows of the thermal storage connected to condenser and desuperheater (HC3)

Some challenges occur when the desuperheater is included into the model. Heating from a uniform temperature distribution leads to a mixing process caused by natural convection in the thermal storage between condenser inlet and desuperheater inlet. The water temperature at the desuperheater outlet T_{do} (see Eq. 4-6) is the temperature of the desuperheater mass flow $\dot{m}_d$ injected into node one and the temperature at the condenser outlet T_{co} (see Eq. 4-4) is the temperature of the condenser mass flow $\dot{m}_c$ injected into node

46

three. The mass flows of the forced convection are calculated with the equations for *mode two* presented in chapter 4.1.2. The velocities for the first and second node are calculated with Eq. 4-20 and the velocities for the fourth and fifth node are calculated with Eq. 4-21. The term for the forced convection of the third node is written as Eq. 4-22. The whole system of equations can be found in the Appendix A-4.

$$u_{vel,d} = \frac{\dot{m}_d}{\rho\,A_j}$$ <div style="text-align:right">**Eq. 4-20**</div>

$$u_{vel,c} = \frac{\dot{m}_c}{\rho\,A_j}$$ <div style="text-align:right">**Eq. 4-21**</div>

$$\dot{Q}_{conv,3} = -\frac{u_{vel,d}\,\Delta\tau}{\Delta x}(T_{S3}^N - T_{S2}^N) - \frac{(u_{vel,c} - u_{vel,d})\,\Delta\tau}{\Delta x}(T_{S3}^N - T_{co})$$ <div style="text-align:right">**Eq. 4-22**</div>

Figure 4-13 compares the curves of the node temperatures of the thermal storage obtained by a TRNSYS simulation with the results obtained by a MATLAB simulation based on the nonlinear model. The initial temperature distribution and the consideration of the loads are equal to the simulation for hydraulic circuit HC1 and HC2. Figure 4-13 shows the simulation results for a compressor frequency of $f = 40\,Hz$. On the left the result of the MATLAB simulation is based on the five node model. The differences between the curves are significantly higher than in the simulations for the hydraulic circuits HC1 and HC2. A reason for this is that the model implemented in TRNSYS uses a discretization of 80 nodes. The temperature curves shown in these figures represent spatially averaged values. The difference between the curves may be reduced by increasing the number of nodes in the MATLAB model (see Figure 4-13 on the right). Figure 4-14 shows these simulations for a compressor frequency of $f = 90\,Hz$.

Figure 4-13 and Figure 4-14 show that the temperature curve of the top node increases through the injection of the desuperheater mass flow till the temperature of $55\,°C$ is reached. The temperature of the second node increases simultaneously with the temperature of the third node at the beginning of the heating process. This is due to the mixing process caused by natural convection. At the end of the heating process the temperature of the second node rises higher than the temperature of node three. This is due to the forced convective heat flow of the top node caused by the mass flow of the desuperheater. This effect also acts on the third node. The temperature curves of the fourth and fifth node are influenced by the forced convective heat flow caused by the mass flow through the condenser and desuperheater.

Despite the differences between the temperature curves obtained by TRNSYS simulations and the temperature curves obtained by MATLAB simulations the five node model of the thermal storage is used. The reasons for this are that a charging of the thermal storage over

such a large temperature difference is rarely during the operation and the slope at the beginning of the charging process fits reasonably. However, the temperature at the bottom is important because this temperature is used to determine the quantities of the heat pump. The inaccuracies of this model have to be compensated by the feedback of the controller.

Figure 4-13: Comparison of simulated charging processes of the thermal storage with the desuperheater for hydraulic circuit HC3 with a compressor frequency of 40 Hz

Figure 4-14: Comparison of simulated charging processes of the thermal storage with the desuperheater for hydraulic circuit HC3 with a compressor frequency 90 Hz

A reason why the nonlinear models (chapters 4.2.1 and 4.2.2) cannot be used in the optimization algorithm is that if the mass flow is chosen as manipulated variable the convective term would lead to a variable input matrix B. Eq. 4-23 shows this written in the form of a state space model. The input matrix depends on the state variables, in this case the storage temperatures. A linearization is not possible as the behavior of the system between on and off of the heat pump is too different. For this case a hybrid MPC may be used (see chapter 2.4.4).

$$\dot{x} = A \cdot x + B(x) \cdot u$$

If the velocities due to the mass flows are known, the models derived in the chapters 4.2.1 and 4.2.2 can be used for a simulation of the storage temperatures over the prediction horizon.

4.2.3 Linear model of the thermal storage for MPC purpose

The linear model of the thermal storage is used in the optimization algorithm to determine the optimal future control actions. This model is the same as in Pichler (2014). However, the MPC-routine in this work requires the consideration of additional disturbances resulting from forced convection (during the charging process) in response to the manipulated variable. Firstly, the linear model is presented for the temperature at the top node as controlled variable and secondly, the linear model is adapted for the temperature at the middle node as controlled variable.

a) Linear model of the thermal storage for the temperature at the top node as controlled variable

Figure 4-15 shows a schematic representation of the heat flows considered in the linear model if the temperature at the top node is the controlled variable. In this model the required heat flow is injected into the top node. The thermal storage in Figure 4-15 on the right illustrates this due an electrical heater at the top node.
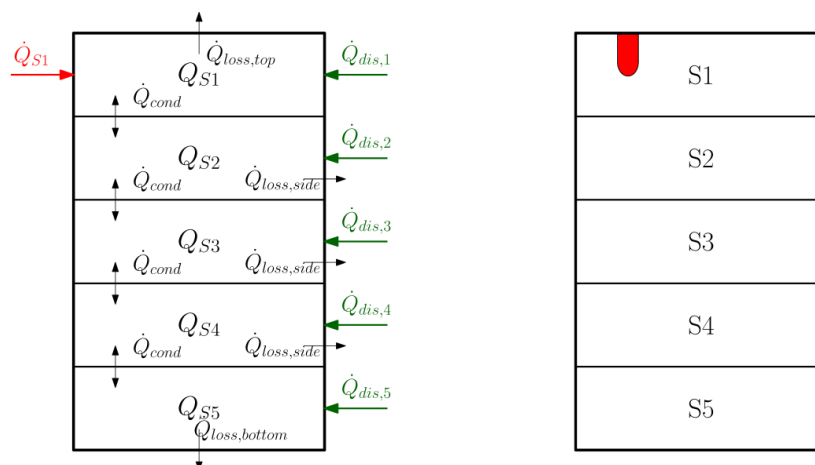
Figure 4-15: Heat flows of the linear model with the temperature at the first node as controlled variable

The energy balance for a node leads to Eq. 4-24.

$$\frac{dT_j}{d\tau} = \frac{1}{m_j c}(\dot{Q}_{cond,j+1} + \dot{Q}_{cond,j-1} + \dot{Q}_{loss,j} + \dot{Q}_{aux,S1} + \dot{Q}_{dis,j})$$

<div align="right">Eq. 4-24</div>

Heat conduction $\dot{Q}_{cond}$ is considered between neighboring nodes with Eq. 4-25 and Eq. 4-26.

$$\dot{Q}_{cond,j+1} = UA_{j+1}(T_{Sj+1} - T_{Sj})$$

<div align="right">Eq. 4-25</div>

$$\dot{Q}_{cond,j-1} = UA_{j-1}(T_{Sj-1} - T_{Sj})$$

<div align="right">Eq. 4-26</div>

The losses to the ambient $\dot{Q}_{loss}$ are modeled by Eq. 4-27.

$$\dot{Q}_{loss,j} = UA_{loss,j}(T_a - T_{Sj})$$

<div align="right">Eq. 4-27</div>

The energy balance Eq. 4-24 applied on all nodes can also be written in the form of a state space model (see Eq. 4-28). Eq. 4-29 shows the dimension of the matrices and vectors of the state space model. The matrices can be found in Appendix A-5. The state variables x are the temperatures of the nodes T_{Sj} (see Eq. 4-30). The control action u is the heat flow into the top node $\dot{Q}_{S1}$ (see Eq. 4-31). The measured disturbances v are represented by convective disturbances $\dot{Q}_{dis,j}$ and the ambient temperature T_a (see Eq. 4-32). The mixing process caused by natural convection has to be considered in the calculation of the disturbances as the linear model is not able to handle this effect. The calculation of $\dot{Q}_{dis,j}$ is shown in chapter 4.2.4.

$$\dot{x} = A \cdot x + B_u \cdot u + B_v \cdot v$$

<div align="right">Eq. 4-28</div>

$$\begin{bmatrix} 5 \times 1 \end{bmatrix} = \begin{bmatrix} 5 \times 5 \end{bmatrix} \cdot \begin{bmatrix} 5 \times 1 \end{bmatrix} + \begin{bmatrix} 5 \times 5 \end{bmatrix} \cdot \begin{bmatrix} 5 \times 1 \end{bmatrix} + \begin{bmatrix} 5 \times 6 \end{bmatrix} \cdot \begin{bmatrix} 6 \times 1 \end{bmatrix}$$

<div align="right">Eq. 4-29</div>

$$x = [T_{S1}, T_{S2}, T_{S3}, T_{S4}, T_{S5}]^T$$

<div align="right">Eq. 4-30</div>

$$u = [\dot{Q}_{S1}, 0, 0, 0, 0]^T$$

<div align="right">Eq. 4-31</div>

$$v = [\dot{Q}_{dis,1}, \dot{Q}_{dis,2}, \dot{Q}_{dis,3}, \dot{Q}_{dis,4}, \dot{Q}_{dis,5}, T_a]^T$$

<div align="right">Eq. 4-32</div>

b) Linear model of the thermal storage for the temperature at the middle node as controlled variable

Figure 4-16 shows the schematic representation of the heat flows considered in the linear model if the temperature in the middle node is the controlled variable. The difference to the model shown in Figure 4-15 is that the manipulated variable which is the required heat flow is now inserted into the middle node. This is a restriction of the iterative MPC-routine due to

the convective heating process. This means that a controlled variable T_j and a manipulated variable $\dot{Q}_{Sj}$ have to concern the same node. The reason for this is the weak coupling of the nodes in the linear model only due to heat conduction. For instance, if the controlled variable is the temperature at the middle node the MPC determines a heat flow under the assumption that this heat flow is transported by conduction to the middle node. Although in the nonlinear model the heat is transported by forced convection. This may cause the situation that the MPC determines a heat flow which is too high and this is irreversible. Therefore, Eq. 4-33 represents the vector of the manipulated variable for the temperature at the top node as controlled variable.
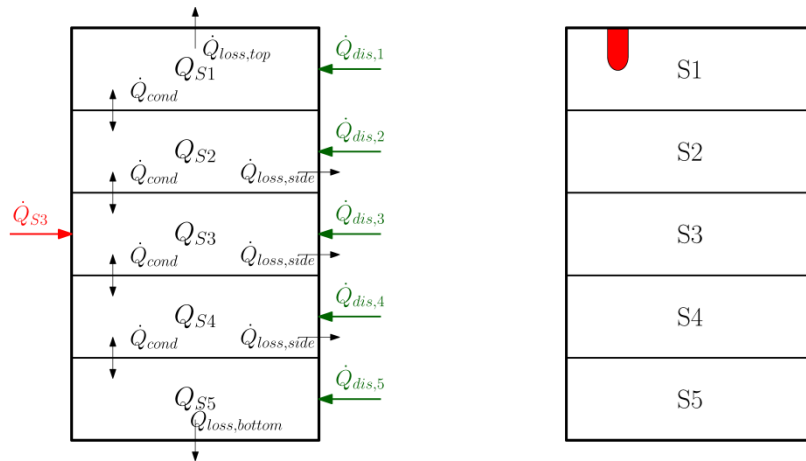
Figure 4-16: Heat flows of the linear model with the temperature at the middle node as controlled variable

$$\boldsymbol{u} = \begin{bmatrix} 0,0,\dot{Q}_{S3},0,0 \end{bmatrix}^T \qquad \text{Eq. 4-33}$$

4.2.4 Conversion of the heat flows into disturbances

The linear model is not able to consider heat flows caused by natural and forced convection. Therefore the convective heat flows have to be converted into disturbances suitable for the linear model. Forced and natural convection is caused by the heating process. Therefore, the required heat flow of the thermal storage determined by the MPC must be known to determine the effect of natural and forced convection. This leads to an iterative process.

This iterative process is independent from the controlled variable in the linear model. This is due to the restriction mentioned in chapter 4.2.3. The iterative process is also similar for the three hydraulic circuits. Therefore, the iterations are explained for a three node model of the thermal storage connected to the condenser with the hydraulic circuit HC1. This is shown in Figure 4-17.

For the further investigations the denomination has to be explained. The subscript j represents the number of the node in the thermal storage. The subscript $k + i|k$ is interpreted as follows. The subscript k on the right of the bar specifies the call of the MPC at

time step k. The subscript i is referred to the prediction horizon p and varies within the range of $0 - (p-1)$. This means that a variable with a subscript $k+i|k$ has to be calculated at each call of the MPC over the prediction horizon. The superscript l specifies the number of the iteration of the iterative process and the superscript L specifies the number of the last iteration.

1st Iteration
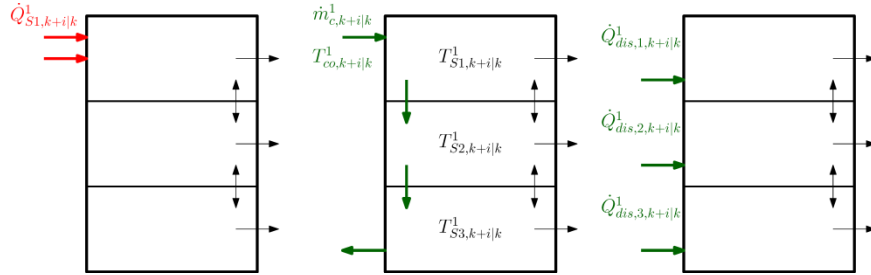
2nd Iteration
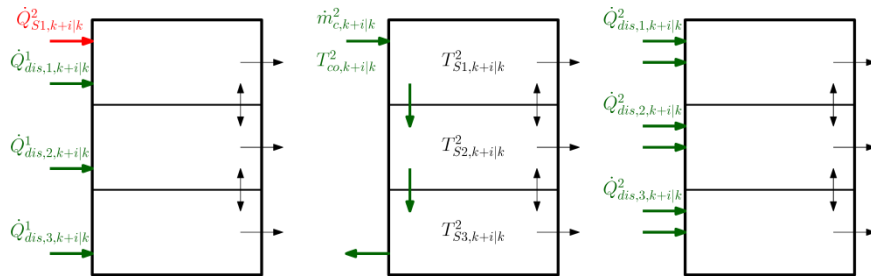
Lth Iteration
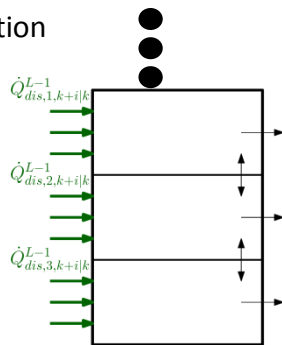
Figure 4-17: Conversion of the convective heat flows into disturbances with heat flux due to conduction shown with black arrows and heat flows due to convection in green

In the first step the MPC is called upon to determine the required heat flows $\dot{Q}^1_{S1,k+i|k}$ (see Figure 4-17, 1st Iteration on the left). These heat flows are a trajectory within the prediction horizon and are used to calculate the mass flows $\dot{m}^1_{j,k+i|k}$ through the nodes of the thermal storage over the prediction horizon. These mass flows are used with the trajectory of the condenser outlet temperatures $T^1_{co,k+i|k}$ in the nonlinear model to obtain the node temperatures $T^1_{Sj,k+i|k}$ of the thermal storage over the prediction horizon (see Figure 4-17, 1st Iteration in the middle). The calculation of the disturbances $\dot{Q}^1_{dis,j,k+i|k}$ with Eq. 4-34 - Eq. 4-37 completes this iteration (see Figure 4-17, 1st Iteration on the right).

In the second iteration the MPC determines the required heat flows $\dot{Q}^2_{S1,k+i|k}$ under consideration of the disturbances calculated in the previous iteration $\dot{Q}^1_{S1,k+i|k}$ (see Figure 4-17 (2nd Iteration on the left)). The mass flows $\dot{m}^2_{j,k+i|k}$ of the second iteration are calculated based on the sum of the heat flows determined in this iteration $\dot{Q}^2_{S1,k+i|k}$ and the heat flows determined in the previous iteration $\dot{Q}^1_{S1,k+i|k}$. The mass flows $\dot{m}^2_{j,k+i|k}$ are used with the condenser outlet temperatures $T^2_{co,k+i|k}$ in the nonlinear model to obtain the node temperatures $T^2_{Sj,k+i|k}$. After the nonlinear simulation the disturbances of the second iteration $\dot{Q}^2_{dis,j,k+i|k}$ are obtained with Eq. 4-34 - Eq. 4-37.

This can be repeated until the MPC determines no additional heat flow for the thermal storage $\left(\dot{Q}^l_{S1,k+i|k} = 0\right)$ as the objective of the cost function is minimized (see Figure 4-17, L^{th} Iteration on the left). For the implementation a termination criterion is defined according to Eq. 4-38. This means that the iteration is terminated if the Euclidean norm (see Eq. 4-39) of the heat flow over the prediction horizon $\left|\dot{Q}^l_{S1,k+i|k}\right|_2$ is smaller than the heat output of the heat pump at minimum compressor speed $\dot{Q}_{HP,min}$. The Euclidean norm is specified with two bars and the subscript 2. The Euclidean norm is calculated for a vector as the root of the sum of the squares of the components (see Eq. 4-39). This is a strict criterion. Another possibility for a weaker criterion would be the maximum norm of the heat flow over the prediction horizon. The maximum norm specifies the highest absolute value of a vector.

$$T^l_{co,k+i|k} = T^l_{S3,k+i|k} + 5\ K \qquad \text{Eq. 4-34}$$

$$\dot{Q}^l_{dis,1,k+i|k} = \dot{m}^l_{c,k+i|k}\ c\ (T^l_{co,k+i|k} - T^l_{S1,k+i|k}) \qquad \text{Eq. 4-35}$$

$$\dot{Q}^l_{dis,2,k+i|k} = \dot{m}^l_{c,k+i|k}\ c\ (T^l_{S1,k+i|k} - T^l_{S2,k+i|k}) \qquad \text{Eq. 4-36}$$

$$\dot{Q}^l_{dis,3,k+i|k} = \dot{m}^l_{c,k+i|k}\ c\ (T^l_{S2,k+i|k} - T^l_{S3,k+i|k}) \qquad \text{Eq. 4-37}$$

$$\left|\dot{Q}^l_{S1,k+i|k}\right|_2 < \dot{Q}_{HP,min} \qquad \text{Eq. 4-38}$$

$$\left|\dot{Q}^l_{S1,k+i|k}\right|_2 = \sqrt{\dot{Q}^2_{S1,k|k} + \cdots + \dot{Q}^2_{S1,k+p-1|k}} \qquad \text{Eq. 4-39}$$

As already mentioned, the calculation of the disturbances for the linear model based on the hydraulic circuit with the desuperheater HC3 (see Figure 4-12) is similar to that without desuperheater. The disturbances for the forced convection are calculated with Eq. 4-40 - Eq. 4-42.

$$\dot{Q}^l_{dis,1,k+i|k} = \dot{m}^l_{d,k+i|k}\ c\ (T_{do,k+i|k} - T^l_{S1,k+i|k}) \qquad \text{Eq. 4-40}$$

$$\dot{Q}^l_{dis,2,k+i|k} = \left(\dot{m}^l_{c,k+i|k} - \dot{m}^l_{d,k+i|k}\right) c \left(T^l_{co,k+i|k} - T^l_{S2,k+i|k}\right)$$
$$+ \dot{m}^l_{d,k+i|k}\ c \left(T^l_{S1,k+i|k} - T^l_{S2,k+i|k}\right)$$

Eq. 4-41

$$\dot{Q}^l_{dis,3,k+i|k} = \dot{m}^l_{c,k+i|k}\ c \left(T^l_{S2,k+i|k} - T^l_{S3,k+i|k}\right)$$

Eq. 4-42

In the hydraulic circuit HC3 natural convection may occur. The heat flow caused by natural convection has also to be considered in the calculation of the disturbances. The calculation of the disturbances caused by natural convection is performed with Eq. 4-43 and Eq. 4-44 based on the mass of one node m_j and the sampling time τ_S of the nonlinear simulation.

$$\dot{Q}^l_{dis,nat,j,k+i|k} = \frac{m_j\ c}{\tau_s} \left(\frac{T^l_{Sj+1,k+i|k} + T^l_{Sj,k+i|k}}{2} - T^l_{Sj,k+i|k} \right)$$

Eq. 4-43

$$\dot{Q}^l_{dis,nat,j+1,k+i|k} = \frac{m_{j+1}\ c}{\tau_s} \left(\frac{T^l_{Sj+1,k+i|k} + T^l_{Sj,k+i|k}}{2} - T^l_{Sj+1,k+i|k} \right)$$

Eq. 4-44

Figure 4-18 shows an overview on the calculation stages performed during the MPC-routine (compare Figure 4-1). The process can be broken down into the following stages:

- The preparation of the external input variables (see chapter 4.3)
- The iterative optimization
  - The online optimization (MPC)
  - The simulation of the convective heat flows
- The conversion of the required heat flow into the compressor frequency
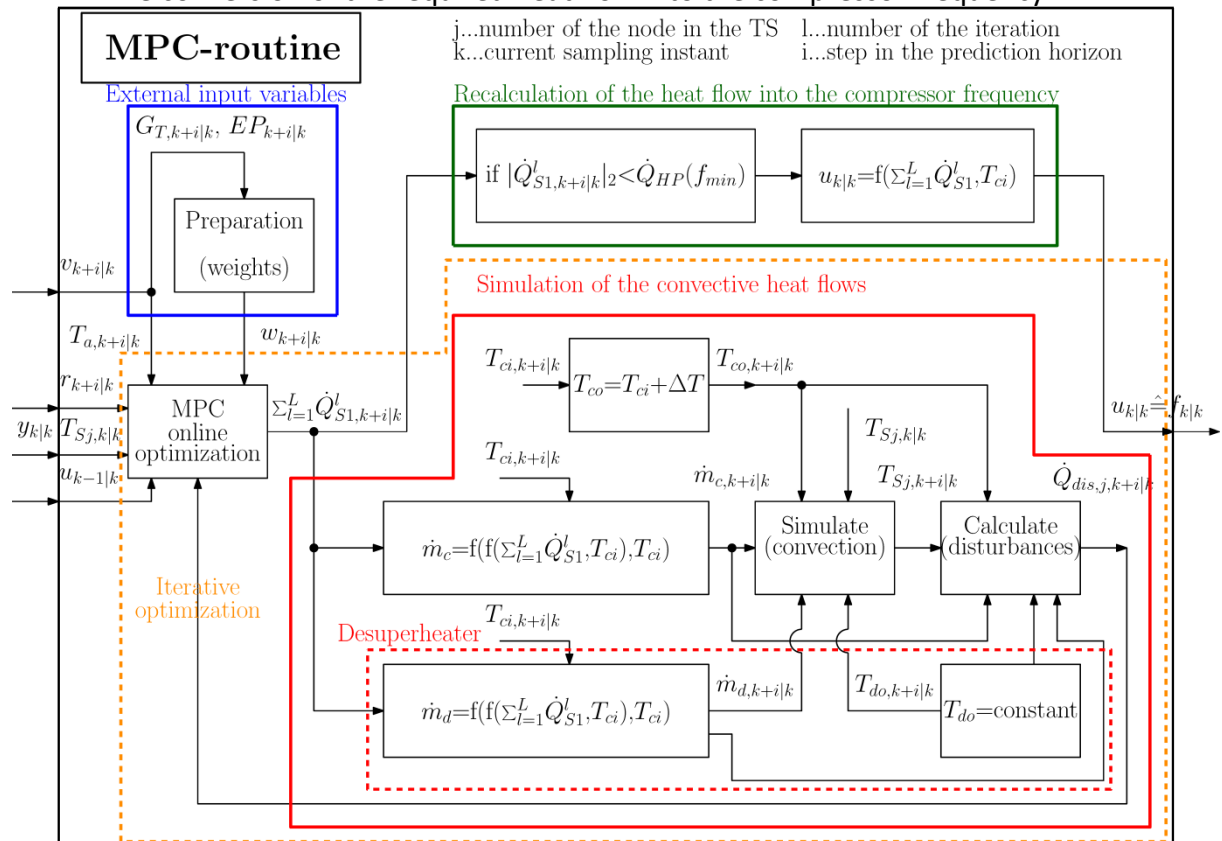
Figure 4-18: Detailed overview of the routines during a MPC call

First of all the external input variables $(T_{a,k+i|k}, G_{T,k+i|k}, EP_{k+i|k})$ are prepared as disturbances and weighting factors $w_{k+i|k}$ for the whole prediction horizon. The MPC receives them with the measured output of the plant y_k and the last manipulated variable $u_{k-1|k}$. Based on these values the optimization of the first iteration is performed to obtain the required heat flows of the first node $\dot{Q}^1_{S1,k+i|k}$. After this the required heat flows are used to calculate the mass flows $(\dot{m}^1_{c,k+i|k}, \dot{m}^1_{d,k+i|k})$ of the thermal storage. These mass flows are used in combination with the temperatures at the condenser outlet $T^1_{co,k+i|k}$, the temperatures at the desuperheater outlet $T^1_{do,k+i|k}$ and the measured node temperature $T_{Sj,k|k}$ in the nonlinear model of the thermal storage. The temperatures of the thermal storage $T^1_{Sj,k+i|k}$ over the prediction horizon are the result of this simulation. Now the convective heat flows are converted into disturbances $\dot{Q}^1_{dis,j,k+i|k}$ affecting each node. In the next iteration the MPC receives these disturbances and determines again the required heat flow of the first node $\dot{Q}^2_{S1,k+i|k}$. These heat flows $\dot{Q}^2_{S1,k+i|k}$ are summarized with the heat flows of the first iteration $\dot{Q}^1_{S1,k+i|k}$ and the simulation of the convective heat flows is performed again. This is repeated until the termination criterion is fulfilled. The conversion of the resulting heat flow for the first step of the prediction horizon $\sum_{l=1}^{L} \dot{Q}^l_{S1,k|k}$ into the compressor frequency $u_{k|k} = f_{k|k}$ for the plant finishes the MPC routine. For the hydraulic circuit without desuperheater the calculation of the mass flow through the desuperheater as well as the temperature at the desuperheater outlet are omitted.

4.3   Modeling of external input variables

This chapter deals with the modeling of the external input variables. These are the DHW demand, the electricity prices and the PV output. Furthermore, the ambient temperature of the thermal storage which is used for the calculation of the losses, and the ambient temperature outside of the building which affects the ground temperature are seen as an external input variable. These variables are chosen as constant $15\,°C$ for the ambient temperature of the thermal storage and as constant $10\,°C$ for the evaporator inlet temperature of the brine. Therefore, a further processing of these quantities is not necessary. The COP is affected by the ground temperature, the temperature at the heat sink and the compressor frequency. External input variables are predicted independently from the state or manipulated variables. A prediction of the COP based on the heat sink temperature which depends on a state variable (temperature at the bottom of the thermal storage) and the compressor frequency which depends on the manipulated variable is a further challenge. This is discussed in chapter 4.3.4.

In the context of MPC, different possibilities for the consideration of predicted external input variables exist. Firstly, they can be considered as predicted disturbances in the system equations. This is the case for the ambient temperature of the thermal storage and would

also be possible for the DHW demand predictions. Secondly, variables which do not affect the state of the system, similar to the electricity prices or the PV output, are considered as weighting factors in the cost function. These variables influence the priority of the objectives defined in the cost function. Thirdly, the reference trajectory can be used to influence the behavior of the MPC. This method is proposed for the prediction of the DHW demand (see chapter 4.3.1).

4.3.1 Domestic hot water demand

As already mentioned there are two different possibilities available to consider the prediction of the DHW draw offs. The first one is to assume a load prediction which corresponds to an expected DHW demand and to consider the draw off as predicted measured disturbance. Pichler et al. (2014) performed investigations based on this method. For this the daily peaks of the DHW demand were modeled by two Gaussian curves. The results have shown that this method leads to undesirable energy consumption. However, the prediction of DHW demand based on recorded DHW demand data can be a more accurate prediction method than the modeling with Gaussian curves. The second possibility is to raise the reference value of the temperature in the thermal storage in times when DHW draw offs are predicted. In this work a prediction of DHW demand is not considered.

4.3.2 Electricity prices

The prediction of electricity prices is used to operate the heat pump in times of surplus electricity. This data is summarized hourly and varies within a range of $0 - 140\ EUR/MWh$ (see Table 3-7). For the use as a weighting factor this data has to be scaled in a range of $0 - 1$. To achieve this the electricity prices over the prediction horizon $EP_{k+i|k}$ are considered and referred to at the maximum value of this horizon (see Eq. 4-45). This is performed at each sampling instant with shifted values.

$$w_{k+i|k}^{EP} = \frac{EP_{k+i|k}}{\max\left(EP_{k+1|k}\right)} \qquad i = 0, \dots, p-1 \qquad \textbf{Eq. 4-45}$$

4.3.3 Photovoltaic output

The prediction of the PV output is used, similar to the electricity prices, to maximize self consumption. To achieve that, calculations are necessary to obtain the predicted output with available weather forecast data. For this a simplified model is used which is based on measured data provided by the manufacturer of the PV array. These values are the same as for the TRNSYS model (see chapter 3.4) and the model introduced in this chapter.

As the PV array is connected to the Grid and HP with a MPPT (see Figure 2-4), a simplified model to predict the PV output can be used because only the power at the MPP is of interest and the current voltage curve does not need to be evaluated. This can be made with one

algebraic equation, which is based on the module efficiency (see Fry, 1998). The module efficiency η can be written as the ratio of useful electrical power output P_{MPP} to incident solar irradiation G_T referred to the area of the PV module (see Eq. 4-46).

$$\eta = \frac{P_{MPP}}{G_T\,A}$$

Eq. 4-46

The module efficiency at reference conditions can be written with Eq. 4-47 as Eq. 4-48.

$$P_{MPP} = U_{MPP}\,I_{MPP}$$

Eq. 4-47

$$\eta_{ref} = \left(\frac{U_{MPP,ref}\,I_{MPP,ref}}{G_{T,ref}\,A}\right)_{T=T_{ref}}$$

Eq. 4-48

In Fry (1998) the efficiency coefficient model is based on the assumption that the efficiency varies linearly in accordance with the temperature. Therefore, the derivative of the module efficiency is constant. This leads to Eq. 4-49. The derivative of the efficiency at reference condition can be written with the chain rule of calculus as Eq. 4-50.

$$\frac{d\eta}{dT} = \frac{d\eta_{ref}}{dT}$$

Eq. 4-49

$$\frac{d\eta_{ref}}{dT} = \frac{1}{G_{T,ref}\,A}\,\frac{d}{dT}\left(U_{MPP,ref}\,I_{MPP,ref}\right)$$
$$= \frac{1}{G_{T,ref}\,A}\left(I_{MPP,ref}\,\frac{dU_{MPP,ref}}{dT} + U_{MPP,ref}\,\frac{dI_{MPP,ref}}{dT}\right)$$

Eq. 4-50

Furthermore, Fry (1998) mentioned a relation between the derivative of voltage and current with respect to the temperature. Therefore, these derivatives can be written with the temperature coefficients at open circuit μ_{Uoc} and short circuit μ_{Isc} with Eq. 4-51 and Eq. 4-52. The temperature coefficient at open circuit was already used in chapter 3.4 to obtain the parameters for the TRNSYS model.

$$\frac{dU_{MPP,ref}}{dT} = \frac{U_{MPP,ref}}{U_{oc,ref}}\mu_{Uoc}$$

Eq. 4-51

$$\frac{dI_{MPP,ref}}{dT} = \frac{I_{MPP,ref}}{I_{sc,ref}}\mu_{Isc}$$

Eq. 4-52

Substituting Eq. 4-51 and Eq. 4-52 for the corresponding terms into Eq. 4-50 leads to Eq. 4-53. This equation can be calculated with the data provided by the manufacturer.

$$\frac{d\eta_{ref}}{dT} = \frac{U_{MPP,ref}\,I_{MPP,ref}}{G_{T,ref}\,A}\left(\frac{\mu_{Uoc}}{U_{oc,ref}} + \frac{\mu_{Isc}}{I_{sc,ref}}\right)$$

Eq. 4-53

The integration of Eq. 4-49 and the substitution of Eq. 4-53 for the derivative of the efficiency at reference conditions lead with the definition of the efficiency (see Eq. 4-46) to Eq. 4-54. This is a function for the maximum power of the module dependent on G_T and T_{cell}.

$$P_{MPP,module} = \frac{G_T}{G_{T,ref}} U_{MPP,ref} I_{MPP,ref} \left(1 + \left(\frac{\mu_{Uoc}}{U_{oc,ref}} + \frac{\mu_{Isc}}{I_{sc,ref}} \right) \left(T_{cell} - T_{cell,ref} \right) \right)$$ **Eq. 4-54**

The cell temperature depends mainly on the ambient temperature and the absorbed incident irradiation and is calculated with Eq. 4-55. $\tau_{\alpha ave}$ is a constant average ratio of the absorbed to the incident irradiation and U_L is an overall heat loss coefficient (see Eq. 4-56) obtained from the normal operation cell temperature (NOCT) test of the manufacturer (see Eckstein, 1990).

$$T_{cell} = T_a + \frac{G_T \tau_{\alpha ave}}{U_L} \left(1 - \frac{\eta_{MPP,ref}}{\tau_{\alpha ave}} \right)$$ **Eq. 4-55**

$$U_L = \frac{G_T \tau_{\alpha ave}}{T_{cell,NOCT} - T_{a,NOCT}}$$ **Eq. 4-56**

The power output of the whole PV array can be calculated with the number of modules in series (NMS) and the number of modules in parallel (NMP) as Eq. 4-57.

$$P_{max,array} = P_{max,module} \ NMS \ NMP$$ **Eq. 4-57**

Figure 4-19 compares the power output of the PV array which is used in this work (see manufacturer data Appendix A-1). The power output of the four parameter model is the result of a TRNSYS simulation and the power output of the efficiency coefficient model is obtained by a MATLAB simulation. The four parameter model predicts higher change of PV output with changing temperature. By contrast, the change of PV output matches the four parameter model and the efficiency coefficient model accurately. Fry (1998) performed similar simulations for the Siemens SR100 crystalline module and the results are similar to the results obtained with the PV module of this work.

The output of the PV array varies within the range of $0 - 2.6 \ kW$ (see Table 3-5). This range has to be scaled for the use as a weighting factor, similar to the electricity prices. For this the predicted PV output is considered and referred to the maximum value of the prediction horizon. These calculations are performed each time the MPC is called upon.

$$w_{k+i|k}^{PV} = \frac{max \left(P_{PV,k+i|k} \right) - P_{PV,k+i|k}}{max \left(P_{PV,k+i|k} \right)} \quad i = 0, \dots, p - 1$$ **Eq. 4-58**
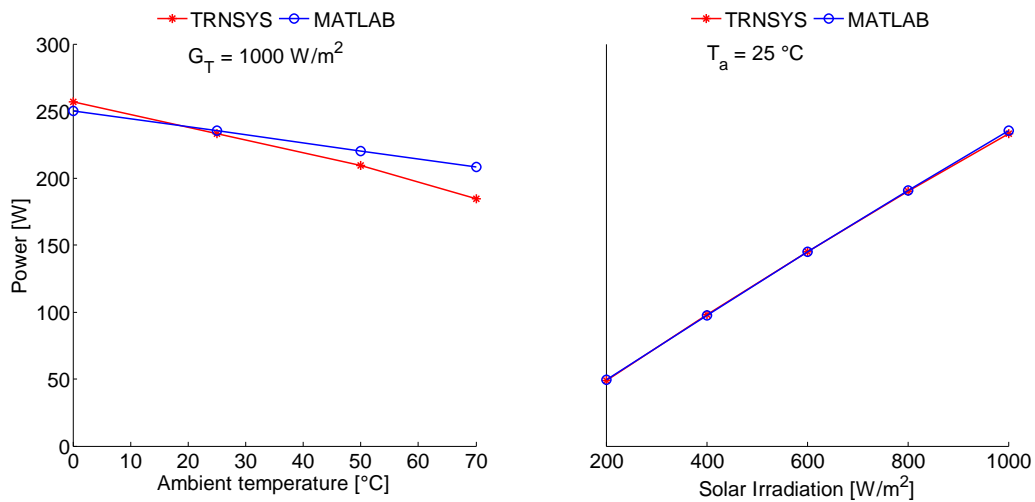
Figure 4-19: Comparison of the four parameter TRNSYS model with the efficiency coefficient MATLAB model

4.3.4 COP

A further challenge is the consideration of the COP. As already mentioned, the COP depends on the heat source inlet temperatures and the heat sink inlet temperature as well as on the compressor frequency. The temperatures at the outlet of the heat source and the heat sink are calculated with the inlet temperatures and the constant temperature differences of the condenser and evaporator (see chapter 3.3.2). The heat sink inlet temperature is the thermal storage temperature at the bottom given as a state variable, and the frequency of the compressor depends on the required heat flow, which is the manipulated variable. Only the heat sink inlet temperature is an external input variable which is constant in this work. Therefore, the dependence of the COP on the temperature at the sink is not investigated.

Wimmer (2004) used a heat pump with air as heat source and a compressor with constant speed. The temperature at the heat sink was considered with a nominal value for the calculation of the COP. This enables to consider the COP dependent on the ambient temperature with characteristic diagrams based on the temperature forecast mentioned in chapter 3.5.1. This approach leads to the situation that the COP can be predicted over the prediction horizon with the ambient temperature as an external input variable.

Bianchi (2006) investigated a brine/water heat pump and a compressor with constant speed. The sink temperature was also not considered in the COP. For the prediction of the brine temperature a similar approach as for the temperature forecast of the ambient temperature was used. The temperature profile of the brine of the last day was corrected to the actual measured temperature of the brine.

Despite these facts, an approach considering the temperature at the sink and/or the compressor frequency for the calculation of the COP is investigated to a certain extend.

a) Consideration of the COP in dependence of the condenser inlet temperature and the compressor frequency

The COP affects the weights similar to the electricity prices and the PV output. If the COP is considered as a function of the frequency and the temperature at the sink a number of questions arise. The first question is in which stage of the MPC-routine the weights have to be updated for the optimization. One option is to calculate the COP during the conversion of the convective heat flows into disturbances. A drawback of this method is that the optimization problem differs during the calculation of the convective disturbances. The iterative method determines in the iterations a trajectory of required heat flows. This heat flows are used to calculate new weights. Therefore each optimization problem differs in the weights from iteration to iteration. This may cause further problems. Another option is to determine the COP based on the results determined at the end of the iterative process. After the last iteration the COP is calculated and the new weights are updated. Then the iterative process is repeated considering these new weights. This method requires more computational effort but it has the advantage that the weights do not change during the iterative process. Therefore, the second possibility is investigated here (see Figure 4-20).
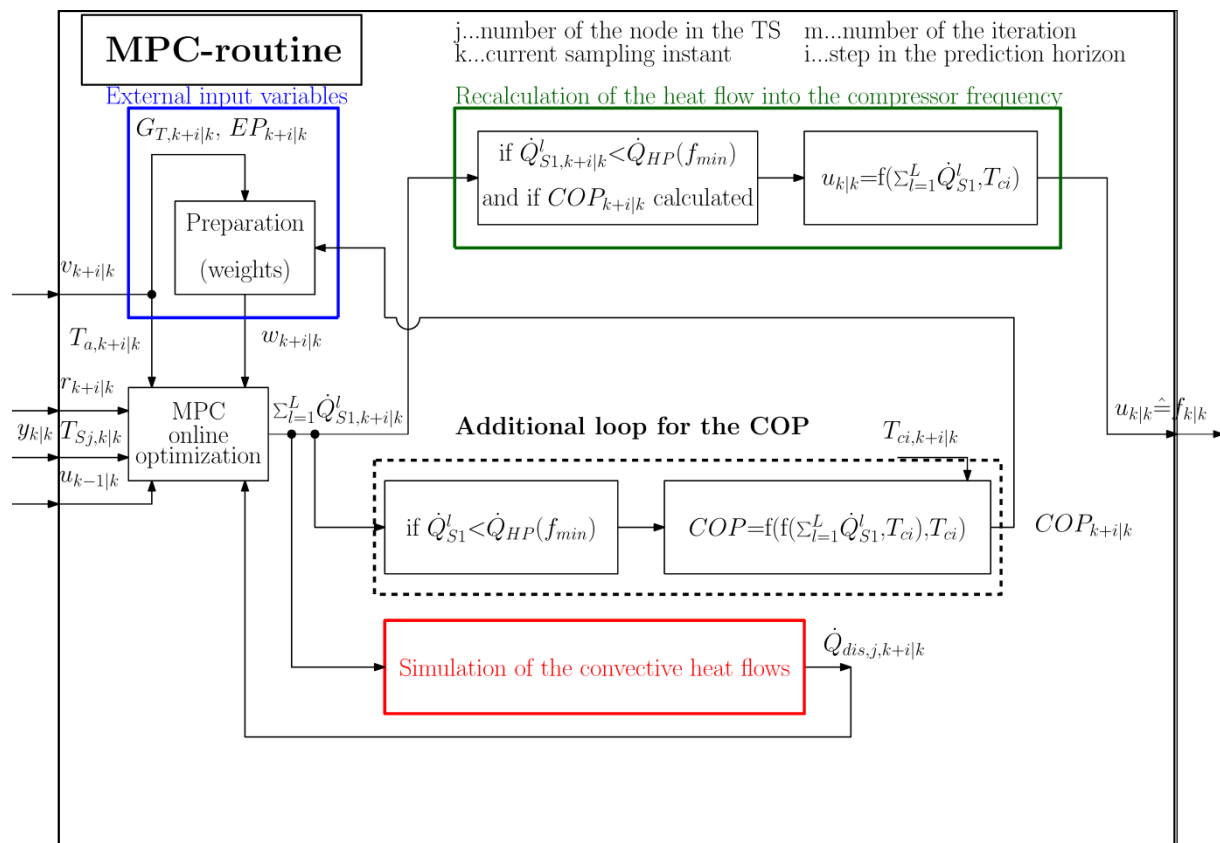
Figure 4-20: Detailed overview of the routines during a MPC call including the COP calculation

Figure 4-20 shows the MPC routine including the COP calculation loop. This figure is based on Figure 4-18. For clarity of presentation the simulation of the convective heat flows is shown in a simplified form. The loop of the COP is superior to the loop for the simulation of the convective disturbances. The routine starts with the preparation of the external input variables. At this point the COP trajectory of the last call of the MPC-routine may be used with shifted values. Then the iterations for the simulation of the convective heat flows are performed. If the termination criterion is fulfilled the *additional loop* for the COP is processed. This starts with the calculation of the COP ($COP_{k+i|k}$) based on the required heat flows $\sum_{l=1}^{L} \dot{Q}_{S1,k+i|k}^{l}$. The COP values are further processed with the external input variables as weights $w_{k+i|k}$ for the optimization problem. Then the iterative optimization is performed again considering these new weights. After this the conversion of the heat flow into the compressor frequency finishes the MPC-routine.

The optimization problem formulation within the MPC toolbox is only able to consider constraints in the range of $0 - f_{max}$ (see chapter 4.4.3). Therefore, a way has to be found to avoid compressor frequencies for the range of $0 - f_{min}$. Figure 4-21 shows two different possibilities to assume values in this range. The first one is to assume the COP as constant in this range with regard to the value at the minimum frequency and the according temperature at the condenser inlet. The second approach can be to assume a parabola in this range with the aim to penalize this range (similar to that discussed in chapter 4.4.3). Another possibility would be to extrapolate the real physical COP .
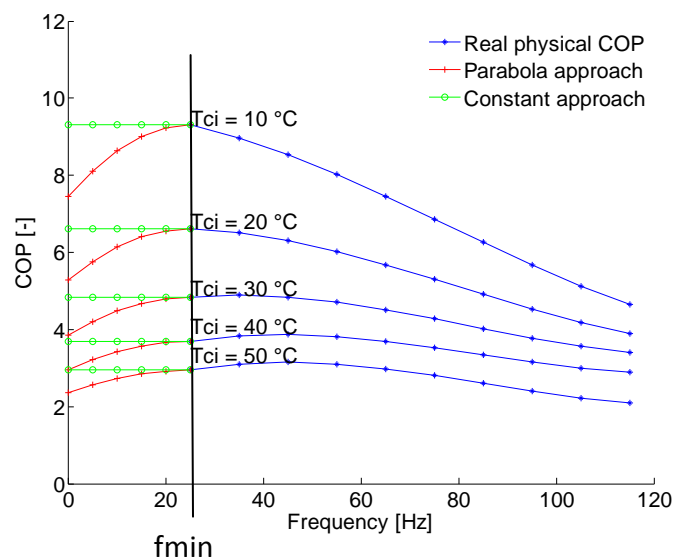
Figure 4-21: Approaches to model the COP in the range between 0-fmin (without desuperheater)

Figure 4-22 shows exemplary weights for the *constant approach* simulated over two days. The top figure shows the temperature of the bottom storage node which equals the condenser inlet temperature. The influence of the condenser inlet temperature on the weight can be seen when the heat pump is off (see Figure 4-22 below, right ordinate). The

weight decreases with increasing COP values in accordance with decreasing condenser inlet temperatures. The frequency, shown in Figure 4-22 below on the left ordinate, results in a jump of the weight. The effect on the optimization is not pronounced as only a small range of $0 \leq w^{COP} \leq 1$ is used. This has to be evaluated with long term simulations.
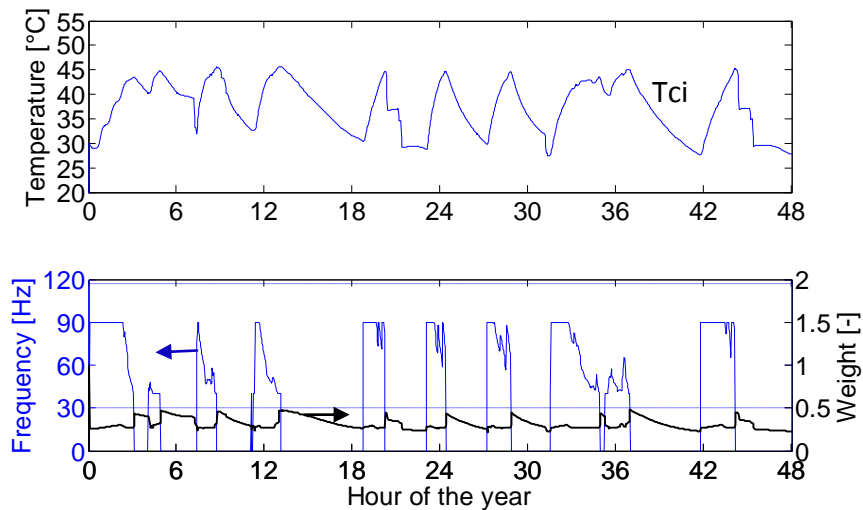
Figure 4-22: Weighting factor of the COP in dependence of the condenser inlet temperature and the compressor frequency

b)   Consideration of the COP in dependence of the condenser inlet temperature and a nominal value for the compressor frequency

Another method would be to assume a nominal value for the frequency that the COP depends only on the temperature at the condenser inlet. This has the advantage that a modeling of the COP for the range of $0 - f_{min}$ would not be necessary. The first question that arises is the same as in the previous method: At which step should the weights be updated. This question can be answered similarly to the method presented in chapter 4.3.4a. Another question is which frequency should be chosen for the nominal value. As the COP curves differ for different frequencies (see Figure 4-23), the effect on the weight would differ according to the chosen nominal value.
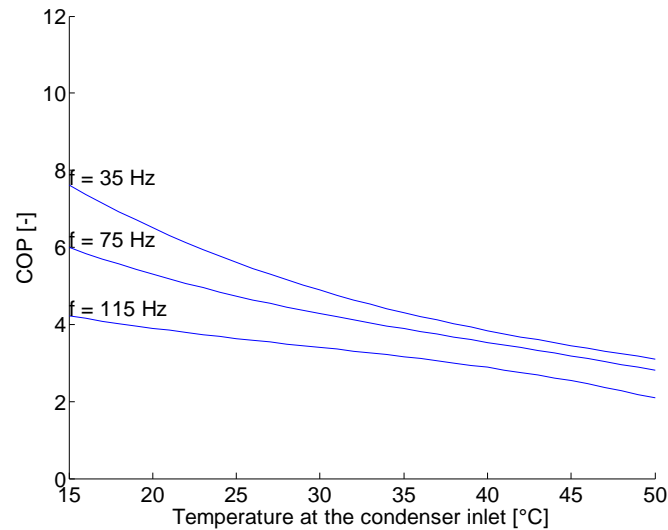
Figure 4-23: COP in dependence of the condenser inlet temperature for different frequencies (without desuperheater)

Figure 4-24 shows the resulting weights for the COP in dependence of the condenser inlet temperature and for a nominal value of the frequency $f_{nom} = 40\ Hz$. This definition leads to the situation that the range of $0 < w^{COP} < 1$ is further decreased than in the method presented in chapter 4.3.4a.
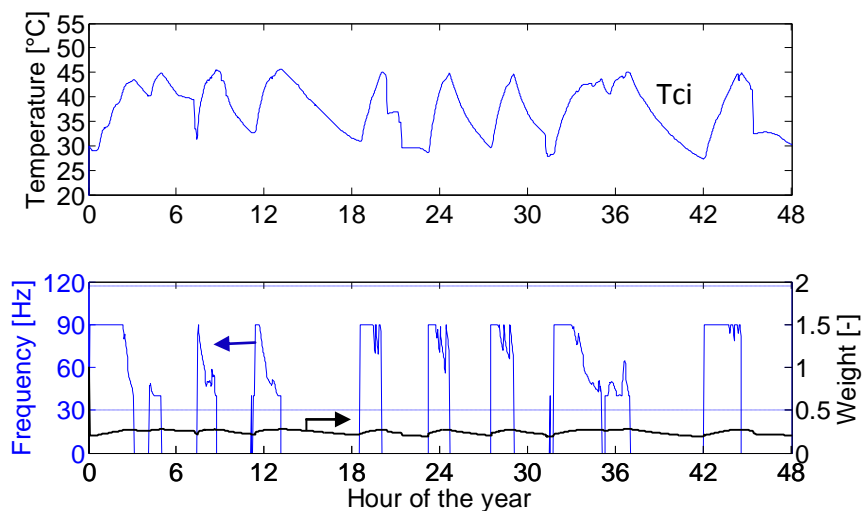
Figure 4-24: Weighting factor of the COP in dependence of the condenser inlet temperature

c) Scaling of the COP for the weights

Furthermore, the COP has to be scaled to the range of $0 - 1$ for the use as a weighting factor in the cost function. This is shown in Eq. 4-59. The COP in the denominator of Eq. 4-59 is predicted over the prediction horizon. The value for the COP in the nominator of Eq. 4-59 is chosen, similar to the weighting factor of the electricity prices and the PV output, to a characteristic value over the prediction horizon. In this case, the minimum COP value is appropriate.

$$w_i^{COP} = \frac{\min (COP_i)}{COP_i} \qquad\qquad i = 0, \dots, p-1 \qquad\qquad \text{Eq. 4-59}$$

4.4 Parameterization of the MPC

This chapter discusses the parameter settings for the MPC. Guidelines for setting controller parameters are not available. A reason for this may be that the settings differ for each system. Therefore, different parameter settings have to be analyzed in simulations. The following chapters discuss the parameters in general.

The prediction horizon for the MPC is set to 48 hours with a sampling time of 20 min. These values have been taken from the work of Pichler et al. (2014).

4.4.1 Cost function

The cost function (see Eq. 4-61) used in this work is equal to the cost function introduced in chapter 2.4.3. The first term of the cost function minimizes the deviation of the top node temperature from the reference value. The second term is used to minimize the changes of the manipulated variable and the third term minimizes the manipulated variable. The last term penalizes the violation of the soft constraints and is mainly influenced by the ECR factors (see chapter 2.4.3).

$$y_{ref} = 50\,°C \qquad\qquad \text{Eq. 4-60}$$

$$\min_{\Delta u(k|k), \dots, \Delta u(m-1+k|k), \epsilon} \left\{ \sum_{i=0}^{p-1} \left[\left(w_{i+1}^y \left(y_1(k+i+1|k) - y_{ref}(k+i+1) \right) \right)^2 \right. \right.$$
$$\left. \left. + \left(w_i^{\Delta u} \, \Delta u(k+i|k) \right)^2 + \left(w_i^u \, u(k+i|k) \right)^2 \right] + \rho_\epsilon \epsilon^2 \right\} \qquad \text{Eq. 4-61}$$

An additional parameter arises with the termination criterion through the iterative process caused by the convective heating process. This parameter is also discussed in this chapter. With the Figure 4-25 and Figure 4-26 the differing behavior of the system is shown step by step for different cost functions and termination criterions. These investigations are based on the hydraulic circuit HC1 (see chapter 4.1.1a) and the temperature at the top node of the thermal storage is the controlled variable. The figures show the predictions of the state variables over the prediction horizon from the perspective of the MPC and are similar to Figure 2-7. The upper picture in the figures shows the curve of the storage temperatures resulting from the trajectory of manipulated variables shown in the lower picture ($\sum_{l=1}^{L} \dot{Q}_{S1}^l$). Furthermore, the lower picture shows the heating trajectories $\dot{Q}_{S1}^l$ resulting from the iterations (see chapter 4.2.4). The sum of these trajectories is the resulting trajectory of the manipulated variable ($\sum_{l=1}^{L} \dot{Q}_{S1}^l$). It will be reinforced again that only the first value of the

resulting trajectory of the manipulated variable is converted into a frequency and used in the plant.

Figure 4-25 on the left shows the predictions for a trajectory of manipulated variables determined by minimizing the cost function shown in Eq. 4-62. The aim of this cost function is to minimize the deviation of the temperature at the top node from the reference temperature. Furthermore a small limit for the termination criterion is used (see Eq. 4-63) this leads to 40 iterations for the formation of a trajectory of manipulated variables.

$$\min_{\Delta u(k|k),\dots,\Delta u(m-1+k|k),\epsilon} \left\{ \sum_{i=0}^{p-1} \left[\left(w_{i+1}^y \left(T_{S1}(k+i+1|k) - T_{ref}(k+i+1) \right) \right)^2 \right] + \rho_\epsilon \epsilon^2 \right\} \qquad \textbf{Eq. 4-62}$$

$$\left| \dot{Q}_{S1} \right|_2 < 0.3 \; kW \qquad \textbf{Eq. 4-63}$$

The main point in Figure 4-25 on the left is that the reference temperature is reached by the temperature in the top node. Reasons for this are that the required heat flow for the thermal storage is fairly accurate calculated and a minimization of the heat flow is not considered in the cost function (see Eq. 4-62).
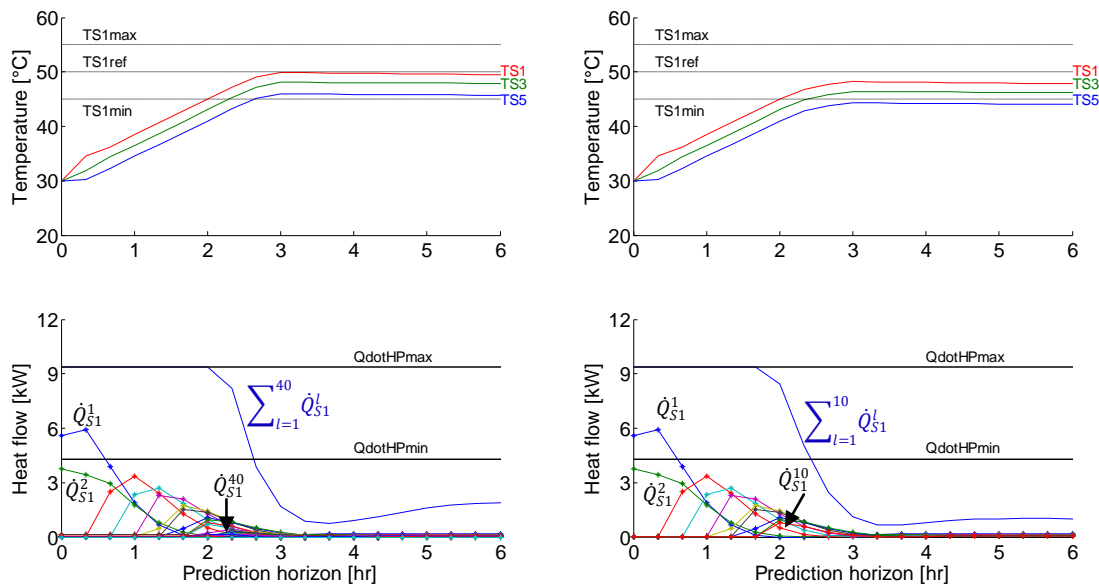
Figure 4-25: Resulting trajectories within the prediction horizon for a cost function which minimizes the deviation from the reference temperature and a low termination criterion (left) and a termination criterion equal the heat flow at minimum compressor speed (right)

In the next step the limit for the termination criterion is set to the heat flow at minimum compressor speed (see Eq. 4-64). This is shown in Figure 4-25 on the right and leads to a reduction of the number of iterations to 10. Figure 4-25 on the right shows the effect on the

storage temperatures resulting in a higher deviation from the reference temperature. A reason for this is that less heat flow is collected as in the previous step.

$$\left|\dot{Q}_{aux}\right|_2 < \dot{Q}_{hp,f_{min}=40Hz} = 4.3\ kW$$

<div align="right">**Eq. 4-64**</div>

In the last step a further term is added to the cost function which minimizes the required heat flow (see Eq. 4-65). This leads to a further deviation of the temperature in the top node from the reference temperature (see Figure 4-26).

$$\min_{\Delta u(k|k),\ldots,\Delta u(m-1+k|k),\epsilon}\left\{\sum_{i=0}^{p-1}\left[\left(w_{i+1}^{y}\left(y_1(k+i+1|k)-r(k+i+1)\right)\right)^2\right.\right.$$
$$\left.\left.+\left(w_i^u\ u(k+i|k)\right)^2\right]+\rho_\epsilon\epsilon^2\right\}$$

<div align="right">**Eq. 4-65**</div>
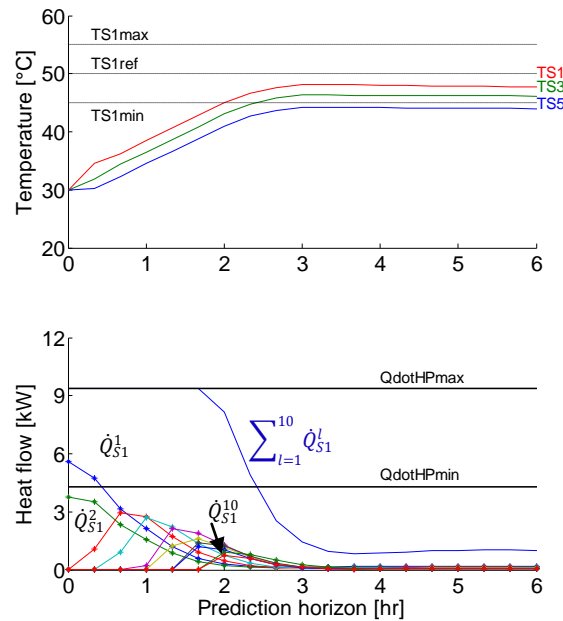
Figure 4-26: Resulting trajectories within the prediction horizon for a cost function which minimizes the deviation from the reference temperature and the heat flow and a termination criterion equal the heat flow at minimum compressor speed

4.4.2 Weights

This chapter explains how the weights w_{i+1}^{y}, $w_i^{\Delta u}$, w_i^u are formed for the use in the cost function (see Eq. 4-61). The weight for the output variable (w_{i+1}^{y}) is set to one as there is freedom to set one weight to one, since only the relation between the weights matter. The weight for the manipulated variable rate ($w_i^{\Delta u}$) is also constant (e.g. $w_i^{\Delta u} = 0.5$) and is used for a smoothing of the manipulated variables. With a high value for the weight of the manipulated variables rate a high number of on and off cycles or oscillations concerning the compressor frequency can be avoided.

$$w_{i+1}^y = 1$$

<div align="right">Eq. 4-66</div>

$$w_i^{\Delta u} = constant$$

<div align="right">Eq. 4-67</div>

The weight for the manipulated variable (w_i^u) is calculated according to Eq. 4-69. The factor w^{Base} in Eq. 4-69 is called base weight and is a constant factor (e.g. $w^{Base} = 1$) (see Eq. 4-68) which is set in relation to the output variable. The base weight corresponds to an upper limit for the curve of the weight. The upper limit for the base weight is determined in simulations by raising the value of the base weight until constraints are violated. This base weight is further processed with the weights of electricity price, PV output and COP (see Eq. 4-69).

$$w^{Base} = constant$$

<div align="right">Eq. 4-68</div>

$$w_i^u = w^{Base}\, w_i^{EP}\, w_i^{PV}\, w_i^{COP}$$

<div align="right">Eq. 4-69</div>

Figure 4-27 shows the resulting weights over two days, for which w_i^{COP} is set to 1. The curve of the resulting weight w_i^u and considers the influences of the individual weights (see Eq. 4-69). The functionality of the base weight as an upper limit can be seen at the 18 hour. This is the worst case the electricity prices are at a maximum value and PV output is not available. Even at this time the constraints on the controlled variable have to be fulfilled.
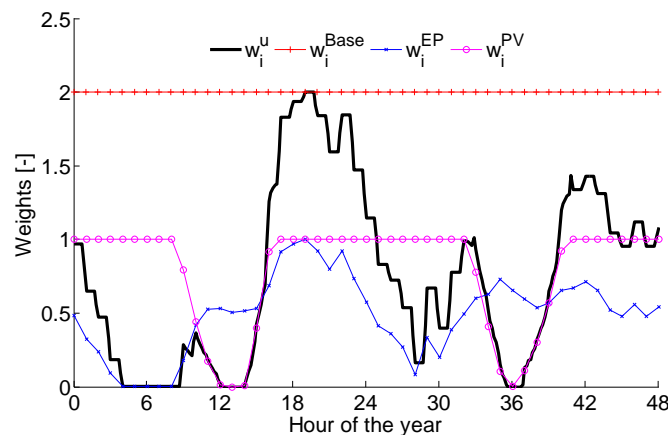
Figure 4-27: Resulting weight of a two day simulation, weight COP equals one and weight base equals two

Figure 4-28 shows the resulting weight for a two day simulation if the weight for the COP is included. The effect on the resulting weight w_i^u compared to Figure 4-27 is significant. Although the weight of the COP varies in a small range a new value for the base weight has to be found. This example shows the challenge to find good parameter settings.
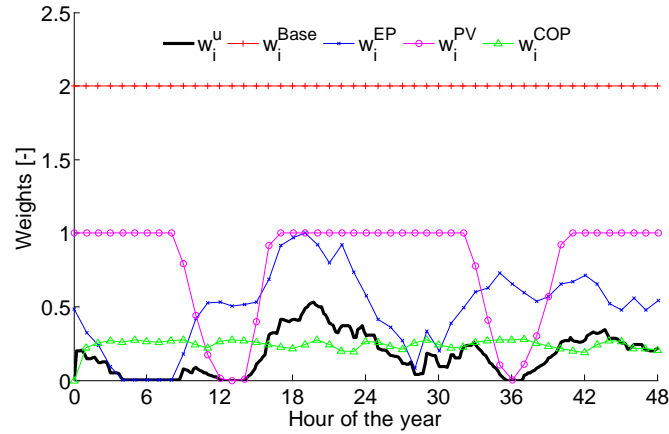
Figure 4-28: Resulting weight of a two day simulation with COP

4.4.3   Constraints

For the output variable, the manipulated variable rate and the manipulated variable constraints have to be defined.

a)   Constraints on the controlled variable

The lower constraint for the controlled variable is set to $45\,°C$. This results in the minimum required temperature in the thermal storage (see chapter 3.1). For the upper constraint a value above the reference temperature is chosen (see Eq. 4-70). This quantity is negligible, as higher values than the reference temperature are rarely reached for the hydraulic circuit without desuperheater. For the hydraulic circuit with desuperheater the upper limit is the constant water temperature at the desuperheater outlet.

$$45\,°C \le T_{S1} \le 55\,°C$$

Eq. 4-70

b)   Constraints on the manipulated variable rate

The constraints on the manipulated variable rate Δu are written in Eq. 4-73. The upper constraint defines the maximum possible step of the manipulated variable u in two successive time steps of the MPC. The lower limit is set to a high value to enable quick switching off. The upper limit is estimated with the time constant ($5\,tau$) found in chapter 4.1.6. The slope of the manipulated variable can be calculated with the time constant (see Eq. 4-71). To estimate the constraint on the manipulated variable rate the time constant is further processed with the sampling time of the MPC $\Delta\tau_{MPC} = 20\,min$ in Eq. 4-72. Due to the high sampling time of the MPC the whole operating range ($\dot{Q}_{HP,min}, \dot{Q}_{HP,max}$) of the heat pump can be covered within the sampling time. For the MPC used in this work the constraint on the manipulated variable rate will not be reached.

$$5 \, tau = 1/5 \, du/d\tau$$

<div align="right">Eq. 4-71</div>

$$\Delta u_{max} = \frac{1}{5} \frac{du}{d\tau} \Delta\tau_{MPC}$$

<div align="right">Eq. 4-72</div>

$$-Inf \leq \Delta u \leq \Delta u_{max}$$

<div align="right">Eq. 4-73</div>

c)   Constant constraints on the manipulated variable

The consideration of the constraints on the manipulated variable is another challenging topic. Even without the limits discussed in chapter 3.3.3 a consideration of the constraints in the form of Eq. 4-74 is not possible in the MPC toolbox. A reason for this is that the constraint in Eq. 4-74 leads to a non convex optimization problem which cannot be solved by the solver used in the MPC toolbox. This is another point where the alternative toolbox presented in chapter 2.4.4 would be superior to the MPC toolbox.

$$f = 0 \text{ or } f_{min} \leq f \leq f_{max}$$

<div align="right">Eq. 4-74</div>

For the MPC toolbox the constraints of the compressor have to be considered in the form of Eq. 4-75. Furthermore, the indirect optimization determines the required heat flow of the thermal storage. Therefore, the constraints have to be defined as heat flow. This means the constraints in Eq. 4-75 are further processed with the equation found in chapter 4.1.1 to obtain Eq. 4-76.

$$0 \leq f \leq f_{max}$$

<div align="right">Eq. 4-75</div>

$$0 \leq \dot{Q}_{HP} \leq \dot{Q}_{HP,max}$$

<div align="right">Eq. 4-76</div>

As already mentioned, a consideration of the lower constraint is not possible in the optimization algorithm. This results in the range of $0 - \dot{Q}_{HP,min}$ for the manipulated variable determined by the optimization. This effect can already be seen in Figure 4-25 and Figure 4-26. Within 2-3 hours of the prediction horizon the trajectory falls below the lower constraint. For this situation a rule is defined in Eq. 4-77. This rule is already used in the conversion of the convective heat flows into disturbances and is further necessary for the calculation of the frequency which is sent to the compressor.

$$\dot{Q}_{HP} = \begin{cases} \dot{Q}_{HP,min} & if & \dfrac{\dot{Q}_{HP,min}}{2} \leq \dot{Q}_{HP} \leq \dot{Q}_{HP,min} \\ 0 & if & 0 \leq \dot{Q}_{HP} < \dfrac{\dot{Q}_{HP,min}}{2} \end{cases}$$

<div align="right">Eq. 4-77</div>

The impact of this rule on the controlled variable is demonstrated by Figure 4-29. The left side of this figure is equal to Figure 4-26. At the point when the required heat flow falls

below $\dot{Q}_{HP,min}/2$ the temperature in the thermal storage stops increasing. The reason for this is that the rule introduced by Eq. 4-77 is already considered. This means that only a part of the heat flow determined by the optimization is used (values in the range $0 \leq \dot{Q}_{HP} < \dot{Q}_{HP,min}/2$ are not considered) which leads, similar to a higher termination criterion, to a deviation with respect to the reference temperature. A way to avoid values in this range would be to penalize the corresponding range in the prediction horizon with a high weight for the manipulated variable. To achieve that, the result of the iterative optimization is used to determine the range of the time horizon where values of the manipulated variable are below $\dot{Q}_{HP,min}/2$. Then the iterative optimization is performed again penalizing this range with a high weight. The effect of this method is shown on the right side of Figure 4-29. The deviation with respect to the reference temperature is reduced and fewer values of the manipulated variable are below $\dot{Q}_{HP,min}/2$. The effect of this method in the simulation, however, is probably not as pronounced as for the prediction results in the MPC. A reason for this is that only the first value of the resulting trajectory shown in Figure 4-29 is actually used for the compressor and the corrected values are normally at the end of the prediction horizon. This method increases the accuracy similar to a low termination criterion with less computational effort. The number of iterations for a low termination criterion lies about 40 iterations and with this method the iterative process has to be carried out twice with only 10 iterations in each loop.
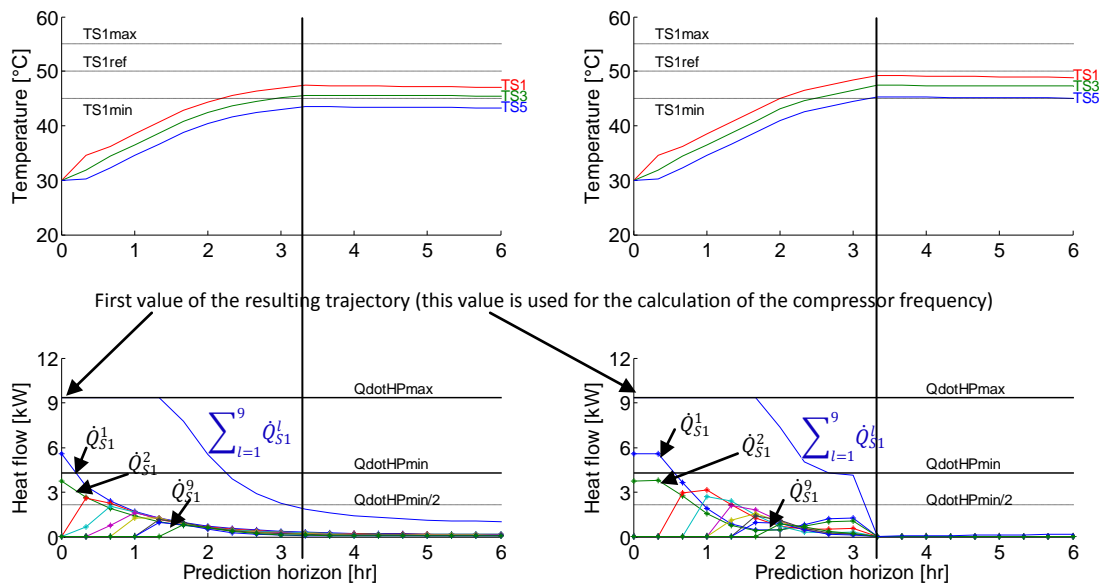
Figure 4-29: Resulting trajectories within the prediction horizon without an additional correction of the manipulated variable (left) and with an additional correction of the manipulated variable (right)

d)   Variable constraints on the manipulated variable

If the operating range of the compressor, presented in chapter 3.3.3, is considered a similar situation as with the COP arises (see chapter 4.3.4). This is because the constraints on the

manipulated variable depend on the compressor speed and the water temperature at the inlet of the condenser. Possible frequencies have to be chosen with the refrigerant condensing temperature T_{cr} and the refrigerant evaporating temperature T_{er} according to the envelopes provided by the manufacturer (see chapter 3.3.3). The condensing and evaporating temperatures are determined with the equations found in chapter 4.1.4. Based on this data the constraints for the heat flow can be written with Eq. 4-78 and Eq. 4-79.

$$\dot{Q}_{HP,min} = g(T_{cr}(f,T_{ci}), T_{er}(f,T_{ci})) \qquad \text{Eq. 4-78}$$

$$\dot{Q}_{HP,max} = g(T_{cr}(f,T_{ci}), T_{er}(f,T_{ci})) \qquad \text{Eq. 4-79}$$

The operating range of the compressor cannot be considered in the iteration for the convective heating process because for increasing frequencies the range decreases. This may lead to the situation that with an additional $\dot{Q}_{S1}^{l}$ the envelope is left. This is shown in Figure 4-30 with the points 1 and 2. For instance, point 1 is reached with the frequency of $f = 75\ Hz$ the maximum possible frequency would be $f = 117\ Hz$. If the frequency will be increased even the condensing temperature increases (see point 2). This would lead to an irreversible violation of the constraint. Therefore, the variable constraints lead to an additional call of the iterative optimization. The illustrated points 3,4 are discussed in connection with Figure 4-32.
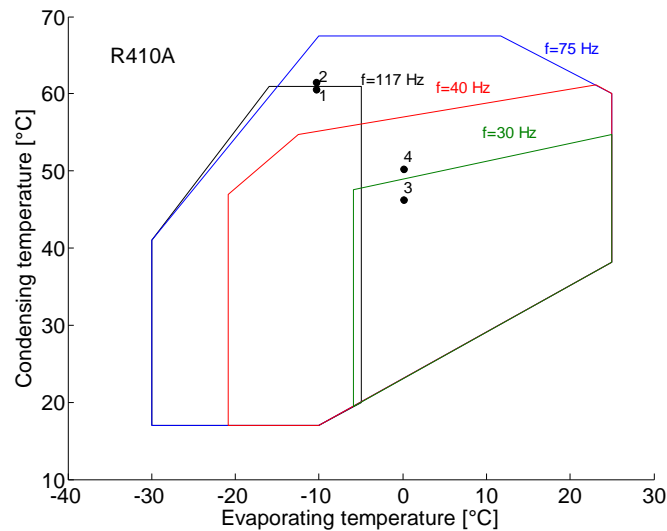
Figure 4-30: Resulting trajectories within the prediction horizon including variable constraints

Figure 4-31 shows the MPC-routine including the loop for the consideration of the variable constraints. The loop for the variable constraints is superior to the loop for the simulation of the convective heat flows. The routine starts with the preparation of the external input variables. At this point the trajectory of the constraints of the last call of the MPC-routine may be used with shifted values. Then the iterations for the simulation of the convective heat flows are performed. If the termination criterion is fulfilled the additional loop for the

variable constraints is processed. This starts with the calculation of the condensing and evaporating temperatures $(T_{cr,k+i|k}, T_{er,k+i|k})$ based on the required heat flows $\sum_{l=1}^{L} \dot{Q}_{S1,k+i|k}^{l}$. Then the constraints $(\dot{Q}_{HP,max,k+i|k}, \dot{Q}_{HP,min,k+i|k})$ are calculated. The upper constraints $\dot{Q}_{HP,max,k+i|k}$ are directly used within the MPC. Then the iterative optimization is performed again under consideration of these new constraints. After this the first value of the lower constraint $\dot{Q}_{HP,min,k|k}$ is used for the conversion of the heat flow into the compressor frequency which finishes the MPC-routine.
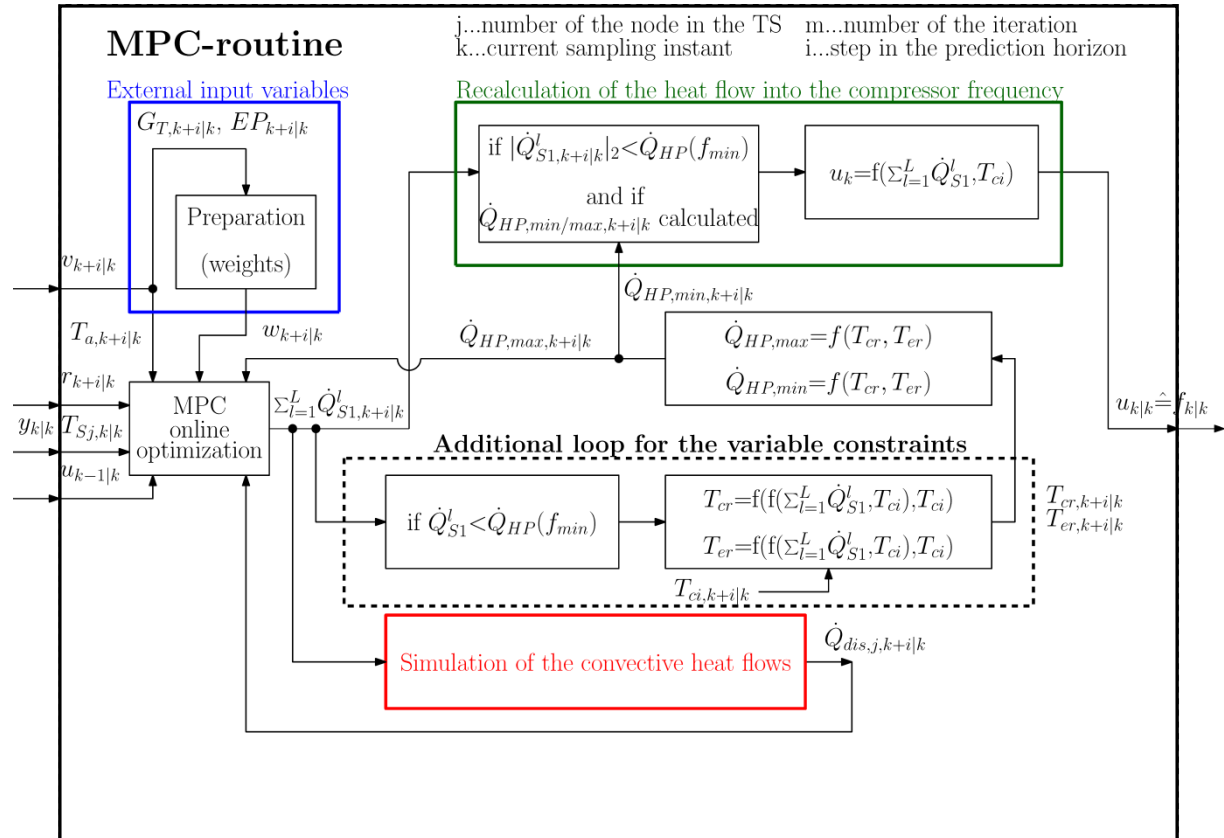
Figure 4-31: Detailed overview of the routines during a MPC call including the variable constraints of the compressor

Figure 4-32 shows the variable constraints within the prediction horizon. The top figure shows the curve of the storage temperatures resulting of the heat flow trajectory in the middle figure. At the bottom the curve of the condensing T_{cr} and evaporating T_{er} temperature is shown. The change of the lower constraints occurs at two successive sampling instants as the envelope of $30\ Hz$ is left (compare with the points 3,4 in Figure 4-30).
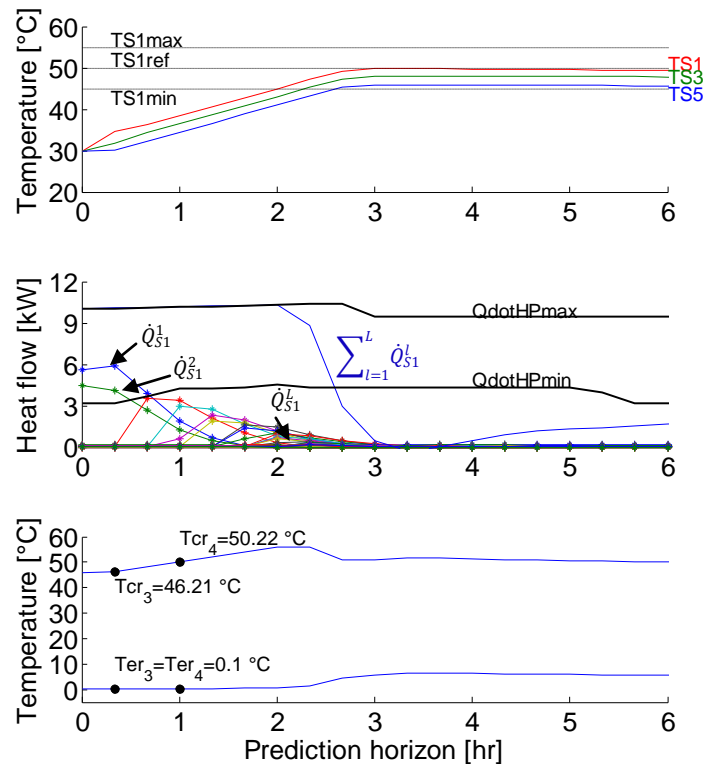
Figure 4-32: Curve of the condensing and evaporating temperature within the prediction horizon

The consideration of the variable constraints for the compressor speed leads to an additional loop. An alternative would be to choose constant constraints for the expected operating range in the MPC. Then solely the frequency, which is set as compressor speed in the plant has to be monitored if it is inside the envelope. This is recommended, as the variable constraints cannot be considered in the iteration for the convective heating process. Furthermore, the accuracy for the variable constraints based on the envelopes for ten different frequencies is low. However, whether a consideration of the variable constraints in the optimization is necessary has to be evaluated with long term simulations.

4.4.4 ECR factors

The ECR factors are used to soften the constraints. These are mainly used for the constraints on the output variables. In this work they are also used for the manipulated variable. This is because the iterative determination of the control move may lead to a violation of the constraints. As high values of the ECR factors lead to soft constraints, the factors for the softening are chosen low. A reason for this is that low ECR factors avoid an unstable system if the constraints are violated. On the other hand, if the ECR factors are chosen too high unnecessary violations may occur. The parameter settings are for all simulation the same (see Table 4-6). The value of the ECR factor for the upper constraint of the controlled

variable $ECR^{y,max}$ is set to a high value. This is as the upper limit for the controlled variable is negligible (see chapter 4.4.3). The values for the ECR factor of lower constraint on the controlled variable $ECR^{y,min}$ and the ECR factors of the lower and upper constraints on the manipulated variable ($ECR^{u_{min}}$, $ECR^{u_{max}}$) are chosen very low to avoid unnecessary violations of the corresponding constraints. The ECR factors for the lower and upper constraints of the manipulated variables rate are defined as hard constraints. This is as these limits cannot be violated with the time step of the MPC.

Table 4-6: Parameter settings for the ECR factors

Parameter	Value [-]
$ECR^{y,max}$	10
$ECR^{y,min}$	10^{-3}
$ECR^{u_{min}}$	10^{-3}
$ECR^{u_{max}}$	10^{-3}
$ECR^{\Delta u_{min}}$	0
$ECR^{\Delta u_{max}}$	0

5   Results and discussion

The simulation results presented in this chapter are based on a simplified TRNSYS model. This has two reasons, firstly, the load profiles of the reference system used in the project "The Bat" are not finished yet and, secondly, simulations including the building lead to higher computation time. Therefore, the TRNSYS model in these simulations is based on the model used in the work of Pichler (see Pichler et al., 2014). This model is used in an adapted form, the solar thermal system and the auxiliary heater are removed and the photovoltaic system and the heat pump are added. The thermal storage has a total volume of $1200 \, l$. This is a deviation from the reference system. The load profile which is used in these simulations represents DHW demand and SH. Both loads are directly coupled to the thermal storage (see Figure 5-1). This is another deviation from the reference system. As in the reference system the heat pump is directly coupled to the building and/or the thermal storage (see chapter 3).
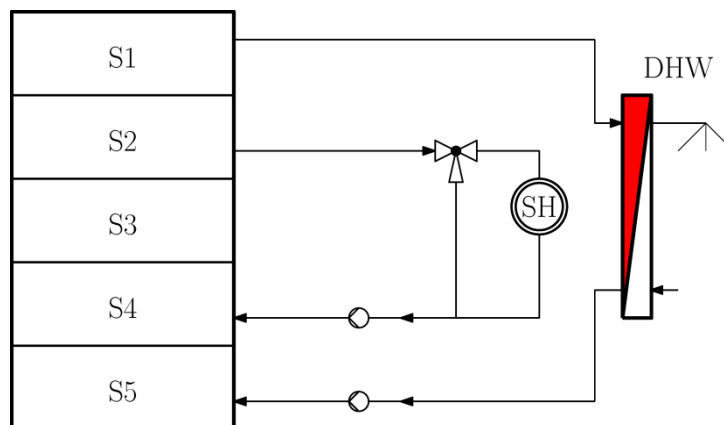
Figure 5-1: Connections of the loads to the thermal storage used for the simulations

The reason why SH was not removed for the simulations is that additional disturbances represent no further simplification but rather a more complicated situation. An exemplary of the load profile is shown in Figure 5-2. The simulation results concerning the thermal input into the thermal storage as well as the energy consumption of the compressor are significantly different among each simulation. The reason for this is linked with the load profiles and cannot be explained due to lack of time. Therefore, the simulation results obtained with these load profiles can only be interpreted qualitatively. Despite these differences, the simulation results can be used for the further implementation of the MPC in the reference system used in the project "The Bat".
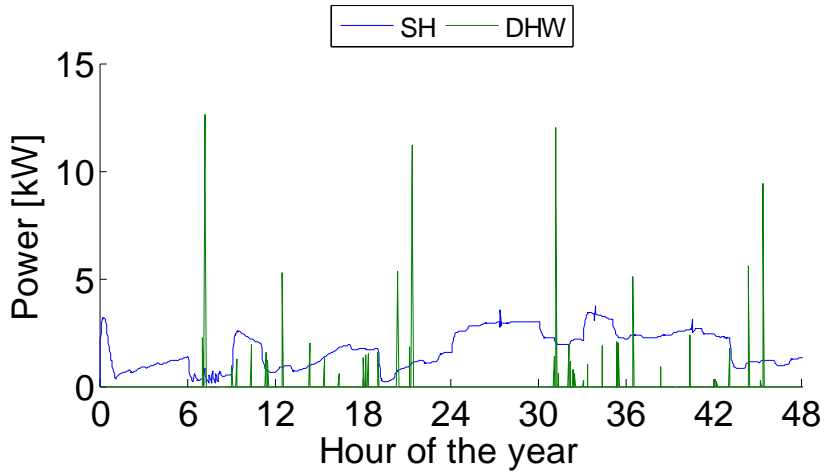
Figure 5-2: Exemplary load profiles for SH and DHW

5.1 Review on the boundary conditions for the simulations

The simulations for different hydraulic circuits and controlled variables of the MPC are compared with simulations based on the classical control concept. The classical control uses a hysteresis to switch the heat pump on if the controlled temperature in the thermal storage falls below $45\,°C$ and off if the controlled temperature in the thermal storage exceeds $50\,°C$. The sensor position to monitor the controlled temperature was set, in accordance with the MPC, to the height of the top node or the height of the middle node. The compressor frequency for the classical control is set to $75\,Hz$ as this frequency covers the largest operating range. This is a disadvantage of the classical control compared to the MPC. The reason for this simplification is that a control concept for a hysteresis with variable compressor speed has not been available.

The relevant parameter settings for the MPC are shown in Table 5-1. These are the prediction horizon p, the control horizon m, the sampling time $\Delta\tau_{MPC}$, the constant value for the weight of the manipulated variable w^{Base} and the constant value for the weight of the manipulated variable rate $w^{\Delta u}$. In the following simulations the effect of the COP on the weights is not considered (see chapter 4.3.4). This means $w^{COP} = 1$. Furthermore, the variable constraints on the manipulated variable are not considered (see chapter 4.4.3d). The minimum for the compressor frequency is set to $f_{min} = 40\,Hz$ and the maximum is set to $f_{max} = 90\,Hz$. The resulting upper constraints on the manipulated variable u_{max} is the heat output at the frequency f_{max}. The upper constraint is different for *mode one* (heat pump with condenser) and *mode two* (heat pump with condenser and desuperheater) of the heat pump. The lower constraint on the manipulated variable u_{min} is zero (see chapter 4.4.3). The upper constraint on the manipulated variable rate Δu_{max} is calculated with equation Eq. 4-72. The theoretical behavior (see chapter 4.4.3) is clear if this value is compared with the upper constraint on the manipulated variable. The value of u_{max} is lower

than the value Δu_{max}. The value for the lower constraint on the manipulated variable rate Δu_{min} is set, as already mentioned, to a very high value to enable quick switching off. The values for the reference y_{ref} and the constraints on the controlled variable y_{min}, y_{max} are chosen similar to the classical control concept. The termination criterion for the iterative optimization of the required heat flow into the thermal storage is set to $\dot{Q}_{HP,min}$. The manipulated variable is corrected for the range of $0 - f_{min}$ with Eq. 4-77. To avoid frequencies below f_{min} the weights are updated in another loop to penalize these values (see Figure 4-29). The ECR values were already shown in Table 4-6. Furthermore, predictions of DHW demand are not considered. The comparison of the simulation results in chapter 5.2.1, chapter 5.2.2 and chapter 5.3 does not consider the differing energy content at the end of the simulation.

Table 5-1: Parameter settings of the MPC application

Parameter	Value
$p \ [hr]$	24
$m \ [hr]$	8
$\Delta\tau_{MPC} \ [min]$	20
$w^{Base} \ [-]$	1
$w^{\Delta u} \ [-]$	0.5
$\Delta u_{min} \ [kW \ per \ \Delta\tau_{MPC}]$	-Inf
$\Delta u_{max} \ [kW \ per \ \Delta\tau_{MPC}]$	14.1
$u_{min} \ [kW]$	0
$u_{max,mode \ 1} \ [kW]$	9
$u_{max,mode \ 2} \ [kW]$	9.3
$y_{ref} \ [°C]$	50
$y_{min} \ [°C]$	45
$y_{max} \ [°C]$	55

5.2 Analysis of the results based on two day simulations

This chapter analyzes the results based on two day simulations. The aim of these simulations is to show the effect on the temperature at the top node. This is the relevant temperature for the comfort limit as DHW draw off is taken from the top node. The comfort limit of $45 \ °C$ was defined in chapter 3.1. The load profiles for these two days represent a DHW demand of approximately 41 kWh/48h and SH demand of 82 kWh/48h. The heat losses of the thermal storage to the ambient were not recorded.

Firstly, the *temperature at the top node of the thermal storage is set as controlled variable* (see Figure 5-3 left). The results show that the *temperature at the top node as controlled variable* leads to violations of the comfort limit for all hydraulic circuits. Secondly, the

temperature at the middle node of the thermal storage is set as controlled variable (see Figure 5-3 right). This configuration fulfills the comfort limits for all hydraulic circuits significantly better.
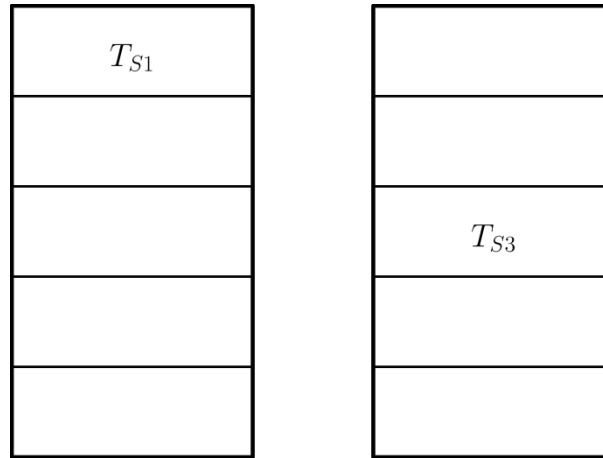
Figure 5-3: Temperature at the top node as controlled variable (left) and temperature at the middle node as controlled variable (right)

The figures presented in the subchapters 5.2.1 and 5.2.2 show the simulation results of the classical control on the left and the simulation results of the MPC on the right. In subchapter 5.2.1 the *temperature at the top node is the controlled variable* and in subchapter 5.2.2 the *temperature at the middle node is the controlled variable*. The upper figures show the curve of the storage temperatures the lower figures show the frequency of the compressor on the left ordinate and the weight on the right ordinate. The classical control does not consider the weights. Nevertheless, the weights are illustrated for a better comparison of the operating times between the two control concepts.

5.2.1 Temperature at the top node as controlled variable

These simulations are based on the linear model where the *controlled variable is the temperature at the top node* and the required heat flow is assumed to be injected into the top node (see chapter 4.2.3). The *temperature at the top node as controlled variable* has the advantage that a small volume is held at a higher temperature level. This leads to an energy saving potential. The drawback of this method is that large disturbances lead to a violation of the comfort limits. The MPC has one advantage over the classical control. This is that the controlled variable has to be held at the reference temperature. Therefore, the MPC is able to switch on, depending on the weight, before the comfort limit is violated. The classic control switches on when the temperature falls below the set value $(45\ °C)$ which is equal to the comfort limit.

a)   Hydraulic circuit HC1

Figure 5-4 shows the simulation results of hydraulic circuit HC1 (see Figure 4-8). Both control concepts are incapable to hold the temperature of the top node within the comfort limits. The classical control shows a higher violation of the comfort limit than the MPC. This is due to the already mentioned advantage of the MPC.

The MPC already shows a desired behavior. The low weight at hour 13 is used to raise the temperature to the reference value (see marking at hour 13). Another effect is shown at hour 42. The temperature at the top node decreases although the heat pump is operating. This is due to the hydraulic circuit. The water at the bottom has a temperature of $30\,°C$. The temperature is increased in the heat exchanger by $5\,K$ and the heated water is inserted at the top with $35\,°C$. This leads to a further decrease of the temperature at the top node until the temperature at the bottom is increased (see marking at hour 42). The violation is not as high as with the classical control. However, it has to be mentioned that this example at hour 42 does not represent the worst case. Higher violations may occur with higher disturbances or if the weight is at the maximum value.
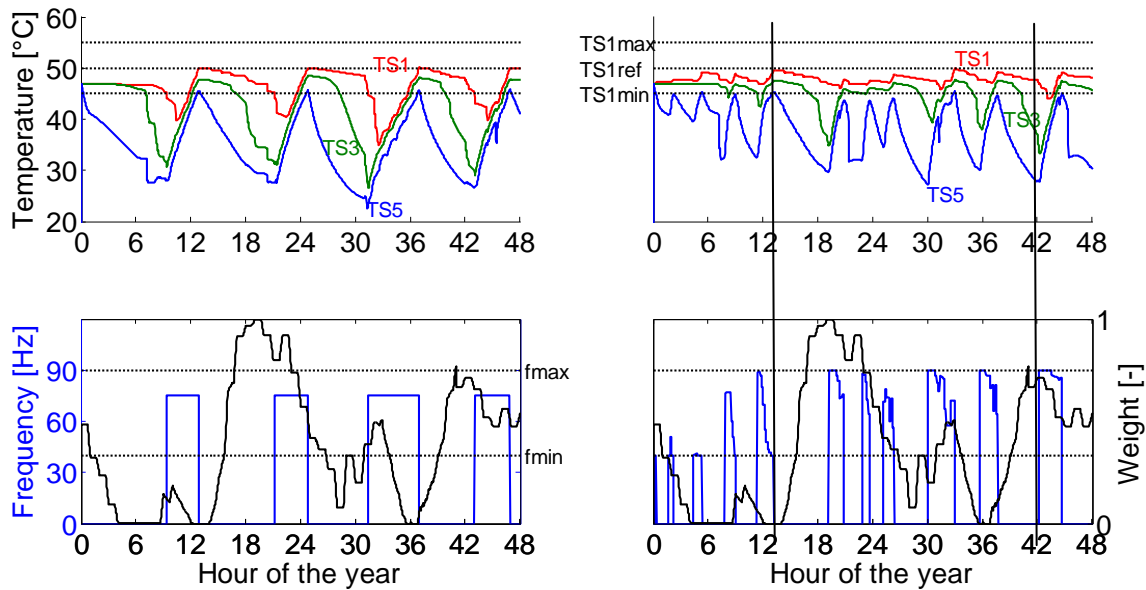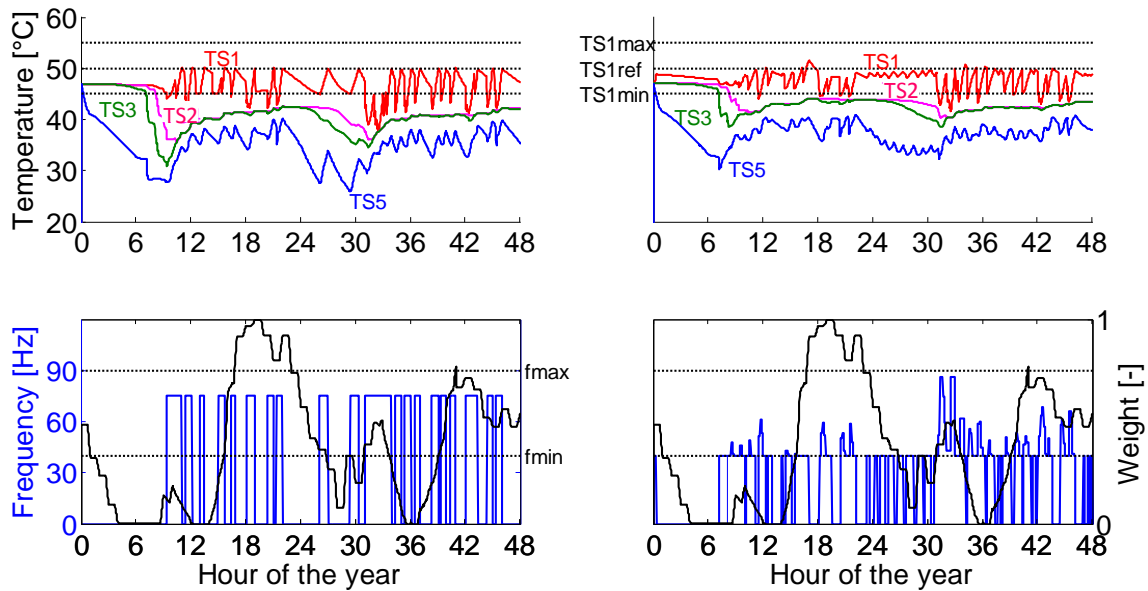

Figure 5-4: Simulation results of two days for the thermal storage connected to the condenser with the top and bottom node without desuperheater (HC1); controlled variable is the temperature at the top node of the thermal storage, classical control (left), MPC (right)

Table 5-2 shows the simulation results obtained for hydraulic circuit HC1. The values for electrical energy consumption of the compressor $W_{Comp,48h}$ and the heat supplied by the condenser $Q_{c,48h}$ are provided but the amount differs significantly among all simulations. The reason for this is assumed to be linked with the load profiles but this could not be confirmed due to lack of time. Therefore, these values are not suitable to make direct comparisons. Despite this the mean frequency $f_{mean,48h}$, the number of operating cycles of

the heat pump $\#_{cycles,48h}$, the mean operating time of the heat pump $\tau_{on,mean,48h}$ and the mean node temperatures of the thermal storage $T_{sj,mean,48h}$ can be interpreted. The MPC achieves a similar compressor frequency as the classical control. The number of operating cycles is higher and the mean operating time is lower with the MPC resulting in a negative impact on the COP's. Furthermore, the mean node temperatures achieved with the MPC are higher with smaller standard deviations. The small temperature fluctuation of the upper nodes is due to the higher number of operating cycles.

Table 5-2: Comparison of the two day simulation results of the classical control with the two day simulation results of the MPC for hydraulic circuit HC1, controlled variable is the temperature at the top node of the thermal storage

Quantity	Value (classical control)	Value (MPC)
$W_{Comp,48h}\ [kWh]$	35.3	34.8
$Q_{c,48h}\ [kWh]$	128	117
$f_{mean,48h}\ [Hz]$	75	74
$\#_{cycles,48h}\ [-]$	4	11
$\tau_{on,mean,48h}\ [hr]$	4.1	1.4
$T_{S1,mean,48h}\ [°C]$	46.4±3.4	47.9±1.6
$T_{S2,mean,48h}\ [°C]$	44.4±4.7	46.6±2
$T_{S3,mean,48h}\ [°C]$	41.8±5.9	45±3.2
$T_{S4,mean,48h}\ [°C]$	38±6.6	41.5±5
$T_{S5,mean,48h}\ [°C]$	34.9±6	37.5±5.2

b) Hydraulic circuit HC2

Figure 5-5 shows the simulation results for hydraulic circuit HC2 (see Figure 4-10). The violation of the comfort limit is higher than in the simulation results of the hydraulic circuit HC1. The reason for this is the higher time delay until the temperature at the top node increases compared to hydraulic circuit HC1. This is caused by the mixing process with the lower nodes due to natural convection.

Table 5-3 shows the simulation results obtained for hydraulic circuit HC2. The values can be interpreted similar to the simulation results obtained for hydraulic circuit HC1 (see chapter 5.2.1a).
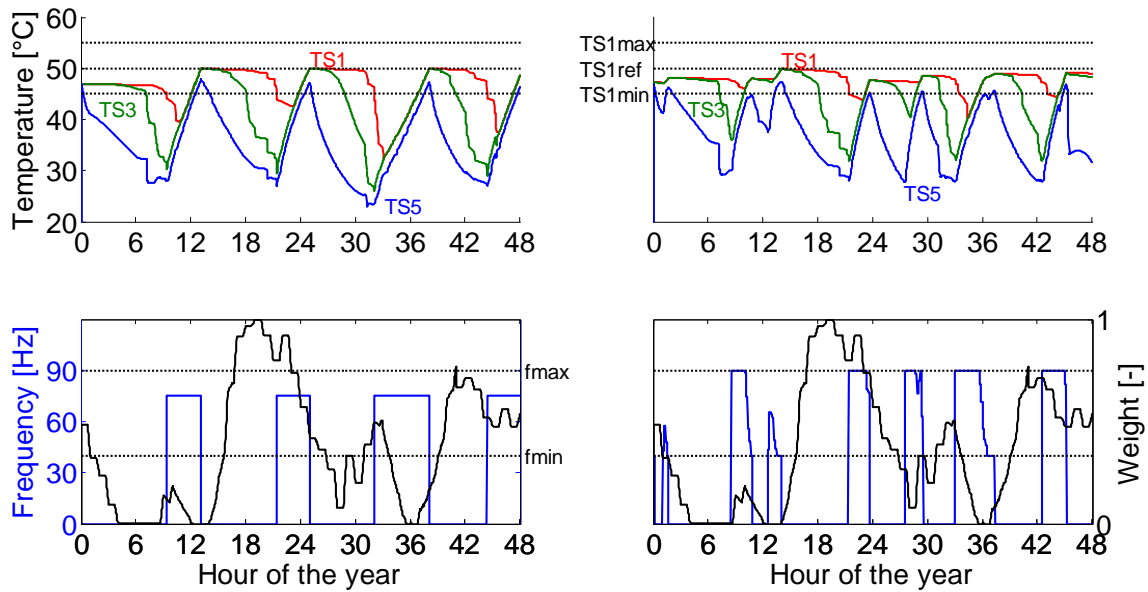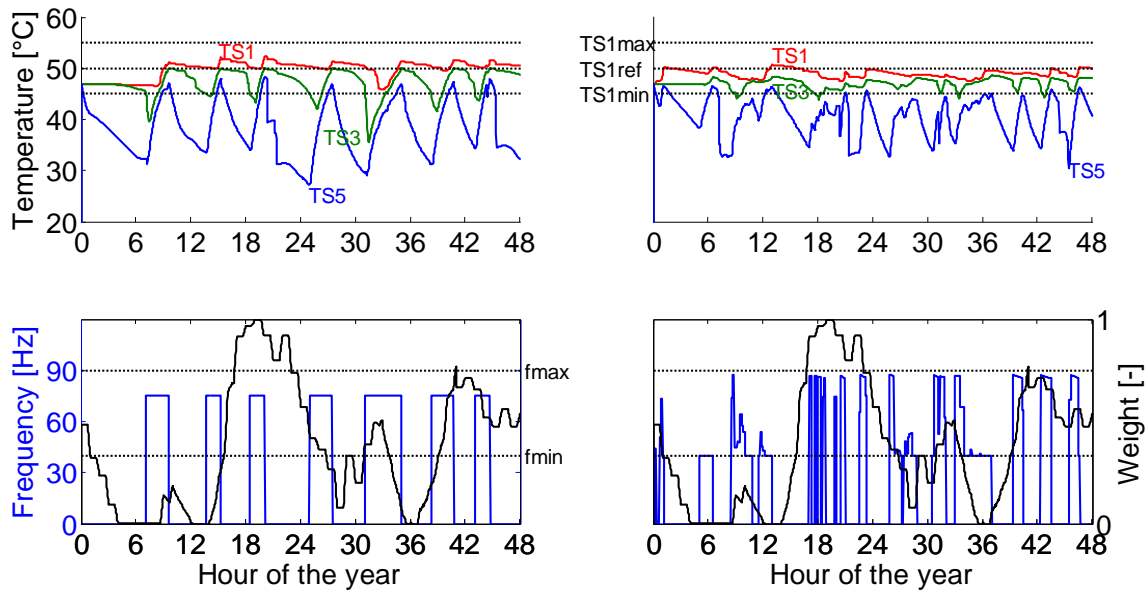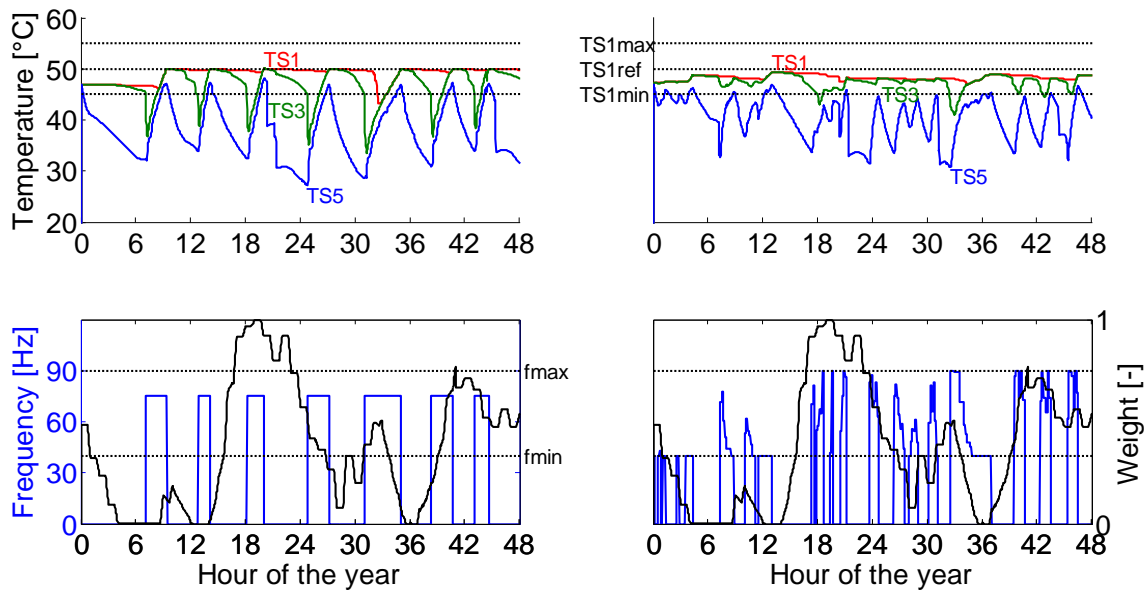
Figure 5-5: Simulation results for the thermal storage connected to the condenser with the middle and bottom node without desuperheater (HC2); controlled variable is the temperature at the top node of the thermal storage, classical control (left), MPC (right)

Table 5-3: Comparison of the two day simulation results of the classical control with the two day simulation results of the MPC for hydraulic circuit HC2, controlled variable is the temperature at the top node of the thermal storage

Quantity	Value (classical control)	Value (MPC)
$W_{Comp,48h}\ [kWh]$	37	37.5
$Q_{c,48h}\ [kWh]$	132	125
$f_{mean,48h}\ [Hz]$	75	77.6
$\#_{cycles,48h}\ [-]$	4	8
$\tau_{on,mean,48h}\ [hr]$	4.3	2
$T_{S1,mean,48h}\ [°C]$	46.4$\pm$4.2	47.8$\pm$2
$T_{S2,mean,48h}\ [°C]$	44.6$\pm$5.4	46.6$\pm$3.5
$T_{S3,mean,48h}\ [°C]$	42.2$\pm$6.6	44.7$\pm$5
$T_{S4,mean,48h}\ [°C]$	38.2$\pm$6.9	41$\pm$6.1
$T_{S5,mean,48h}\ [°C]$	35.1$\pm$6.3	37.1$\pm$5.7

c)   Hydraulic circuit HC3

Figure 5-6 shows the simulation results for the hydraulic circuit HC3 (see Figure 4-12). The operating times of the heat pump are significantly shorter and much more frequently than in the results of the simulations for the hydraulic circuits HC1 and HC2. This occurs with the classical control concept as well as with the MPC. A further insight of this simulations is that the number of comfort violations increases with the number of operating cycles of the heat pump.

In hydraulic circuit HC3 the top node is rapidly heated to the reference temperature with the high temperature of the water mass flow at the desuperheater outlet. However, the influence of the desuperheater on node two is low. Node two is mainly heated with the heat flow of the condenser due to the mixing process with node three caused by natural convection. The heat flow of the condenser is further used to heat node three and the lower nodes due to forced convection. This leads to a higher temperature difference between the top node and the nodes below and results in the sudden changes of the temperature at the top node, as with a draw off a mixing with the lower temperature of node two occurs. Another difference to the hydraulic circuits HC1 and HC2 is that the MPC operates the heat pump at lower frequencies. This is also a result of the rapid heating process of the top node with the desuperheater.
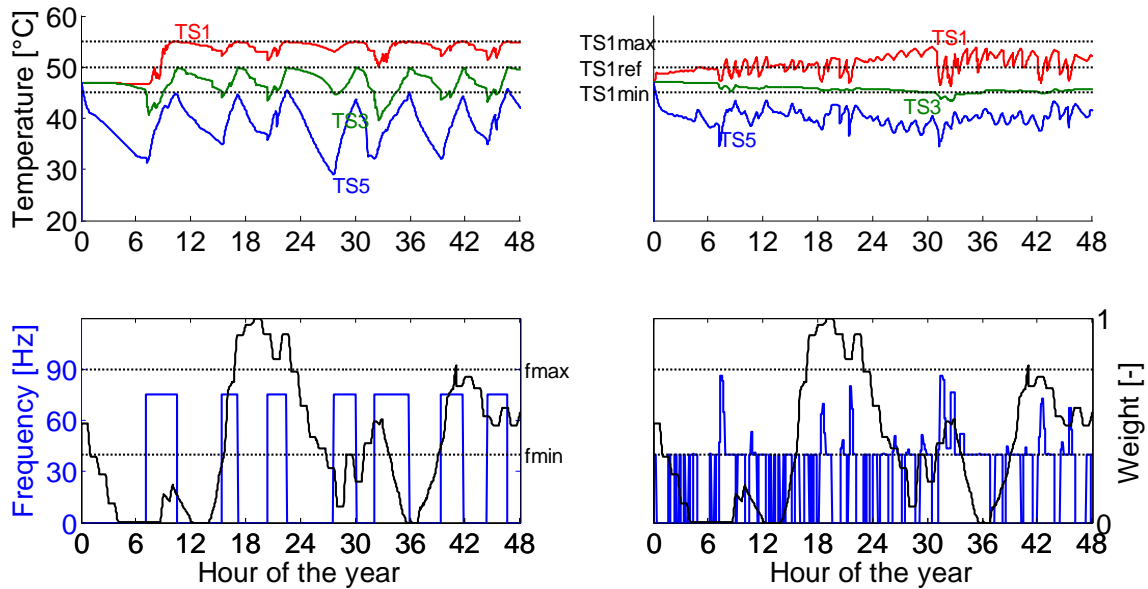

Figure 5-6: Simulation results for the thermal storage connected to the condenser with the middle and bottom node with desuperheater (HC3); controlled variable is the temperature at the top node of the thermal storage, classical control (left), MPC (right)

Table 5-4 shows the simulation results obtained for hydraulic circuit HC3. As already mentioned, the electrical energy consumption of the compressor $W_{Comp,48h}$ and the heat input into the thermal storage $Q_{c+d,48h}$ are not suitable for a direct comparison. The mean operating time $\tau_{on,mean,48h}$ achieved with the MPC is, despite the higher number of operating cycles $\#_{cycles,48h}$, equal to the mean operating time achieved with the classical control. This is due to the lower mean frequency $f_{mean,48h}$ achieved with the MPC. The positive impact of the lower compressor frequencies on the COP's is partly cancelled by the higher starting losses due to the higher number of operating cycles with the MPC. Furthermore, the mean storage temperatures $T_{sj,mean,48h}$ show the high temperature difference of node one and node two compared to the small temperature difference of node two and node three.

Table 5-4: Comparison of the two day simulation results of the classical control with the two day simulation results of the MPC for hydraulic circuit HC3, controlled variable is the temperature at the top node of the thermal storage

Quantity	Value (classical control)	Value (MPC)
$W_{Comp,48h}\ [kWh]$	33.8	34.1
$Q_{c+d,48h}\ [kWh]$	126.1	125.9
$f_{mean,48h}\ [Hz]$	75	45
$\#_{cycles,48h}\ [-]$	20	31
$\tau_{on,mean,48h}\ [hr]$	0.9	0.9
$T_{S1,mean,48h}\ [°C]$	46.7$\pm$2.6	47.8$\pm$2.1
$T_{S2,mean,48h}\ [°C]$	41.6$\pm$3	43.6$\pm$2.1
$T_{S3,mean,48h}\ [°C]$	40.8$\pm$3.5	43$\pm$2.3
$T_{S4,mean,48h}\ [°C]$	38.5$\pm$4	41.3$\pm$2.5
$T_{S5,mean,48h}\ [°C]$	35$\pm$3.7	37.3$\pm$2.6

5.2.2 Temperature at the middle node as controlled variable

These simulations are based on the linear model where the *controlled variable is the temperature at the middle node* and the required heat is assumed to be injected into the middle node (see chapter 4.2.3). With this setting almost all comfort violations are eliminated. Only the classical control concept based on hydraulic circuit HC2 shows a violation of the comfort limit.

The *temperature at the middle node as controlled variable* holds the thermal storage at a higher temperature level. This leads, as already mentioned to higher electrical energy consumptions. Furthermore, the operating cycles of the heat pump are shorter and more frequently. This may be reduced by the MPC through an increased value for the weight of the manipulated variable $w^{\Delta u}$.

a) Hydraulic circuit HC1

Figure 5-7 shows the simulation results for the hydraulic circuit HC1 (see Figure 4-8). The mean temperature of the top node, achieved with the classical control, is higher than the mean temperature achieved with the MPC. The reason for this is that the classical control switches off if the temperature at the middle node exceeds $50\ °C$. The MPC switches off in a range below the reference temperature depending on the weight.

Table 5-5 shows the simulation results obtained for hydraulic circuit HC1. As already mentioned, the electrical energy consumption of the compressor $W_{Comp,48h}$ and the heat input into the thermal storage $Q_{c,48h}$ are not suitable for a direct comparison. Despite this, a further comparison with the simulation results presented in chapter 5.2.1a shows a higher number of operating cycles $\#_{cycles,48h}$ and a lower operating time of the heat pump

$\tau_{on,mean,48h}$ for the MPC and the classical control. This is due to the higher storage volume which has to be held at the required temperature. Furthermore, the MPC achieved a lower mean compressor frequency $f_{mean,48h}$ compared to the simulation results presented in chapter 5.2.1a. This is due to lower thermal input needed to heat the thermal storage to the required temperature as the mean node temperatures of the thermal storage $T_{sj,mean,48h}$ are higher than in the simulations with the temperature at the top node as controlled variable.

Figure 5-7: Simulation results for the thermal storage connected to the condenser with the top and bottom node without desuperheater (HC1); controlled variable is the temperature at the middle node of the thermal storage, classical control (left), MPC (right)

Table 5-5: Comparison of the two day simulation results of the classical control with the two day simulation results of the MPC for hydraulic circuit HC1, controlled variable is the temperature at the middle node of the thermal storage

Quantity	Value (classical control)	Value (MPC)
$W_{Comp,48h}\ [kWh]$	37.4	37.7
$Q_{c,48h}\ [kWh]$	124	124
$f_{mean,48h}\ [Hz]$	75	60.8
$\#_{cycles,48h}\ [-]$	7	19
$\tau_{on,mean,48h}\ [hr]$	2.3	1.1
$T_{S1,mean,48h}\ [°C]$	49.8$\pm$2.1	48.9$\pm$1.5
$T_{S2,mean,48h}\ [°C]$	48.9$\pm$2.1	48$\pm$1.5
$T_{S3,mean,48h}\ [°C]$	47.2$\pm$2.9	47$\pm$1.6
$T_{S4,mean,48h}\ [°C]$	42.7$\pm$4.8	44.8$\pm$2.9
$T_{S5,mean,48h}\ [°C]$	38.1$\pm$5.3	40.5$\pm$3.9

b)   Hydraulic circuit HC2

Figure 5-8 shows the simulation results of the hydraulic circuit HC2 (see Figure 4-10). The simulation results of the classical control show a violation of the comfort criterion. This occurs at hour 33, at this time occurs also the largest violation in the simulation for hydraulic circuit HC2 with the *temperature at the top node as controlled variable* (see Figure 5-5).

Figure 5-8: Simulation results for the thermal storage connected to the condenser with the middle and bottom node without desuperheater (HC2); controlled variable is the temperature at the middle node of the thermal storage

Table 5-6 shows the simulation results obtained for hydraulic circuit HC2. The change of the number of operating cycles $\#_{cycles,48h}$, lower mean operating time $\tau_{on,mean,48h}$ and mean frequency $f_{mean,48h}$ compared to the simulation results of chapter 5.2.1b can be interpreted similar to the simulation results obtained for hydraulic circuit HC1 (see chapter 5.2.2a).

Table 5-6: Comparison of the two day simulation results of the classical control with the two day simulation results of the MPC for hydraulic circuit HC2, controlled variable is the temperature at the middle node of the thermal storage

Quantity	Value (classical control)	Value (MPC)
$W_{Comp,48h}\ [kWh]$	36.4	36.8
$Q_{c,48h}\ [kWh]$	121	122
$f_{mean,48h}\ [Hz]$	75	60
$\#_{cycles,48h}\ [-]$	7	20
$\tau_{on,mean,48h}\ [hr]$	2.3	1
$T_{S1,mean,48h}\ [°C]$	49$\pm$1.9	48.3$\pm$1.4
$T_{S2,mean,48h}\ [°C]$	48.6$\pm$2.3	48$\pm$1.5
$T_{S3,mean,48h}\ [°C]$	46.8$\pm$3.5	47.4$\pm$1.8
$T_{S4,mean,48h}\ [°C]$	42.5$\pm$4.7	44.9$\pm$3.3
$T_{S5,mean,48h}\ [°C]$	37.9$\pm$5.3	40.4$\pm$4.2

c)   Hydraulic circuit HC3

Figure 5-9 shows the simulation results of the hydraulic circuit HC3 (see Figure 4-12). The simulation results show the highest mean temperature at the top node for both control concepts compared to the hydraulic circuits HC1 and HC2.

Figure 5-9: Simulation results for the thermal storage connected to the condenser with the middle and bottom node with desuperheater (HC3); controlled variable is the temperature at the middle node of the thermal storage

Table 5-7 shows the simulation results for the hydraulic circuit HC3. A comparison with the simulation results presented in chapter 5.2.1c shows that the classical control achieves a significantly reduced number of operating cycles $\#_{cycles,48h}$. This is due to the hysteresis which heats up the middle node to a higher temperature than the MPC. The number of operating cycles is further increased with the MPC. The operating time $\tau_{on,mean,48h}$ and the mean compressor frequency $f_{mean,48h}$ achieved with the MPC are further decreased compared to the simulation results presented in chapter 5.2.1c. These results may be improved due to a better adaption of the water temperature at the desuperheater outlet.

Table 5-7: Comparison of the two day simulation results of the classical control with the two day simulation results of the MPC for hydraulic circuit HC3, controlled variable is the temperature at the middle node of the thermal storage

Quantity	Value (classical control)	Value (MPC)
$W_{Comp,48h}\ [kWh]$	38.4	37.6
$Q_{c+d,48h}\ [kWh]$	140	128.6
$f_{mean,48h}\ [Hz]$	75	44.3
$\#_{cycles,48h}\ [-]$	7	39
$\tau_{on,mean,48h}\ [hr]$	2.6	0.8
$T_{S1,mean,48h}\ [°C]$	52.7$\pm$3.2	50.7$\pm$2.1
$T_{S2,mean,48h}\ [°C]$	50$\pm$2.8	46$\pm$1.4
$T_{S3,mean,48h}\ [°C]$	46.8$\pm$2.4	45.7$\pm$1.4
$T_{S4,mean,48h}\ [°C]$	42.6$\pm$3.9	44.5$\pm$1.7
$T_{S5,mean,48h}\ [°C]$	38.7$\pm$4	40.2$\pm$1.9

5.3 Analysis of the results based on annual simulations

The annual simulations are performed for each hydraulic circuit for the *temperature at the middle node as controlled variable*. The simulations show the robustness of the implemented MPC routine. As for this wide range of states no errors occurred. Furthermore, the compliance of the comfort limits can be presented for a longer period. The reduction of thermal energy input into the thermal storage can also not be evaluated for the annual simulations. The differences of thermal energy input among the simulations are more pronounced in the annual simulations than in the two day simulations. As already mentioned, the reason for this is assumed to be linked with the load profiles, but this cannot be confirmed. Therefore, also the SPF has to be evaluated carefully. In addition to the simulations of chapter 5.2, the amount of PV output used to drive the heat pump $W_{PV,used}$ is provided for the classical control and the MPC.

The annual load profiles represent a DHW demand of 8276 kWh/a and SH demand of 6411 kWh/a. The heat losses of the thermal storage to the ambient differ for each hydraulic cycle according to the temperature in the thermal storage. The heat losses of hydraulic cycle HC1 based on the classical control concept are approximately 477 kWh/a. The heat losses of the other hydraulic cycles were not recorded. The weather data represents the climate in Strasbourg. The annual PV output is approximately 2767 kWh/a.

a) Hydraulic circuit HC1

Figure 5-10 shows the curve of the temperature at the top node for the hydraulic circuit HC1 for an annual simulation. Both control concepts have rarely violations of the lower constraint. These violations occur through high disturbances caused by DHW and SH demand.
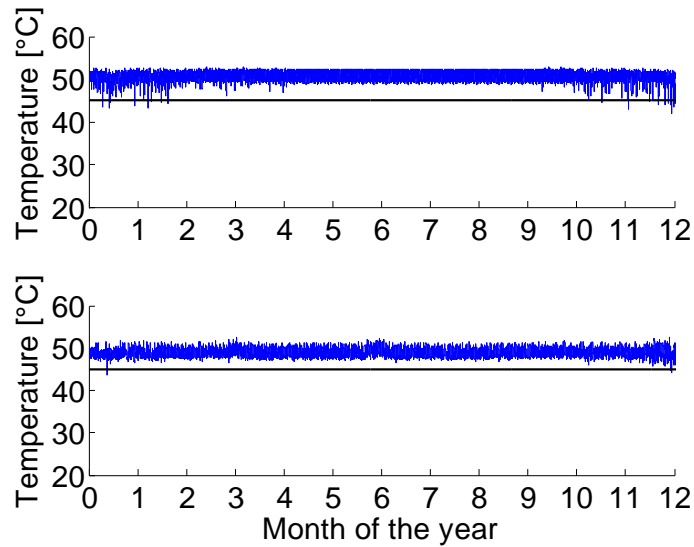
Figure 5-10: Annual simulation of the thermal storage connected to the condenser with the top and bottom node (HC1); based on the classical control (top), based on MPC (bottom)

Table 5-8 shows the simulation results of hydraulic circuit HC1. The values for the electrical energy consumption of the compressor W_{Comp} and the heat supplied by the condenser Q_c are unsuitable for a direct comparison. The lower SPF achieved with the MPC is mainly caused by the higher starting losses due to the higher number of operating cycles compared to the classical control. The mean frequency f_{mean}, the number of operating cycles of the heat pump $\#_{cycles}$, the mean operating time of the heat pump $\tau_{on,mean}$ and the mean node temperatures of the thermal storage $T_{sj,mean}$ are similar to the results of the two day simulation (see chapter 5.2.2a). The self consumption of PV output $W_{PV,used}$ achieved with the MPC is approximately 14 % higher than with the classical control concept.

Table 5-8: Comparison of the annual simulation results of the classical control with the annual simulation results of the MPC for hydraulic circuit HC1, controlled variable is the temperature at the middle node of the thermal storage

Quantity	Value (classical control)	Value (MPC)
W_{Comp} $[kWh]$	4808	4487
Q_c $[kWh]$	15754	14246
SPF $[-]$	3.28	3.17
$W_{PV,used}$ $[kWh]$	633	721
f_{mean} $[Hz]$	75	70.6
$\#_{cycles}$ $[-]$	967	2499
$\tau_{on,mean}$ $[hr]$	2.1	0.8
$T_{S1,mean}$ $[°C]$	50.8±0.9	49±1
$T_{S2,mean}$ $[°C]$	50±1.1	48±0.8
$T_{S3,mean}$ $[°C]$	48±2.2	47.1±0.9
$T_{S4,mean}$ $[°C]$	43±4.9	45.2±2.4
$T_{S5,mean}$ $[°C]$	38±5.4	40.7±3.9

b)   Hydraulic circuit HC2

Figure 5-11 shows the curve of the temperature at the top node for the hydraulic circuit HC2 for an annual simulation. As already seen in the two day simulation, the classical control is not able to hold the temperature at the top node within the comfort limits. The MPC shows rarely violations of the comfort limit.
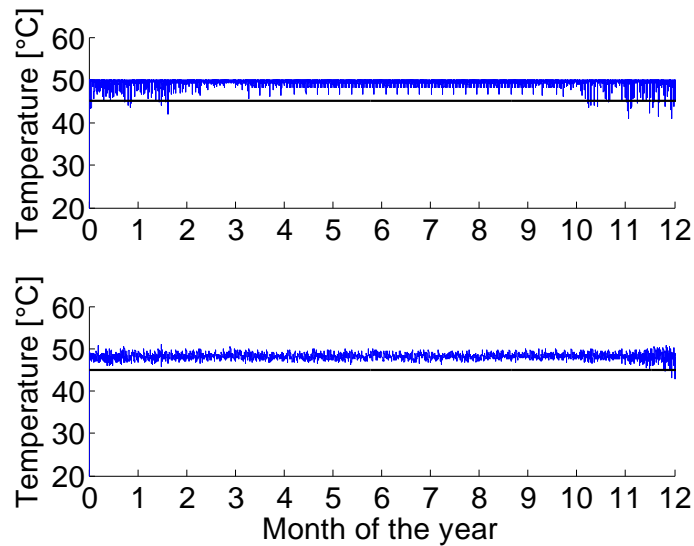
Figure 5-11: Annual simulation of the thermal storage connected to the condenser with the middle and bottom node (HC2); based on the classical control (top), based on MPC (bottom)

Table 5-7 shows the results of the annual simulation of hydraulic circuit HC2. The results are similar to those obtained by the two day simulation (see chapter 5.2.2b). The self consumption of PV output $W_{PV,used}$ is with the MPC approximately 15 % higher than with the classical control concept.

Table 5-9: Comparison of the annual simulation results of the classical control with the annual simulation results of the MPC for hydraulic circuit HC2, controlled variable is the temperature at the middle node of the thermal storage

Quantity	Value (classical control)	Value (MPC)
W_{Comp} $[kWh]$	4635	4273
Q_c $[kWh]$	15169	13887
SPF $[-]$	3.27	3.25
$W_{PV,used}$ $[kWh]$	618	712
f_{mean} $[Hz]$	75	64.7
$\#_{cycles}$ $[-]$	985	2744
$\tau_{on,mean}$ $[hr]$	2	0.8
$T_{S1,mean}$ $[°C]$	49.6±0.6	48.4±0.7
$T_{S2,mean}$ $[°C]$	49.2±1.2	48.1±0.8
$T_{S3,mean}$ $[°C]$	47.7±2.9	47.5±1.3
$T_{S4,mean}$ $[°C]$	43.8±4.2	45.2±2.6
$T_{S5,mean}$ $[°C]$	36.8±5.7	40.7±3.9

c)   Hydraulic circuit HC3

Figure 5-12 shows the curve of the temperature at the top node for the hydraulic circuit HC3 for an annual simulation. Both control concepts hold the comfort limit.
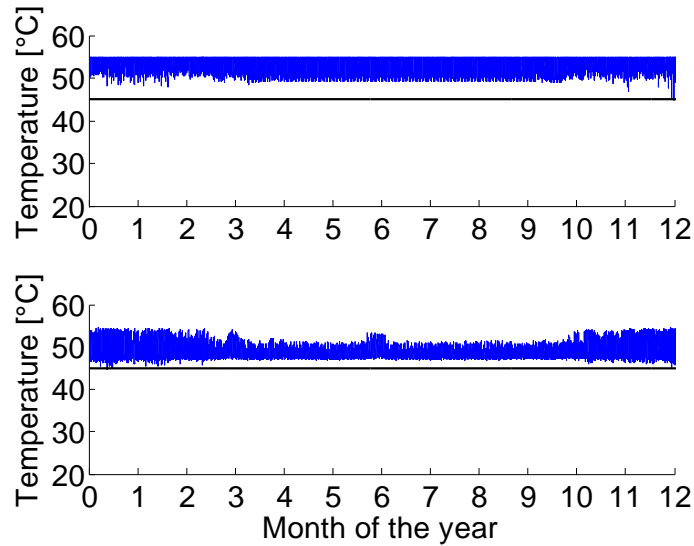
Figure 5-12: Annual simulation of the thermal storage connected to the condenser and desuperheater (HC3); based on the classical control (top), based on MPC (bottom)

Table 5-10 shows the results of the annual simulation of hydraulic circuit HC3. The simulation results are similar to the results obtained by the two day simulation (see chapter 5.2.2c). The mean compressor frequency f_{mean} achieved with the MPC is lower than in the simulation results of the other hydraulic cycles. Furthermore, the number of operating cycles of the heat pump $\#_{cycles}$ is higher which leads to the lower mean operating time of the heat pump $\tau_{on,mean}$. The impact of the high number of operating cycles on the SPF is partly compensated by the lower mean frequency achieved with the MPC. The self consumption of PV output $W_{PV,used}$ is with the MPC approximately 41 % higher than with the classical control concept. This high amount of self consumption of PV output compared to hydraulic circuit HC1 and HC2 may be partly due to the high number of operating cycles.

Table 5-10: Comparison of the annual simulation results of the classical control with the annual simulation results of the MPC for hydraulic circuit HC3, controlled variable is the temperature at the middle node of the thermal storage

Quantity	Value (classical control)	Value (MPC)
W_{Comp} $[kWh]$	4526	4233
Q_{c+d} $[kWh]$	16140	13960
SPF $[-]$	3.56	3.29
$W_{PV,used}$ $[kWh]$	620	875
f_{mean} $[Hz]$	75	44.5
$\#_{cycles}$ $[-]$	960	4832
$\tau_{on,mean}$ $[hr]$	2.2	0.7
$T_{S1,mean}$ $[°C]$	53.6±1.4	49.9±1.6
$T_{S2,mean}$ $[°C]$	50.8±2.2	46.5±0.7
$T_{S3,mean}$ $[°C]$	47.6±2	46.2±0.8
$T_{S4,mean}$ $[°C]$	44.4±3.4	45.2±1.2
$T_{S5,mean}$ $[°C]$	40.6±4.5	42.5±2.6

6 Summary and conclusion

Summary

An MPC approach was designed for the heating of a thermal storage with a heat pump. For this an iterative MPC-routine is used to model the nonlinear processes in a linear MPC. The MPC-routine was implemented in MATLAB. The MPC toolbox of MATLAB was used to solve the optimization problem. The required quantities of the heat pump were modeled with polynomials. Nonlinear models were derived for different hydraulic circuits of the thermal storage. Furthermore, predictions of electricity prices and PV output were used to operate the heat pump in times of surplus energy. Simulations for different hydraulic circuits and controlled variables were analyzed and compared to a classical control based on a hysteresis.

The reference system of the project "The Bat" was implemented as a simulation model in TRNSYS by the University of Innsbruck. It mainly consists of a heat pump, a thermal storage, a building and a PV array. External input variables are the DHW demand and the weather data. The weather data represents the climate in Innsbruck. This work focused on the heating of the thermal storage with the heat pump. A direct heating of the building with the heat pump as well as the division of the heat flow between building and thermal storage were not investigated in this work. This is why the building was not modeled. The heating demand for SH may be considered if the required heat is taken from the thermal storage.

After an analysis of the reference system the modeling started with the heat pump. To keep the problem simple the temperature of the heat source at the inlet of the evaporator was assumed as constant. For this a TRNSYS model of the heat pump with matching parameters was used to create characteristic diagrams for a defined operating range. Two different modes were investigated. In mode one the heat pump is only equipped with the condenser and in mode two the desuperheater is added. For both modes the characteristic diagrams were used to fit polynomials for the heat flows of the heat exchangers at the heat sink, for the mass flows through the heat exchangers at the heat sink, for the temperature at the desuperheater outlet, for the COP as well as for the evaporation and condensation temperatures.

The heating of the thermal storage was investigated for different hydraulic circuits. Firstly, the condenser was connected to the thermal storage at the top and bottom node. Secondly, the condenser was connected to the thermal storage at the middle and bottom node. Thirdly, the condenser and the desuperheater were connected to the thermal storage at the top, middle and bottom node. For each hydraulic circuit a five node model was derived to simulate the nonlinear heating process. These models consider the effect of forced

convection, natural convection, conduction inside the thermal storage and heat exchange with the ambient. Furthermore, a linear model was presented which is used within the linear MPC to control the temperature at the top node of the thermal storage as well as the temperature at the middle node of the thermal storage.

Predictions for PV output were based on ideal weather forecasts. To calculate the PV output in dependence of the cell temperature and the total incident irradiation an algebraic equation was derived based on measured data provided by the PV manufacturer. Historical data was used to obtain realistic values for the electricity price development. This data was used within the MPC-routine as predicted data.

To consider the nonlinear processes in the linear model, used within the linear MPC, an iterative MPC-routine was implemented in MATLAB. This routine prepares the external input variables for the use as weights and disturbances within the MPC. Then the linear model is used to determine the required heat flow into the thermal storage within the prediction horizon. Furthermore, a nonlinear model of the thermal storage is used to simulate the convective heat flow of the heating process within the prediction horizon. Then the heat flows are converted into disturbances affecting each node of the thermal storage. These disturbances are considered within the MPC and the required heat flow is determined again. This is repeated until a termination criterion is fulfilled.

Furthermore, investigations were performed to consider the COP within the MPC. These showed that the dependence of the COP on the condenser water inlet temperature and the frequency of the compressor led to a wide range of different possibilities for the consideration within the MPC. The consideration of the operating envelopes of the compressor within the MPC was also investigated. The gained insights were discussed and concepts for a further implementation were presented.

The parameter settings of the MPC application of this work were discussed in general to provide some insights into the different effects which can be achieved. In addition to the parameter settings provided by the MPC toolbox some parameters have arisen through the iterative MPC-routine as well as through the lower constraint of the compressor frequency.

Finally, simulations over a short period of two days were performed for the three hydraulic circuits with different controlled variables. The simulation results based on the MPC were compared with simulation results obtained with a classical control concept based on a hysteresis. The results showed that with the temperature at the top node as controlled variable the comfort limits were violated with all hydraulic circuits. This occurred for the classical control as well as for the MPC. The MPC showed lower violations. The simulation results for the temperature at the middle node as controlled variable did not show these violations for all hydraulic circuits controlled with the MPC. This was also observed for the

classical control concept for two hydraulic circuits. Only the hydraulic circuit with the thermal storage connected to the condenser with the middle and bottom node showed a violation of the comfort limit. Furthermore, annual simulations were performed to test the robustness of the MPC routine and to provide first results for the use of PV output compared to the classical control.

Conclusion

An iterative MPC approach for the control of the heating of a thermal storage with a heat pump incorporating predictions for PV output and electricity prices was investigated.

Annual simulation results for the temperature at the middle node as controlled variable showed the robustness of the iterative MPC approach. Furthermore, the MPC fulfills the comfort limits for all hydraulic cycles better than the classical control. An improvement with the MPC was the increased self consumption of PV output compared to the classical control (10% for HC1, 15% for HC2 and 40% for HC3). The high amount of self consumption with hydraulic circuit HC3 may be partly due to the high number of operating cycles of the heat pump. This was already achieved with first parameter settings. An adaption of the parameter settings may further increase the self consumption of PV output.

The simulation results with respect to the thermal energy input into the thermal storage are not meaningful. The amount of thermal energy input into the thermal storage differs significantly among all the simulations. It is assumed that the reason for this is linked with the load profiles, but this could not be confirmed due to lack of time. Therefore, also the SPF obtained by these simulations should be interpreted carefully. The SPF achieved with the MPC is for all hydraulic circuits lower than with the classical control. The reasons for this are the higher starting losses due to the short and frequently operating times of the heat pump and the higher mean temperature at bottom of the thermal storage with the MPC. The MPC achieved the highest SPF for hydraulic circuit HC3 (SPF=3.29). This is mainly due to the low mean compressor frequency of approximately 44 Hz which is partly compensated by the high number of operating cycles (4832 cycles with a mean operating time of 0.7 hours). The SPF may be further improved if the number of operating cycles of the heat pump is reduced. This may be achieved by a higher value for the weight of the manipulated variables rate.

Further improvements of the simulation results may be achieved due to a reduced temperature at the desuperheater outlet and a better adaption of the position of the controlled variable in the thermal storage.

The computational effort of an MPC based on online optimization is higher than for a classical control. This effort is further increased through the iterative MPC approach. The termination criterion is relevant for the number of iterations and has in this work been very

strict. To find a balance between accuracy and computational effort further investigations are necessary.

The prediction horizon and the sampling time of the MPC were taken from the work of Pichler et al. (2014). An analysis with the aim to reduce the steps in the prediction horizon can help to reduce the computational effort. This can be done by increasing the sampling time and/or decreasing the prediction horizon.

Bibliography

Beckmann, W., De Soto, W., Klein, S. (2006), Improvement and validation of a model for photovoltaic array performance, Solar Energy, 80: 78-88.

Bemporad, A., Morari, M., Ricker, N. (2014), Model Predictive Control Toolbox, Users Guide, The MathWorks, Inc., 3 Apple Hill Drive Natick, MA 01760.

Bianchi, M. (2006), Adaptive Modellbasierte Prädiktive Regelung einer Kleinwärmepumpenanlage, PhD thesis, Eidgenössische Technische Hochschule Zürich.

Bitzer, (2008), Kältemittel Report 15. Auflage, Bitzer Kühlmaschinenbau GmbH, Eschenbrünnlestraße 15, 71065 Sindelfingen.

Brenn, G., Meile, W. (2010), Strömungslehre und Wärmeübertragung 1, Skriptum, Institut für Strömungslehre und Wärmeübertragung, Technische Universität Graz.

Brychta, M. (2014), Referenzsystem, "The Bat" Interner Projektbericht, Arbeitsbereich Energieeffizientes Bauen, Universität Innsbruck.

Camacho, E., Bordons, C. (1999), Model Predicitive Control, Springer-Verlag London Limited, 236 Gray's Inn Road, London WC1X 8HB.

Coelho, R., Martins, D. (2012), An Optimized Maximum Power Point Tracking Method Based on PV Surface Temperature Measurement, Sustainable Energy - Recent Studies, Dr. Alemayehu Gebremedhin (Ed.), http://www.intechopen.com/books/sustainable-energy-recent-studies/an-optimized-maximum-power-point-tracking-method-based-on-pv-surface-temperature-measurement, 25.10.2014.

Copeland, (2013), Scroll Compressors for Heat Pumps with R410A, Emerson Climate Technologies, http://www.emersonclimate.com/europe/en-eu/resources.

Eckstein, J. (1990), Detailed modelling of photovoltaic system components, Master thesis, University of Wisconsin - Madison.

Fry, B. (1998), Simulation of grid tied building integrated photovoltaic systems, Master thesis, University of Wisconsin - Madison.

Gencer, E., Al-musleh, E., Mallapragada, D., Agrawal, R. (2014), Uninterrupted renewable power through chemical storage cycles, Current Opinion in Chemical Engineering, 5: 29-36.

Girodo, M. (2006), Solarstrahlungsvorhersage auf der Basis numerischer Wettermodelle, PhD thesis, Carl von Ossietzky Universität Oldenburg.

Grötschel, M., Lucas, K., Mehrmann, V. (2008), Produktionsfaktor Mathematik, acatech - Deutsche Akademie der Technikwissenschaften, Berlin.

Heinz, A., Haller, M. (2014), Description of TRNSYS Type 887, Internal report, Institute of Thermal Engineering, Graz University of Technology.

Heliotherm, (2014), Heliotherm Frischwassersystem, Heliotherm Wärmepumpentechnik Ges.m.b.H., www.heliotherm.com/media/frischwassersystem-pb_2014_3mail.pdf, 17.09.2014.

Hochenauer, C. (2012), Wärmetechnik 1, Skriptum, Institut für Wärmetechnik, Technische Universität Graz.

Hofer, A. (2014), Entwurf optimaler Systeme, Skriptum, Institut für Regelungs- und Automatisierungstechnik, Technische Universität Graz.

Hofer, A. (2009), Regelungstechnik 1, Skriptum, Institut für Regelungs- und Automatisierungstechnik, Technische Universität Graz.

Horn, M., Dourdoumas, N. (2004), Regelungstechnik, Pearson Education Deutschland GmbH, Lilienthalstr. 2, 85399 Hallbergmoos.

Löfberg, J. (2014), YALMIP Wiki, -, http://users.isy.se/johanl/yalmip/, 08.09.2014.

Maciejowski, J. (2000), Predictive Control with Constraints, Pearson Education Deutschland GmbH, Lilienthalstr. 2, 85339 Hallbergmoos.

Miara, M., Günther, D., Kramer, T., Oltersdorf, T., Wapler, J. (2011), Wärmepumpen Effizienz, Fraunhofer-Institut für Solare Energiesysteme ISE, Heidenhofstraße 2, 79110 Freiburg.

Morari, M., Ricker, N. (1998), Model Predictive Control Toolbox User's Guide, The MathWorks, Inc., 3 Apple Hill Drive Natick, MA 01760.

Pichler, M., Lerch, W., Heinz, A., Goertler, G., Schranzhofer, H., Rieberer, R. (2014), A novel linear predictive control approach for auxiliary energy supply to a solar thermal combistorage, Solar Energy, 101: 203-219.

Reiner, G., Shafai, E., Wimmer, R., Zogg, D., Gabathuler, H., Mayer, H., Bruderer, H. (1998), Kurztestmethode für Wärmepumpenanlagen, Schweizer Bundesamt für Energie, Kirchstutz 3, 3414 Oberburg.

Rieberer, R. (2012), Heizungs-, Lüftungs-, Klimatechnik, Skriptum, Institut für Wärmetechnik, Technische Universität Graz.

Rieberer, R., Moser, H., Halozan, H. (2009), Wärmepumpentechnik, Skriptum, Institut für Wärmetechnik, Technische Universität Graz.

Sanz, W. (2012), Computational Fluid Dynamics, Skriptum, Institut für Thermische Turbomaschinen und Maschinendynamik, Technische Universität Graz.

Self, S., Reddy, B., Rosen, M. (2013), Ground source heat pumps for heating: Parametric energy analysis of a vapor compression cycle utilizing an economizer arrangement, Applied Thermal Engineering, 52: 245-254.

Thron, U. (2001), Vorausschaunde selbstadaptierende Heizungsregelung für Solarhäuser, PhD thesis, Universität Hannover.

Townsend, T. (1989), A method for estimating the long-term performance of direct coupled photovoltaic systems, Master thesis, University of Wisconsin - Madison.

TRNSYS, (2012), TRNSYS 17 Manual, Solar Energy Laboratory, University of Wisconsin-Madison, 22 North Carroll Street - suite 370 Madison, WI 53703.

Webasto, T. (2000), Schulungshandbuch Kälte-Klima, Webasto Thermosysteme GmbH, D-82131 Stockdorf.

Wimmer, R. (2004), Regelung einer Wärmepumpenanlage mit Model Predictive Control, PhD thesis, Eidgenössische Technische Hochschule Zürich.

Nomenclature and abbreviations

Hydraulic circuit & heat pump

T	temperature	$[K]$
t	temperature	$[°C]$
τ	time	$[s]$
m	mass	$[kg]$
$\dot{m}$	mass flow	$[kg/s]$
p	pressure	$[bar]$
P	power	$[kW]$
W	work	$[kJ]$
G_T	total solar radiation	$[W/m^2]$
c	specific heat capacity	$[J/(kg\ K)]$
A	area	$[m^2]$
Q	thermal energy	$[J]$
$\dot{Q}$	thermal power	$[W]$
ρ	density	$[kg/m^3]$
u_{vel}	velocity	$[m/s]$
λ	thermal conductivity	$[W/(m\ K)]$
a	thermal diffusivity	$[m^2/(kg\ s)]$
U	thermal transmittance	$[W/(m^2\ K)]$
α	heat transfer coefficient	$[W/(m^2\ K)]$
f	frequency	$[Hz]$
b	coefficients of the polynomials	
π	pressure ratio	

Photovoltaic

V	voltage	$[V]$
I	current	$[A]$
R	resistance	$[\Omega]$
k	Boltzmann constant	$[J/K]$
q	electron charge constant	$[C]$
γ	shape factor	$[-]$

Control

J	cost function	$[-]$
p	prediction horizon	$[s]$
m	control horizon	$[s]$
y_{ref}, r	reference value/set point	$[°C]$
v	measured disturbances	$[°C], [W]$
d	unmeasured disturbances	
y	controlled variable	$[°C]$
u	manipulated variable	$[W]$
Δu	manipulated variable rate	$[W/\Delta\tau_{MPC}]$
x	state variable	$[°C]$
V	ECR factors	
ϵ	slack variable	

A	dynamic matrix
B	input matrix
C	output matrix

Subscripts

Hydraulic circuit & heat pump

cr	condensation refrigerant
er	evaporation refrigerant
a	ambient
$conv$	convection
$cond$	conduction
x	in x direction
yz	in y and z direction
$Comp$	compressor
H	heating
c	condenser
d	desuperheater
w	water
el	electrical
r	refrigerant
b	brine
S	storage
GF	ground floor
$1st\ Fl.$	first floor
ci	condenser inlet
co	condenser outlet
di	desuperheater inlet
do	desuperheater outlet
op	operating
$surf$	surface
rad	radiation
$loss$	losses to the ambient
HP	heat pump
air	room air temperature
J	number of the node in the thermal storage

Photovoltaic

L	light current
O	reverse saturation current
D	diode current
SC	shortcircuitcurrent
OC	open circuit voltage
MPP	maximum power current/voltage
S	series resistance
$cell$	cell
T	total incident irradiation
Ref	values at standard test conditions

Control

i i steps ahead in relation to k; $i = 0, \dots, p-1$

k current sampling instant

h h steps ahead in relation to k; $h = m, \dots, p-1$

min lower constraint

max upper constraint

$k + i|k$ the subscript k on the right side of the bar specifies the call of the MPC at time step k; the subscript i is referred to the prediction horizon and varies within the range $0 - (p-1)$; This means a variable with the subscript $k + i|k$ is calculated at each call of the MPC over the time horizon $0 - (p-1)$.

Superscripts

Hydraulic circuit & heat pump

N time step

Control

L last iteration of the iterative optimization

l current iteration number of iterative optimization; $l = 1, \dots, L$

$Base$ base weight

y referred to the controlled variable

u referred to the manipulated variable

Δu referred to the manipulated variable rate

Abbreviations

COP   coefficient of performance

MPP   maximum power point

MPPT   maximum power point tracker

ECR   equal concern for relaxation

PV   photovoltaic

DHW   domestic hot water

MPC   model based predictive control

ODP   ozone depletion potential

GWP   global warming potential

LQR   linear quadratic regulator

SPF   seasonal performance factor

SH   space heating

List of Figures

List of tables

Appendix

A-1 Manufacturers data of Solarwatt 60P

This chapter presents the measured data of the PV module Solarwatt 60P provided by the manufacturer (http://www.photovoltaikdirekt24.de, 02.06.2014). This PV module consists of 60 crystalline solar cells. One cell has a size of 156x156 mm. The electrical properties at standard test conditions (STC) are shown in Table A- 1. The standard test conditions refer to a solar irradiance of $1000\ W/m^2$ and an ambient temperature of $25\ °C$.

Table A- 1: Electrical properties of the PV-module Solarwatt 60P at standard test conditions (STC)

Property	Value
Nominal power [W]	250
Nominal voltage [V]	30.6
Nominal current [A]	8.18
Open circuit voltage [V]	37.4
Short circuit current [A]	8.73

Table A- 2 shows the electrical properties of the PV module Solarwatt 60P at normal operation cell temperature (NOCT). The normal operation cell temperature conditions refer to a solar irradiation of $800\ W/m^2$ and an ambient temperature of $20\ °C$.

Table A- 2: Electrical properties of the PV-module Solarwatt 60P at normal operation cell temperature (NOCT)

Property	Value
Nominal Power [W]	186
Nominal Voltage [V]	28.4
Nominal Current [A]	32.2
Open circuit voltage [V]	35.2
Short circuit current [A]	7.07

Table A- 3 shows the thermal properties of the PV module Solarwatt 60P. These are the temperature coefficient of open circuit voltage and short circuit voltage.

Table A- 3: Thermal properties of the PV-module Solarwatt 60P

Property	Value
Temperature coefficient of open circuit voltage [%/V]	-0.3
Temperature coefficient of short circuit current [%/A]	0.06

A-2 System of equations for hydraulic circuit HC1

The system of equations for the simulation of the convective heating process of hydraulic circuit HC1 is written in Eq. A- 1 - Eq. A- 5. Each equation corresponds to one node. The velocity $u_{vel,c}$ is calculated with the mass flow through the condenser (see Eq. 4-18). The temperature in the ghost cells (T_{S0}, T_{S6}) is calculated with Eq. 4-16-Eq. 4-17.

$$T_{S1}^{N+1} = T_{S1}^{N} - \frac{u_{vel,c}\,\Delta\tau}{\Delta x}(T_{S1}^{N} - T_{co}^{N}) - \frac{a\,\Delta\tau}{\Delta x^2}(T_{S2}^{N} - 2T_{S1}^{N} + T_{S0}^{N}) - \frac{UA_1\Delta\tau}{m_1\,c}(T_{S1} - T_a)$$ **Eq. A- 1**

$$T_{S2}^{N+1} = T_{S2}^{N} - \frac{u_{vel,c}\,\Delta\tau}{\Delta x}(T_{S2}^{N} - T_{S1}^{N}) - \frac{a\,\Delta\tau}{\Delta x^2}(T_{S3}^{N} - 2T_{S2}^{N} + T_{S1}^{N}) - \frac{UA_2\Delta\tau}{m_2\,c}(T_{S2} - T_a)$$ **Eq. A- 2**

$$T_{S3}^{N+1} = T_{S3}^{N} - \frac{u_{vel,c}\,\Delta\tau}{\Delta x}(T_{S3}^{N} - T_{S2}^{N}) - \frac{a\,\Delta\tau}{\Delta x^2}(T_{S4}^{N} - 2T_{S3}^{N} + T_{S2}^{N}) - \frac{UA_3\Delta\tau}{m_3\,c}(T_{S3} - T_a)$$ **Eq. A- 3**

$$T_{S4}^{N+1} = T_{S4}^{N} - \frac{u_{vel,c}\,\Delta\tau}{\Delta x}(T_{S4}^{N} - T_{S3}^{N}) - \frac{a\,\Delta\tau}{\Delta x^2}(T_{S5}^{N} - 2T_{S4}^{N} + T_{S3}^{N}) - \frac{UA_4\Delta\tau}{m_4\,c}(T_{S4} - T_a)$$ **Eq. A- 4**

$$T_{S5}^{N+1} = T_{S5}^{N} - \frac{u_{vel,c}\,\Delta\tau}{\Delta x}(T_{S5}^{N} - T_{S4}^{N}) - \frac{a\,\Delta\tau}{\Delta x^2}(T_{S6}^{N} - 2T_{S5}^{N} + T_{S4}^{N}) - \frac{UA_5\Delta\tau}{m_5\,c}(T_{S5} - T_a)$$ **Eq. A- 5**

A-3 System of equations for hydraulic circuit HC2

The system of equations for the simulation of the convective heating process of hydraulic circuit HC2 is written in Eq. A- 6 - Eq. A- 10.

$$T_{S1}^{N+1} = T_{S1}^{N} - \frac{a\,\Delta\tau}{\Delta x^2}(T_{S2}^{N} - 2T_{S1}^{N} + T_{S0}^{N}) - \frac{UA_1\Delta\tau}{m_1\,c}(T_{S1} - T_a)$$ **Eq. A- 6**

$$T_{S2}^{N+1} = T_{S2}^{N} - \frac{a\,\Delta\tau}{\Delta x^2}(T_{S3}^{N} - 2T_{S2}^{N} + T_{S1}^{N}) - \frac{UA_2\Delta\tau}{m_2\,c}(T_{S2} - T_a)$$ **Eq. A- 7**

$$T_{S3}^{N+1} = T_{S3}^{N} - \frac{u_{vel,c}\,\Delta\tau}{\Delta x}(T_{S3}^{N} - T_{co}^{N}) - \frac{a\,\Delta\tau}{\Delta x^2}(T_{S4}^{N} - 2T_{S3}^{N} + T_{S2}^{N}) - \frac{UA_3\Delta\tau}{m_3\,c}(T_{S3} - T_a)$$ **Eq. A- 8**

$$T_{S4}^{N+1} = T_{S4}^{N} - \frac{u_{vel,c}\,\Delta\tau}{\Delta x}(T_{S4}^{N} - T_{S3}^{N}) - \frac{a\,\Delta\tau}{\Delta x^2}(T_{S5}^{N} - 2T_{S4}^{N} + T_{S3}^{N}) - \frac{UA_4\Delta\tau}{m_4\,c}(T_{S4} - T_a)$$ **Eq. A- 9**

$$T_{S5}^{N+1} = T_{S5}^{N} - \frac{u_{vel,c}\,\Delta\tau}{\Delta x}(T_{S5}^{N} - T_{S4}^{N}) - \frac{a\,\Delta\tau}{\Delta x^2}(T_{S6}^{N} - 2T_{S5}^{N} + T_{S4}^{N}) - \frac{UA_5\Delta\tau}{m_5\,c}(T_{S5} - T_a)$$ **Eq. A- 10**

A-4 System of equations for hydraulic circuit HC3

The system of equations for the simulation of the convective heating process of hydraulic circuit HC2 is written in Eq. A- 11 - Eq. A- 15.

$$T_{S1}^{N+1} = T_{S1}^N - \frac{u_{vel,d}\,\Delta\tau}{\Delta x}(T_{S1}^N - T_{co}^N) - \frac{a\,\Delta\tau}{\Delta x^2}(T_{S2}^N - 2T_{S1}^N + T_{S0}^N) - \frac{UA_1\Delta\tau}{m_1\,c}(T_{S1} - T_a) \qquad \text{Eq. A- 11}$$

$$T_{S2}^{N+1} = T_{S2}^N - \frac{u_{vel,d}\,\Delta\tau}{\Delta x}(T_{S2}^N - T_{S1}^N) - \frac{a\,\Delta\tau}{\Delta x^2}(T_{S3}^N - 2T_{S2}^N + T_{S1}^N) - \frac{UA_2\Delta\tau}{m_2\,c}(T_{S2} - T_a) \qquad \text{Eq. A- 12}$$

$$T_{S3}^{N+1} = T_{S3}^N - \frac{u_{vel,d}\,\Delta\tau}{\Delta x}(T_{S3}^N - T_{S2}^N) - \frac{(u_{vel,c} - u_{vel,d})\,\Delta\tau}{\Delta x}(T_{S3}^N - T_{co}) $$
$$- \frac{a\,\Delta\tau}{\Delta x^2}(T_{S4}^N - 2T_{S3}^N + T_{S2}^N) - \frac{UA_3\Delta\tau}{m_3\,c}(T_{S3} - T_a) \qquad \text{Eq. A- 13}$$

$$T_{S4}^{N+1} = T_{S4}^N - \frac{u_{vel,c}\,\Delta\tau}{\Delta x}(T_{S4}^N - T_{S3}^N) - \frac{a\,\Delta\tau}{\Delta x^2}(T_{S5}^N - 2T_{S4}^N + T_{S3}^N) - \frac{UA_4\Delta\tau}{m_4\,c}(T_{S4} - T_a) \qquad \text{Eq. A- 14}$$

$$T_{S5}^{N+1} = T_{S5}^N - \frac{u_{vel,c}\,\Delta\tau}{\Delta x}(T_{S5}^N - T_{S4}^N) - \frac{a\,\Delta\tau}{\Delta x^2}(T_{S6}^N - 2T_{S5}^N + T_{S4}^N) - \frac{UA_5\Delta\tau}{m_5\,c}(T_{S5} - T_a) \qquad \text{Eq. A- 15}$$

A-5 Matrices of the linear state space model

The matrices for the state space model are written in continuous form as the values are further processed in MATLAB with the function "c2d – continuous to discrete" where the sampling time is added. Eq. A- 16 shows the state space model written in a matrix equation.

$$\dot{x} = A \cdot x + B_u \cdot u + B_v \cdot v \qquad \text{Eq. A- 16}$$

The vector of the state variables x represents the temperatures in the nodes of the thermal storage (see Eq. A- 17). The corresponding dynamic matrix A is written as Eq. A- 18.

$$x = [T_{S1}, T_{S2}, T_{S3}, T_{S4}, T_{S5}]^T \qquad \text{Eq. A- 17}$$

$$A = \begin{bmatrix} -\dfrac{UA}{m_1c} - \dfrac{UA_{loss,1}}{m_1c} & \dfrac{UA}{m_2c} & 0 & 0 & 0 \\[2mm] \dfrac{UA}{m_1c} & -\dfrac{UA}{m_2c} - \dfrac{UA_{loss,2}}{m_2c} & \dfrac{UA}{m_3c} & 0 & 0 \\[2mm] 0 & \dfrac{UA}{m_2c} & -\dfrac{UA}{m_3c} - \dfrac{UA_{loss,3}}{m_3c} & \dfrac{UA}{m_4c} & 0 \\[2mm] 0 & 0 & \dfrac{UA}{m_3c} & -\dfrac{UA}{m_4c} - \dfrac{UA_{loss,4}}{m_4c} & \dfrac{UA}{m_5c} \\[2mm] 0 & 0 & 0 & \dfrac{UA}{m_4c} & -\dfrac{UA}{m_5c} - \dfrac{UA_{loss,5}}{m_5c} \end{bmatrix} \qquad \text{Eq. A- 18}$$

The input vector of the manipulated variable $\boldsymbol{u}$ differs according to the controlled variable. If the temperature at the top node is the controlled variable Eq. A- 19 is used and if the temperature at the middle node is the controlled variable Eq. A- 20 is used. The corresponding input matrix of the manipulated variable is written in Eq. A- 21.

$$\boldsymbol{u} = \left[\dot{Q}_{S1}, 0, 0, 0, 0\right]^T \qquad \text{Eq. A- 19}$$

$$\boldsymbol{u} = \left[0, 0, \dot{Q}_{S3}, 0, 0\right]^T \qquad \text{Eq. A- 20}$$

$$B_u = \begin{bmatrix} \dfrac{1}{m_1 c} & 0 & 0 & 0 & 0 \\ 0 & \dfrac{1}{m_2 c} & 0 & 0 & 0 \\ 0 & 0 & \dfrac{1}{m_3 c} & 0 & 0 \\ 0 & 0 & 0 & \dfrac{1}{m_4 c} & 0 \\ 0 & 0 & 0 & 0 & \dfrac{1}{m_5 c} \end{bmatrix} \qquad \text{Eq. A- 21}$$

The vector of the disturbances $\boldsymbol{v}$ contains the convective heat flows calculated in chapter 4.2.4 and the ambient temperature of the thermal storage (see Eq. A- 22). The corresponding input matrix of the disturbances is written in Eq. A- 23.

$$\boldsymbol{v} = \left[\dot{Q}_{dis,1}, \dot{Q}_{dis,2}, \dot{Q}_{dis,3}, \dot{Q}_{dis,4}, \dot{Q}_{dis,5}, T_a\right]^T \qquad \text{Eq. A- 22}$$

$$B_v = \begin{bmatrix} \dfrac{1}{m_1 c} & 0 & 0 & 0 & 0 & \dfrac{UA_{loss,1}}{m_1 c} \\ 0 & \dfrac{1}{m_2 c} & 0 & 0 & 0 & \dfrac{UA_{loss,2}}{m_2 c} \\ 0 & 0 & \dfrac{1}{m_3 c} & 0 & 0 & \dfrac{UA_{loss,3}}{m_3 c} \\ 0 & 0 & 0 & \dfrac{1}{m_4 c} & 0 & \dfrac{UA_{loss,4}}{m_4 c} \\ 0 & 0 & 0 & 0 & \dfrac{1}{m_5 c} & \dfrac{UA_{loss,5}}{m_5 c} \end{bmatrix} \qquad \text{Eq. A- 23}$$